MAKİNE MÜHENDİSLİĞİ ALANINDA BİLİMSEL ARAŞTIRMALAR

Editör: Dr.Öğr.Üyesi Semih DURAN

yaz
yayınları

Makine Mühendisliği Alanında Bilimsel Araştırmalar

Editör

Dr.Öğr.Üyesi Semih DURAN

yaz yayınları

2026

yaz yayınları

Makine Mühendisliği Alanında Bilimsel Araştırmalar

Editör: Dr.Öğr.Üyesi Semih DURAN

E_ISBN 978-625-8574-75-3

Mart 2026 – Afyonkarahisar

Dizgi/Mizanpaj: YAZ Yayınları

Kapak Tasarım: YAZ Yayınları

YAZ Yayınları. Yayıncı Sertifika No: 73086

M.İhtisas OSB Mah. 4A Cad. No:3/3
İscehisar/AFYONKARAHİSAR

www.yazyayinlari.com

yazyayinlari@gmail.com

İÇİNDEKİLER

POWDER BED ADDITIVE MANUFACTURING: A GLOBAL BIBLIOMETRIC PERSPECTIVE (2021–2026)

Caner BULUT[1]

Mustafa ÖCAL[2]

1. INTRODUCTION

Manufacturing technologies, one of the fundamental driving forces of human history, have continuously evolved since the industrial revolutions. Increasing design complexity, high performance expectations, and the need for flexibility in production have made the limitations of traditional manufacturing methods more apparent. With advances in digitalization, automation, and materials science, manufacturing processes have evolved into a design and optimization-oriented structure. This transformation has highlighted new approaches offering shorter development times, less material loss, and greater geometric freedom. In this context, additive manufacturing technologies, based on the principle of layered production, offer the possibility of producing complex geometries and lightweight structures by directly transforming digital designs into physical parts, thus providing a strong alternative to traditional methods (Solberg and Berto 2019). According to ISO/ASTM 52900:2021 2021 additive manufacturing is the production of three- dimensional objects by adding material layer by layer using computer-controlled

[1] Dr. Öğr. Üyesi, Iğdır Üniversitesi, Teknik Bilimler MYO, Motorlu Araçlar ve Ulaştırma Teknolojileri Bölümü, ORCID: 0000-0001-5421-300X.

[2] Dr. Öğr. Üyesi, Iğdır Üniversitesi, Teknik Bilimler MYO, Makine ve Metal Teknolojileri Bölümü, ORCID: 0000-0002-6731-8561.

systems. In recent years, academic and industrial interest in this field has intensified significantly (Fig.1).

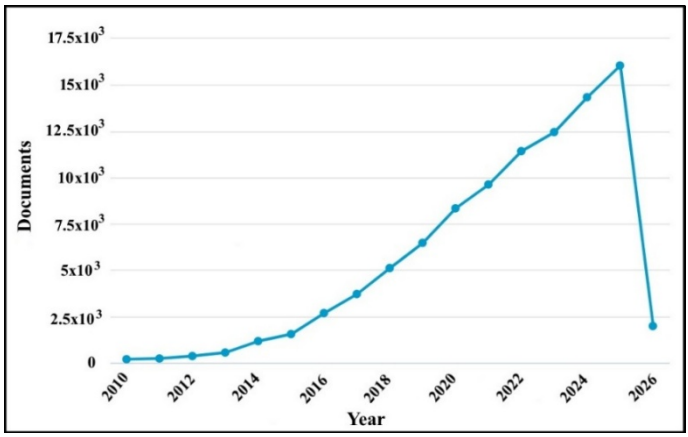

Fig. 1. Distribution of scientific studies on additive manufacturing by year

Additive manufacturing technologies are classified as solid extrusion or wire extrusion (melt deposition modeling, wire arc additive manufacturing, electron beam freeform), powder bed systems (selective laser melting, selective laser sintering, direct metal laser sintering, laser powder bed fusion and electron beam melting), and liquid-based systems (liquid-based system, stereolithography, direct light processing, inkjet printing) (Rajaguru et al. 2020). Powder bed-based (PBF) additive manufacturing methods, included in this classification, are based on the controlled liquefaction of metal powders with high-energy heat sources such as lasers or electron beams and the layer-by-layer solidification of molten or semi-molten material. The most important advantage of these methods is that complex geometries can be produced with high precision without the need for traditional molding and shaping processes (Frazier 2014). This study will address research using powder bed fusion additive manufacturing techniques. These methods, which have similar manufacturing principles, stand out because they offer high

design freedom, superior geometric accuracy and the ability to produce near-final shapes (Zhou et al. 2018).

PBF additive manufacturing methods have created a significant body of knowledge that expands the field through ongoing research, and although many illuminating review articles have been published about material manufacturing with these methods, studies using bibliometric analysis to systematically compile data and visualize trends are limited. In this context, throughout the subsequent sections of the study, these methods are classified under the heading of powder bed fusion/PBF, and the data analyzed using bibliometric analysis techniques (Studio R and VOSviewer programs) are evaluated within this framework. This study uses bibliometric methods to analyze the literature of studies conducted with PBF methods published in the Scopus database between January 1, 2021, and February 1, 2026. Using a data-driven approach and dimensionality reduction techniques, the aim is to map the research environment, identify key trends, and evaluate active researchers, frequently used keywords, prominent institutions, top-publishing journals, and relevant countries.

2. RESULTS AND DISCUSSION

2.1. Descriptive Analysis

Bibliometric analysis is a systematic approach that uses text mining techniques to evaluate and visualize various types of bibliometric networks based on the results of academic research in a specific scientific field (Eck and Waltman 2010). Bibliometric and VOSviewer software allow for the analysis of documents retrieved from SCOPUS, Web of Science, or PubMed. SCOPUS is preferred due to its comprehensive data, which generally contains more scientific publication data than Web of Science and PubMed. With an index containing 49,401 sources

(journals, books, etc.) in various scientific fields, SCOPUS is considered one of the most comprehensive and reliable bibliographic sources. Many studies in the literature have used this database in bibliometric analyses.

In our study, a search was performed in the Scopus database using a query string for "Article Title, Abstract, and Keywords," and a total of 41,822 scientific publication data points of all types were found in all languages and time periods related to PBF. Between January 1, 2021, and February 1, 2026, a total of 25,944 scientific publication data points were found in all languages and for all scientific documents. These documents include 21,119 articles, 1,207 reviews, 2,714 conference proceedings, 585 book chapters, and 16 books. In addition to these documents, there are 303 other scientific studies in the form of documents such as conference reviews, letters, notes, reports, etc. While scientific data published in English is the most prevalent, publications in Chinese (1091), Russian (58), Japanese (99), and German (46) are also prominent, and many other scientific publication documents related to the subject are available in different other languages.

Before statistical analysis, abstracts were manually reviewed to remove irrelevant titles and keywords, and only publications in English and of the original research paper type were filtered. Bibliometric analysis was performed on original research papers, which are considered to best represent the scientific output of the field. Accordingly, a total of 19881 documents were recorded between January 1, 2021, and February 1, 2026, using the specified query string and filtering for original research papers in English, and this data was used for visualizations, interpretations, and analyses in the bibliometric study. Table 1 presents the basic details regarding these scientific publications obtained from the Scopus database. According to the data in Table 1, the annual growth rate of documents globally was

observed to be 23.77%. A total of 23303 authors contributed to 1439 sources, with an average of 11.7 co-authors and an average of 14.61 citations per document. These results demonstrate that researchers' interest in PBF additive manufacturing technologies is steadily increasing.

Table 1. Basic data obtained regarding PBF additive manufacturing

Definition	Result
Timespan	2021-2026
Sources (Journal, etc.)	1439
Documents/Article	19881
Annual growth rate (%)	23.77
Average Document Age	2.64
Average number of citations per document	14.61
References	85680
Keyword Plus (ID)	46128
Author's Keywords (DE)	26902
Authors	23303
Number of co-authors per document	11.7
International co-authorships (%)	25.55
Document Types (Article)	19881
Language	English

Fig.2 shows the annual scientific publication trend data for powder bed-based additive manufacturing methods for the period January 1, 2021 - February 1, 2026. According to the data in Figure 2, a steady annual increase in publication output has been observed since 2021. This significant increase in both annual and cumulative publications reveals the rapidly growing interest of researchers in this field, especially in recent years. A literature review also confirms that scientific studies on material production using additive manufacturing and powder bed-based additive manufacturing methods have increased significantly compared to previous years. Therefore, it is predicted that the current growth trend will continue in the coming years with the development of new application areas for PBF-based additive manufacturing technologies.

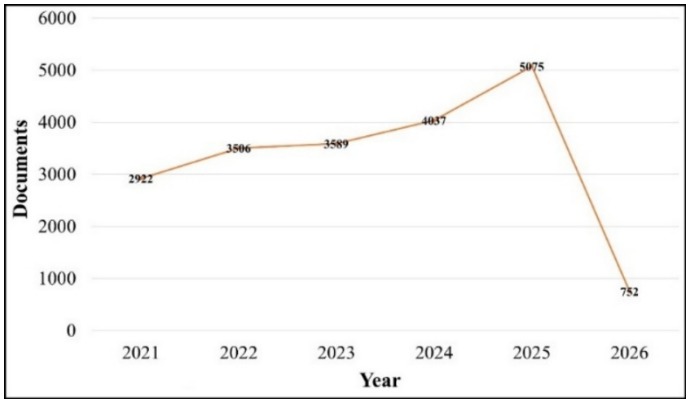

Fig. 2. Distribution of original research articles on PBF methods by year

2.2. Author, Country, and Institutional Analysis

Analyzing inter-institutional collaboration using bibliometric methods is a valuable approach to evaluating the effectiveness of research partnerships between institutions and countries. This analysis helps researchers identify reputable institutions for potential collaboration, facilitating faster development and commercialization of innovative outputs, documents, and products from both industry and laboratories. Fig.3 visually illustrates the author-based time trend of relevant studies on materials produced using PBF-additive manufacturing methods. The publication distribution reveals that some researchers stand out in terms of the number of publications. However, the field has generally developed with moderate contributions from numerous researchers. Researchers have shown significant interest in this field since 2021 and have regularly contributed to scientific studies on the subject in 2022 and beyond. The prevalence of multi-authored and interdisciplinary studies indicates that the field has a collaborative structure. Researchers have generally conducted studies on many materials using PBF-additive manufacturing methods, such as Aluminum (Al) matrix composites, IN718 superalloys, 316L stainless steels, NiTi alloy, Ti6Al4V alloy, and high-entropy

alloys. The data shows that not only leading researchers but also other researchers in the dataset have shown interest in this field and that studies are ongoing.

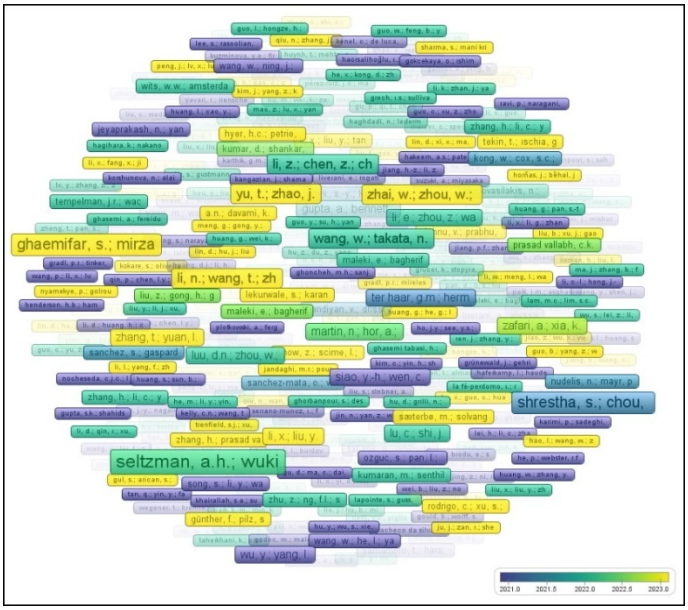

Fig. 3. Most relevant authors in the PBF field.

Fig.4 illustrates the global scientific collaboration network between countries based on the number of publications in PBF-based studies. The size of the nodes represents the total number of published scientific articles. However, when examining the geographical distribution of publications in this field, the analysis of the world map/collaboration network reveals strong collaborative ties between authors from various countries. For example, in research conducted in China, co-authors may be from different countries, and their institutional connections may reflect multiple countries. This dynamic affects the number of publications for each country involved in the research. Similarly, this scenario applies to other countries that have submitted documents on the subject. China stands out as the most productive country with the largest node in the scientific collaboration network, with 7555 documents. China is followed by the USA

and Germany, respectively. The figure shows that other countries and research groups based on each continent have formed intensive and multifaceted joint publication networks, and that these core regions play a decisive role in the development of the field by establishing strong scientific interactions with other countries.

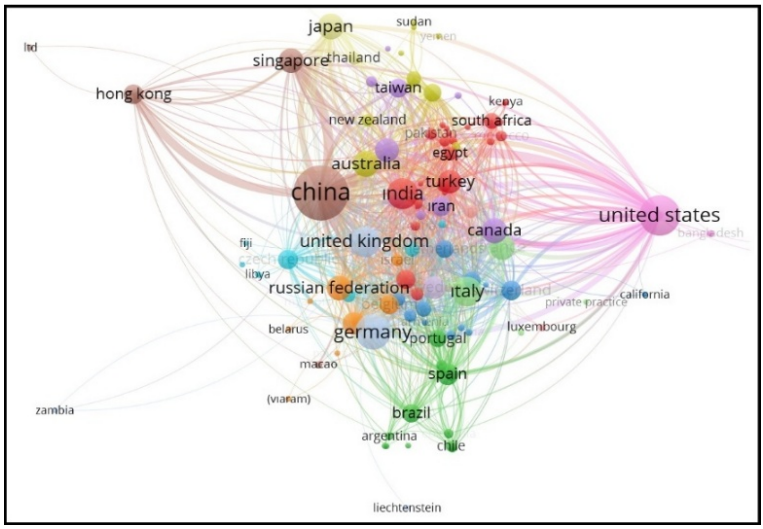

Fig. 4. PBF is a network for international scientific cooperation in additive manufacturing research

Table 2 shows the number of documents and average citations for some countries. China, the USA, and Germany rank in the top three in terms of the number of articles and citations, and these three countries also rank first among important institutions such as universities and institutes. This is among the important factors affecting the production of scientific documents. In addition, China's leading position in output related to this subject can be attributed to factors such as the strong infrastructure and support they need in this field, their interest and approach to the subject, and their sufficient human resources in this field.

Table 2. Number of publications and citations by country

No	Country	Document/ Article	Citations	Average Citations Per Article
1	China	7555	122860	16.26
2	USA	2798	49423	17.67
3	Germany	1826	27348	14.98
4	India	1198	12003	10.02
5	United Kingdom	1114	21592	19.38
6	Italy	1088	14255	13.10
7	Australia	699	19103	27.33
8	Japan	694	9505	13.70
9	Canada	627	11178	17.83
10	France	603	8480	14.06
11	Russia	587	4638	7.90
12	Singapore	568	15791	27.80
13	South Korea	546	8545	15.65
14	Türkiye	482	5749	11.93
15	Sweden	451	6704	14.86

2.3. Sources

The most influential research publications are discussed under these headings. Fig.5 shows the top 10 most active publication sources (journals). “Additive Manufacturing” ranks first with 1075 documents (Elsevier), followed by “Materials Science and Engineering A” with 1062 documents (Elsevier) and “Materials” (MDPI) with 860 documents. All three journals offer peer-reviewed and open-access publications focusing on materials science, metallurgy, and interdisciplinary studies.

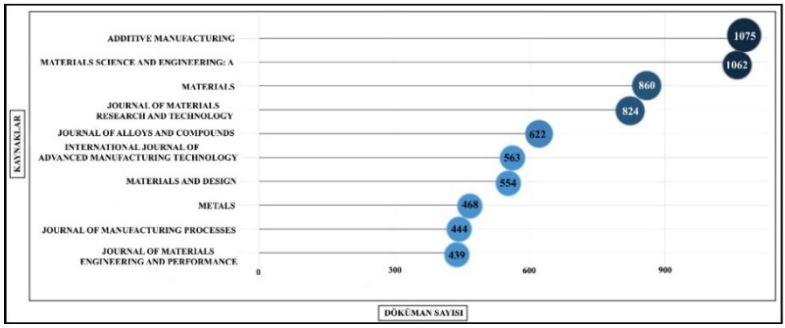

Fig. 5. Most Relevant Publication Sources/Journals

In addition to the original research articles (total 1439) included in the current data package as of 2021, review articles published in English during this period (total 1126) were also considered. Review articles are important resources that help new researchers understand the field and enable established groups to stay informed with current data. By examining these articles in detail, researchers can better contextualize their studies within the existing literature (Palmatier et al. 2018). In this context, the most cited studies and the journals in which they were published within the current data package are listed in Table 3, and the most cited review articles in the journals in which they were published are listed in Table 4. These articles are coded as “Study 1”, “Study 2”, etc. for each table. The article titled “Strong Yet Ductile Nanolamellar High-Entropy Alloys By Additive Manufacturing” by Ren et al. (Study 1) ranks first with a total of 587 citations (Ren et al. 2022). This study highlights that high yield strength (~1.3 GPa) and good ductility (14% elongation) can be achieved simultaneously in $AlCoCrFeNi_{2.1}$ high-entropy alloys produced by the L-PBF method thanks to their dual-phase nanolamellar microstructure. Tang et al.’s article “Alloys-by-Design: Application to New Superalloys for Additive Manufacturing” (Study 2) ranks second with a total of 532 citations (Tang et al. 2021). In this study, the process-microstructure-property relationships were systematically addressed using the alloy-design approach in the development of new superalloys designed

for additive manufacturing, and a framework for high-performance superalloy design suitable for additive manufacturing was presented. When other highly cited studies in Table 3 are examined, it is seen that microstructure, mechanical properties, heat treatment effects, alloy design and performance relationships are systematically addressed in L-PBF and general PBF processes. Some of these studies detail microstructure investigations and thermal stability, while others focus on optimizing critical mechanical performance parameters such as high strength, ductility, and fatigue behavior.

Table 3. Most cited review studies globally within the data package of PBF methods

Study	Journal	Total Citations	Ref.
"Study 1"	Nature	587	(Ren et al. 2022)
"Study 2"	Acta Materialia	532	(Tang et al. 2021).
"Study 3"	Acta Materialia	475	(Voisin et al. 2021)
"Study 4"	Nature Communications	379	(Huang et al. 2022)
"Study 5"	Acta Materialia	342	(Gokcekaya et al. 2021)
"Study 6"	Science	341	(Zhang et al. 2021)
"Study 7"	Engineering Fracture Mechanics	289	(Bao et al. 2021)
"Study 8"	Journal of Materials Processing Technology	262	(Cai et al. 2021)
"Study 9"	International Journal of Fatigue	258	(Wu et al. 2021)
"Study 10"	Additive Manufacturing	257	(Serrano-Munoz et al. 2020)

Table 4. Table 4. Most cited review studies on PBF

Study	Journal	Total Citations	Ref.
"Study 1"	Materials & Design	1824	(Blakey-Milner et al. 2021)
"Study 2"	Additive Manufacturing	575	(Kong et al. 2021)
"Study 3"	Journal of Materials Research and Technology	531	(Chowdhury et al. 2022)
"Study 4"	Additive Manufacturing	510	(Kotadia et al. 2021)
"Study 5"	Journal of Materials Science	509	(Haghdadi et al. 2021)
"Study 6"	Progress in Materials Science	494	(du Plessis et al. 2022)
"Study 7"	Journal of Materials Research and Technology	485	(Nguyen et al. 2022)
"Study 8"	International Journal of Machine Tools and Manufacture	431	(Sanchez et al. 2021)
"Study 9"	Advanced Powder Materials	409	(Wang et al. 2023)
"Study 10"	Journal of Materials Science & Technology	394	(Ostovari et al. 2021)

In Table 4, the article titled "Metal Additive Manufacturing in Aerospace: A Review" by Milner et al. (Blakey-Milner et al. 2021) ranks first with a total of 1824 citations. With an average annual citation rate of approximately 429 as of the publication date, this article demonstrates a high level of impact in the literature. This study is the most cited review article in the field, comprehensively addressing metal additive manufacturing technologies for aerospace applications in terms of processes, materials used, mechanical performance, quality control, and industrial application challenges. It is evident that other review articles listed in Table 4 have also received considerable attention from researchers. These review articles comprehensively evaluate key themes in the PBF and metal additive manufacturing literature, such as microstructure-property relationships, the effects of process defects and flaws, thermal behavior and heat treatments, surface engineering applications, and machine process optimization.

2.4. Keyword Cloud Analysis

Word cloud analysis provides insight into common topics and keywords in a given field by visually representing the most frequently used words in documents (Atenstaedt 2012). In this context, a Word Cloud analysis was performed using the “Author Keywords” and “Abstract” factors from the existing data package. Fig. 6 shows the most frequently used keywords by the authors in the generated Word Cloud. Prominent keywords include additive manufacturing, laser powder bed fusion, selective laser melting, 3D printing, selective laser sintering, microstructure, mechanical properties, heat treatment, powder bed fusion corrosion, surface treatments, and fatigue. The materials produced include titanium and titanium alloys, aluminum alloys, superalloys (IN718, IN625), Ti6Al4V, 316L stainless steel, high-entropy alloys, copper and its alloys, which are the prominent keywords of the author. Based on this data, it is observed that significant studies on these and other materials produced by PBF methods generally focus on determining structural, microstructural, mechanical, surface treatment, fatigue, and corrosion properties. The analysis also shows that research aimed at improving materials produced by the PBF method through additional alloying elements, additives, and process parameters also holds a significant place. These findings are in good agreement with the main theme of the current research. Word cloud analysis reveals that authors use appropriate and highly representative keywords in their studies that reflect the core issues and research trends of the field.

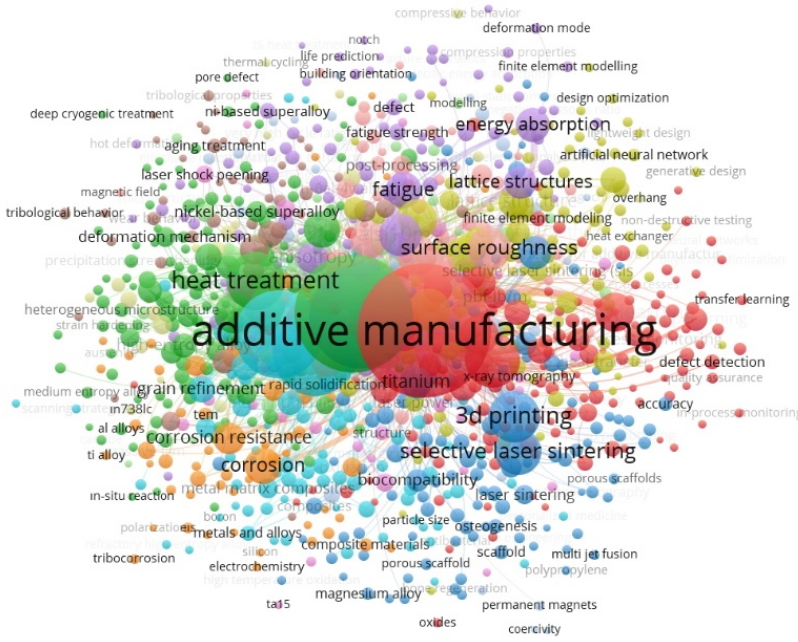

Fig. 6. Word cloud of keywords

2.5. Co-word Analysis

Multiple Correlation Analysis (MCA) was performed to reveal the conceptual structure of this study, and two main clusters were identified as shown in Fig 7. The MCA map shows that the prominent concepts in the literature are grouped under two main clusters. The first dimension (Dim 1) explains 36.34% of the total variance, while the second dimension (Dim 2) contributes 26.18%, and the first two dimensions together represent 62.52% of the conceptual structure. The red cluster mainly consists of concepts related to material types, alloy systems, and powder bed fusion processes. In this cluster, terms such as Ti-6Al-4V, aluminum, nickel, cobalt, chromium, copper and iron-based alloys, binary and ternary alloy systems, grain boundaries, powder bed, laser powder bed fusion, melting pool, laser material interaction, and heat treatment stand out. This conceptual integrity demonstrates that the literature heavily

researches the relationships between production parameters, microstructure formation, and material performance of metallic alloys produced by PBF processes. The blue cluster, while containing a more limited number of concepts, focuses on terms such as selective laser sintering, laser heating, sintering, X-3D printing, and 316L stainless steel. This cluster represents studies focusing on sintering-based production processes and specific material systems within PBF-based approaches. Overall, the MCA results reveal that research in the PBF literature largely focuses on laser powder bed fusion processes, alloy systems, and their microstructure-process relationships; conversely, sintering-based approaches are positioned as a more limited but distinct sub-theme. These findings are consistent with the bibliometric and thematic analysis results of the study and comprehensively reflect the conceptual framework of the field.

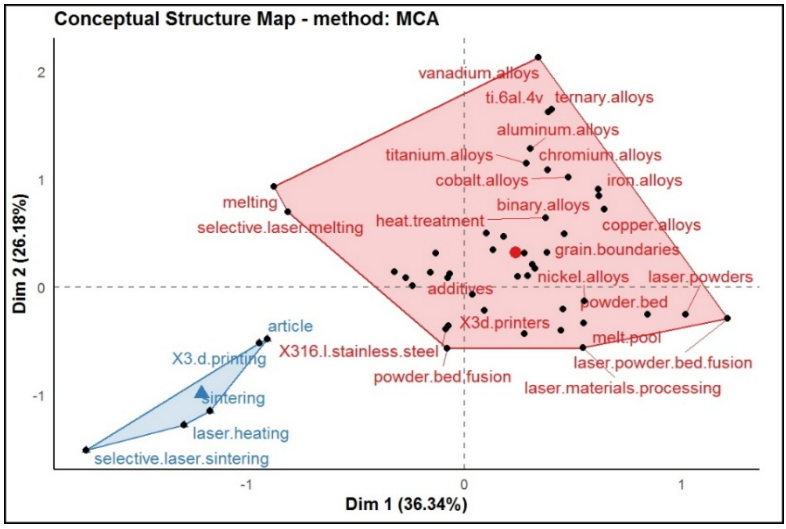

Fig. 7. Conceptual Factor Analysis of the Documents

3. LIMITATIONS

In this study, an initial pool of over 40,000 documents related to additive manufacturing methods in PBF between

January 1, 2021, and February 1, 2026, was reduced to a total of 19,881 documents after necessary filtering. To perform the analysis, we used Bibliometrix software, which facilitates the reduction of the size of main themes within the topics and critical categorization, and in some sections, the VOSviewer application. However, a major limitation of the study is that the analysis was restricted to the WOS Core Collection, excluding other online databases such as Web of Science and PubMed. Therefore, we refrain from making definitive conclusions or strong claims. Instead, we suggest research gaps and future directions based on the frequency of co-occurrence of author keywords. Furthermore, the fact that the analyses are limited to studies published in English and specific databases is among the main limitations of this study. Our observations relate to terms extracted from documents in SCOPUS-indexed journals.

4. CONCLUSION

This study examines published articles on additive manufacturing technologies based on PBF from a holistic perspective, analyzing current developments and limitations. Literature on PBF additive manufacturing research was evaluated using bibliometric analysis (RStudio) and VOSviewer software between January 1, 2021, and February 1, 2026. A total of 19,881 documents were analyzed globally to create a comprehensive bibliometric map revealing the structure, trends, and research focuses of the field. The research findings indicate that additive manufacturing research related to PBF technologies has gained significant momentum and experienced a considerable increase in the number of publications in the post-2021 period. When evaluated on a country basis, China ranks first in terms of the number of publications, followed by the United States and Germany. Prominent journals in this field include “Additive Manufacturing”, “Materials Science and Engineering A”,

"Materials", and "Journal of Materials Research and Technology". According to subject area distribution, the vast majority of studies are concentrated in Materials Science and Engineering, followed by Physics, Chemistry and Chemical Engineering. This study provides a guiding framework for researchers by revealing research trends, collaborations, and prominent themes in PBF-based additive manufacturing.

Acknowledgements

The Bibliometric and VOSviewer-based R-Studio software used in this study are freely available. Both software programs have a user-friendly interface, and the figures presented in the study were automatically generated by the software. The relevant images were derived from keywords used in data searches performed in the SCOPUS database. We would like to thank the developers of these software programs for their significant contributions to the analysis and management of large-scale data.

REFERENCES

Atenstaedt, R. 2012. Word cloud analysis of the BJGP. The British journal of general practice : the journal of the Royal College of General Practitioners, 62(596), 148.

Bao, H., Wu, S., Wu, Z., Kang, G., Peng, X. and Withers, P. J. 2021. A machine-learning fatigue life prediction approach of additively manufactured metals. Engineering Fracture Mechanics, 242, 107508.

Blakey-Milner, B., Gradl, P., Snedden, G., Brooks, M., Pitot, J., Lopez, E., Leary, M., Berto, F. and du Plessis, A. 2021. Metal additive manufacturing in aerospace: A review. Materials & Design, 209, 110008.

Cai, C., Tey, W. S., Chen, J., Zhu, W., Liu, X., Liu, T., Zhao, L. and Zhou, K. 2021. Comparative study on 3D printing of polyamide 12 by selective laser sintering and multi jet fusion. Journal of Materials Processing Technology, 288, 116882.

Chowdhury, S., Yadaiah, N., Prakash, C., Ramakrishna, S., Dixit, S., Gupta, L. R. and Buddhi, D. 2022. Laser powder bed fusion: a state-of-the-art review of the technology, materials, properties & defects, and numerical modelling. Journal of Materials Research and Technology, 20, 2109–2172.

du Plessis, A., Razavi, N., Benedetti, M., Murchio, S., Leary, M., Watson, M., Bhate, D. and Berto, F. 2022. Properties and applications of additively manufactured metallic cellular materials: A review. Progress in Materials Science, 125, 100918.

Eck, N. J. van and Waltman, L. 2010. Software survey: VOSviewer, a computer program for bibliometric mapping. Scientometrics, 84(2), 523–538.

Frazier, W. E. 2014. Metal Additive Manufacturing: A Review. Journal of Materials Engineering and Performance, 23(6), 1917–1928.

Gokcekaya, O., Ishimoto, T., Hibino, S., Yasutomi, J., Narushima, T. and Nakano, T. 2021. Unique crystallographic texture formation in Inconel 718 by laser powder bed fusion and its effect on mechanical anisotropy. Acta Materialia, 212, 116876.

Haghdadi, N., Laleh, M., Moyle, M. and Primig, S. 2021. Additive manufacturing of steels: a review of achievements and challenges. Journal of Materials Science, 56(1), 64–107.

Huang, Y., Fleming, T. G., Clark, S. J., Marussi, S., Fezzaa, K., Thiyagalingam, J., Leung, C. L. A. and Lee, P. D. 2022. Keyhole fluctuation and pore formation mechanisms during laser powder bed fusion additive manufacturing. Nature Communications, 13(1), 1170.

ISO/ASTM 52900:2021. 2021. Additive manufacturing — General principles — Terminology, International Organization for Standardization / ASTM International.

Kong, D., Dong, C., Wei, S., Ni, X., Zhang, L., Li, R., Wang, L., Man, C. and Li, X. 2021. About metastable cellular structure in additively manufactured austenitic stainless steels. Additive Manufacturing, 38, 101804.

Kotadia, H. R., Gibbons, G., Das, A. and Howes, P. D. 2021. A review of Laser Powder Bed Fusion Additive Manufacturing of aluminium alloys: Microstructure and properties. Additive Manufacturing, 46, 102155.

Nguyen, H. D., Pramanik, A., Basak, A. K., Dong, Y., Prakash, C., Debnath, S., Shankar, S., Jawahir, I. S., Dixit, S. and Buddhi, D. 2022. A critical review on additive

manufacturing of Ti-6Al-4V alloy: microstructure and mechanical properties. Journal of Materials Research and Technology, 18, 4641–4661.

Ostovari, Ahmad, M., Shaburova, N. A., Samodurova, M. N., Abdollahzadeh, A. and Trofimov, E. A. 2021. Additive manufacturing of high entropy alloys: A practical review. Journal of Materials Science and Technology, 77, 131–162.

Palmatier, R. W., Houston, M. B. and Hulland, J. 2018. Review articles: purpose, process, and structure. Journal of the Academy of Marketing Science, 46(1), 1–5.

Rajaguru, K., Karthikeyan, T. and Vijayan, V. 2020. Additive manufacturing – State of art. Materials Today: Proceedings, 21, 628–633.

Ren, J., Zhang, Y., Zhao, D., Chen, Y., Guan, S., Liu, Y., Liu, L., Peng, S., Kong, F., Poplawsky, J. D., Gao, G., Voisin, T., An, K., Wang, Y. M., Xie, K. Y., … Chen, W. 2022. Strong yet ductile nanolamellar high-entropy alloys by additive manufacturing. Nature, 608(7921), 62–68.

Sanchez, S., Smith, P., Xu, Z., Gaspard, G., Hyde, C. J., Wits, W. W., Ashcroft, I. A., Chen, H. and Clare, A. T. 2021. Powder Bed Fusion of nickel-based superalloys: A review. International Journal of Machine Tools and Manufacture, 165, 103729.

Serrano-Munoz, I., Mishurova, T., Thiede, T., Sprengel, M., Kromm, A., Nadammal, N., Nolze, G., Saliwan-Neumann, R., Evans, A. and Bruno, G. 2020. The residual stress in as-built Laser Powder Bed Fusion IN718 alloy as a consequence of the scanning strategy induced microstructure. Scientific Reports, 10(1), 14645.

Solberg, K. and Berto, F. 2019. What is going on with fatigue of additively manufactured metals? Material Design & Processing Communications, 1(5), e84.

Tang, Y. T., Panwisawas, C., Ghoussoub, J. N., Gong, Y., Clark, J. W. G., Németh, A. A. N., McCartney, D. G. and Reed, R. C. 2021. Alloys-by-design: Application to new superalloys for additive manufacturing. Acta Materialia, 202, 417–436.

Voisin, T., Forien, J.-B., Perron, A., Aubry, S., Bertin, N., Samanta, A., Baker, A. and Wang, Y. M. 2021. New insights on cellular structures strengthening mechanisms and thermal stability of an austenitic stainless steel fabricated by laser powder-bed-fusion. Acta Materialia, 203, 116476.

Wang, J., Zhu, R., Liu, Y. and Zhang, L. 2023. Understanding melt pool characteristics in laser powder bed fusion: An overview of single- and multi-track melt pools for process optimization. Advanced Powder Materials, 2(4), 100137.

Wu, Z., Wu, S., Bao, J., Qian, W., Karabal, S., Sun, W. and Withers, P. J. 2021. The effect of defect population on the anisotropic fatigue resistance of AlSi10Mg alloy fabricated by laser powder bed fusion. International Journal of Fatigue, 151, 106317.

Zhang, T., Huang, Z., Yang, T., Kong, H., Luan, J., Wang, A., Wang, D., Kuo, W., Wang, Y. and Liu, C.-T. 2021. In situ design of advanced titanium alloy with concentration modulations by additive manufacturing. Science, 374(6566), 478–482.

Zhou, Y., Zeng, X., Yang, Z. and Wu, H. 2018. Effect of crystallographic textures on thermal anisotropy of selective laser melted Cu-2.4Ni-0.7Si alloy. Journal of Alloys and Compounds, 743, 258–261.

PANEL EĞİM AÇISINA BAĞLI GÜNEŞ RADYASYONU EKSERJİSİNİN TEORİK MODELLERLE ANALİZİ: İZMİR İLİ ÖRNEĞİ

Ali Serkan AVCI[1]

1. GİRİŞ

Küresel nüfus artışı, sanayileşme ve teknolojik gelişmeler, dünya genelinde enerjiye olan talebi gün geçtikçe artırmaktadır. Günümüzde bu enerji talebinin büyük bir kısmı fosil yakıtlardan karşılanıyor olsa da, bu durumun yol açtığı çevresel problemler (sera gazı emisyonları, küresel ısınma vb.) ve fosil kaynakların tükenme riski, insanoğlunu temiz, güvenilir ve sürdürülebilir yenilenebilir enerji kaynaklarına yöneltmiştir (Özalp, 2025). Bu bağlamda güneş enerjisi, temiz, çevre dostu ve tükenmez bir enerji kaynağı olması sebebiyle en çok tercih edilen alternatiflerin başında gelmektedir (Luo ve ark., 2025). Güneş enerjisi sistemlerinden elde edilen verimi maksimum düzeye çıkarmak için, yüzeye düşen güneş ışınımı miktarının doğru hesaplanması ve sistem tasarımının bu doğrultuda optimize edilmesi büyük önem taşır. Güneş panellerinin üzerine düşen ışınım miktarını etkileyen en kritik parametrelerden biri, panelin yatay düzlemle yaptığı eğim (tilt) açısıdır (Yadav ve Chandel, 2013). Panellerin güneş ışınlarını en dik açıyla alacak şekilde konumlandırılması, yıl boyunca elde edilecek toplam enerjiyi doğrudan artırmaktadır (Benghanem, 2011). Güneş takip sistemleri bu açıyı dinamik olarak optimize etse de yüksek maliyetleri nedeniyle genellikle sabit eğim açılı sistemler tercih edilmektedir; bu nedenle,

[1] Dr. Öğr. Üyesi, Batman Üniversitesi, Beşiri OSB Meslek Yüksek Okulu, ORCID: 0000-0002-0761-8642.

panellerin kurulacağı coğrafi konuma özgü en uygun sabit eğim açısının belirlenmesi zorunludur. Öte yandan, enerji sistemlerinin performans değerlendirmesinde yalnızca enerji analizi yapmak yeterli olmamakta, enerjinin işe dönüşebilme kalitesini (maksimum faydalı iş potansiyelini) ifade eden ekserji analizinin de yapılması gerekmektedir (Caliskan, 2017). Güneş enerjisi belirli bir entropi barındırdığından gelen radyasyonun tamamı işe dönüştürülemez, bu nedenle termodinamik açıdan elde edilebilecek maksimum faydalı işin doğru modellenmesi verimli sistem tasarımları için vazgeçilmezdir (Saidur ve ark., 2012).

Güneş ışınımı ekserji modelleri incelendiğinde, radyasyonun termodinamik kalitesini belirlemek amacıyla literatürde çeşitli teorik denklemlerin geliştirildiği görülmektedir (Bayrak ve ark., 2017). Bu modellerin temelini, radyasyonun ekserjisini Carnot etkinliğine veya idealize edilmiş termodinamik çevrimlere dayandıran Petela, Spanner ve Jeter gibi araştırmacıların çalışmaları oluşturmaktadır (Rodríguez ve ark., 2022). Petela, ısı ışınımının ekserjisinin hesaplanmasına yönelik termodinamik temelli bir bağıntı sunmuş (Petela, 2003); Spanner, bu yaklaşımı sadeleştirerek doğrudan güneş ışınımı için yaklaşık bir ifade önermiş (Spanner, 1964); Jeter ise radyasyonu bir ısı kaynağı olarak ele alarak Carnot verimine dayalı farklı bir değerlendirme geliştirmiştir (Jeter, 1981). Türkiye ekseninde yapılan güncel araştırmalarda bu modellerin güneş radyasyonunun ekserji potansiyelini belirlemede yaygın olarak kullanıldığı görülmektedir. Bu üç modele ek olarak, Mohammed ve Mengüç (2018) tarafından geliştirilen yaklaşım, güneş radyasyonu ekserji hesabına yerel meteorolojik değişkenleri ve geometrik etkileri birlikte dâhil ederek, çevresel koşulları gözeten daha kapsamlı bir değerlendirme sunmaktadır (Mohammed ve Mengüç, 2018). Örneğin, Beyazit ve ark. (2019) Diyarbakır ili için yaptıkları uzun dönemli analizde Jeter, Petela ve Spanner modellerini kıyaslamış; üç modelin de birbirine yakın sonuçlar

verdiğini ancak Jeter modelinin güneş ışınım ekserji değerini diğerlerine göre bir miktar daha yüksek hesapladığını saptamışlardır (Beyazit ve ark., 2019). Benzer şekilde, Kaltakkıran (2023) Erzurum verileriyle yaptığı analizde Jeter modelinin en yüksek değerleri sunduğunu, Spanner ve Petela modellerinin sonuçlarının ise birbiriyle aynı hesaplandığını ortaya koymuştur (Kaltakkıran, 2023). Uçkan (2017) tarafından Van ili için gerçekleştirilen uzun dönemli çalışmada da Petela ve Spanner modellerinin ekserji–enerji oranlarının neredeyse çakıştığı, Jeter modelinin ise yaklaşık %1.7 oranında daha yüksek ekserji değerleri verdiği rapor edilmiştir (Uçkan, 2017). Çevik (2021) ise Türkiye'deki 8 farklı istasyon için ekserji modellerini incelemiş ve özellikle direkt ile difüz radyasyonu ayrı ayrı ele alan Onyegegbu-Morhenne modelini de değerlendirerek, istatistiksel tahmin yöntemlerinin ekserji analizlerinde başarılı bir şekilde kullanılabileceğini kanıtlamıştır (Çevik, 2021). Uluslararası literatürde de yapılan kapsamlı incelemeler, bu modellerin yıllar içinde en çok kabul gören ve doğruluğu kanıtlanan teorik modeller olduğunu desteklemektedir (Rodríguez ve ark., 2022).

Teorik modellerle radyasyonun iş potansiyeli hesaplanırken, bu potansiyeli uygulamada maksimize etmeyi amaçlayan eğim açısı optimizasyonu üzerine çalışmalar, panel performansını artırmak için kritik bir rol oynamaktadır. Eğim açısının coğrafi konuma ve mevsime göre büyük değişkenlik gösterdiği birçok çalışmayla ortaya konmuştur. Bakırcı (2012), Türkiye'deki çeşitli iller için optimum eğim açılarını matematiksel modellerle incelemiş; İzmir için bu açının Haziran ayında 0°'ye kadar düştüğünü, Aralık ayında ise 61°'ye kadar çıktığını tespit etmiştir (Bakirci, 2012). Yakın dönemde Gürfidan ve ark. (2025), yapay zeka tabanlı bir modelle Türkiye geneli için optimizasyon yapmış ve yıl boyu sabit tutulacak paneller için ortalama 29°'lik bir eğim açısının optimum olduğunu belirterek,

bu açının ekserji verimi üzerindeki doğrudan etkisini vurgulamışlardır (Gürfidan ve ark., 2025). Bir başka çalışmada Kabul ve ark. (2024), Türkiye genelinde farklı eğim açılarının (21°, 30°, 39°, 48°, 57°) güneş ekserji potansiyeli üzerindeki etkisini araştırmış; yıllık ortalamada en yüksek ekserji potansiyelinin 30° eğimli yüzeylerde elde edildiğini ve bu açının yatay düzleme kıyasla yaklaşık %10 daha fazla ekserji sağladığını saptamışlardır (Kabul ve ark., 2024). Bu çalışmalar, sabit açılı panellerde doğru eğim açısının seçilmesinin, enerji kazanımını ve ekserji verimini belirgin düzeyde artırdığını göstermektedir.

Literatürdeki mevcut çalışmaların çoğunlukla ya yatay yüzeylere odaklanması ya da enerji temelli eğim açısı değerlendirmeleriyle sınırlı kalması, belirli bir coğrafya için panel eğim açısına bağlı ekserji değişimlerinin ayrıntılı olarak incelenmesini gerekli kılmaktadır. Bu kitap bölümünde, İzmir ili için farklı panel eğim açıları altında güneş radyasyonunun ekserji potansiyeli; Petela, Spanner, Jeter ve Mohammed–Mengüç teorik modelleri kullanılarak karşılaştırmalı biçimde analiz edilmiştir. Çalışma kapsamında, eğik yüzeylere ulaşan doğrudan, difüz ve yansıyan radyasyon bileşenleri dikkate alınmış; panel eğim açısına bağlı aylık ekserji değişimleri belirlenmiş ve maksimum kullanılabilir iş potansiyelini sağlayan eğim açıları ortaya konulmuştur. Elde edilen bulguların, İzmir özelinde ve benzer iklim koşullarına sahip bölgelerde kurulacak güneş enerjisi sistemlerinin termodinamik temelli tasarımı, performans değerlendirmesi ve optimizasyonu için yol gösterici bir çerçeve sunması amaçlanmaktadır.

2. MATERYAL-YÖNTEM

2.1. Çalışma Alanının Coğrafi ve İklimsel Özellikleri

Bu çalışmada ele alınan İzmir ili, Türkiye'nin batısında, Ege Bölgesi sınırları içerisinde yer almakta olup yaklaşık olarak

38.42° kuzey enlemi ve 27.14° doğu boylamı koordinatlarında konumlanmaktadır. Çalışma alanının Türkiye ve Avrupa ölçeğindeki coğrafi konumu ile il sınırları içerisindeki idari dağılımı Şekil 1'de sunulmuştur. İzmir'in sahip olduğu kıyı şeridi, topoğrafik çeşitlilik ve denizel etki, bölgenin iklimsel özelliklerini ve güneşlenme potansiyelini doğrudan etkilemektedir. Analizlerde kullanılan uzun dönemli meteorolojik veriler; aylık ortalama küresel güneş ışınımı, güneşlenme süresi ve çevre sıcaklığı değerlerini kapsamakta olup, Meteoroloji Genel Müdürlüğü tarafından sağlanan ölçüm kayıtlarından elde edilmiştir. Çalışmada, bölgenin iklim karakteristiklerini güvenilir biçimde temsil edebilmek amacıyla 1991–2020 yılları arasındaki 30 yıllık veri seti esas alınmıştır. Bu uzun dönemli yaklaşım, hem mevsimsel değişkenliğin hem de iklimsel eğilimlerin doğru şekilde yansıtılmasına olanak sağlamaktadır.

Şekil 1. İzmir ilinin coğrafi konumu ve yıllık güneş ışınımı dağılımı.

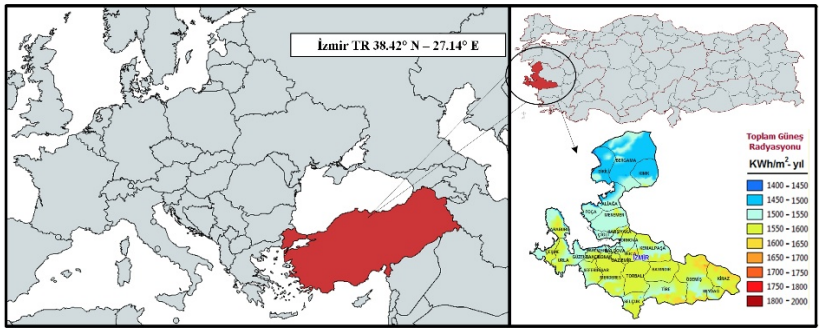

Köppen–Geiger iklim sınıflandırmasına göre İzmir ili, Csa (sıcak yazlı Akdeniz iklimi) sınıfında yer almakta olup, yaz aylarının sıcak ve kurak, kış aylarının ise ılık ve yağışlı geçtiği bir iklim yapısına sahiptir. Yıl boyunca yüksek güneşlenme süresi ve görece düşük bulutluluk oranı, bölgeyi güneş enerjisi uygulamaları açısından avantajlı kılmaktadır. Şekil 2'de görüldüğü üzere, İzmir ili için aylık ortalama günlük küresel

güneş radyasyonu değerleri kış aylarında yaklaşık 1.5–2.5 kWh/m²·gün aralığında seyrederken, yaz aylarında bu değerler 6.0–7.0 kWh/m²·gün seviyelerine ulaşmaktadır. Bu iklimsel koşullar, yalnızca toplam güneş radyasyonu miktarı bakımından değil, aynı zamanda güneş enerjisinin termodinamik açıdan kullanılabilirlik düzeyi (ekserji potansiyeli) açısından da İzmir'i önemli bir çalışma alanı hâline getirmektedir. Bölgeye ulaşan yüksek düzeydeki güneş radyasyonu, hem fotovoltaik hem de güneş termal sistemlerin performansını olumlu yönde etkilemekte; özellikle eğik yüzeylerde yapılan ekserji temelli değerlendirmeler için uygun bir araştırma ortamı sunmaktadır.

Şekil 2. İzmir ili için aylık ortalama küresel güneş ışınımı (W/h-m²-gün) ve çevre sıcaklığı (K) değişimi.

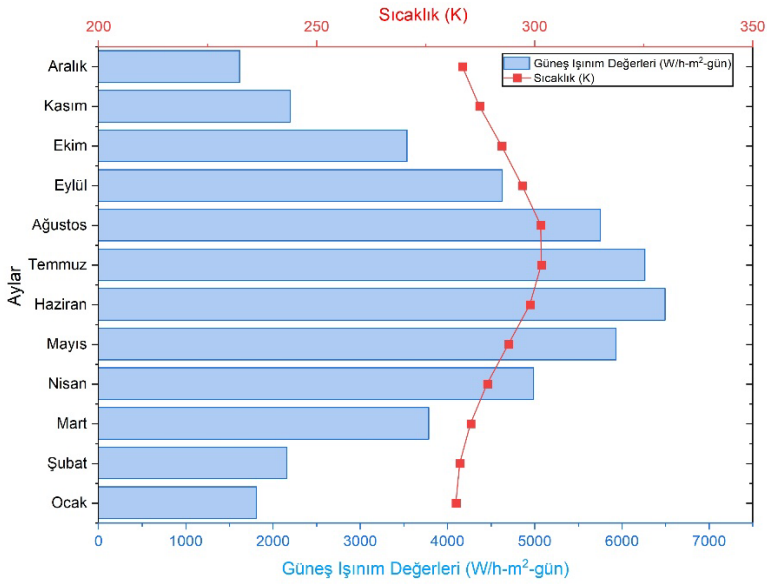

2.2. Güneş Radyasyonu Ekserjisinin Matematiksel Modellenmesi

Bu çalışmada, güneş radyasyonunun ekserji potansiyelinin belirlenmesi amacıyla literatürde yaygın olarak

kullanılan üç klasik model ile daha güncel bir yaklaşım olmak üzere toplam dört farklı teorik model dikkate alınmıştır. Bu modellere ait matematiksel ifadeler Denklem (1)–(4) arasında sunulmuştur. Denklemlerde yer alan T_s, güneşin etkin yüzey sıcaklığını temsil etmekte olup literatürde yaygın kabul gören şekilde yaklaşık 6000 K olarak alınmıştır. T_a ise çalışma alanına ait aylık ortalama çevre sıcaklığını ifade etmekte ve güneş radyasyonu ile çevre arasındaki termodinamik etkileşimi temsil eden temel bir değişken olarak kullanılmaktadır (Hepbasli, 2008). Bu iki sıcaklık arasındaki fark, güneş radyasyonundan elde edilebilecek maksimum teorik iş potansiyelinin belirlenmesinde kritik bir rol oynamakta ve ekserji hesaplarının temelini oluşturmaktadır.

Klasik modellerden ilki olan Petela modeli, güneş ışınımının termodinamik doğasını dikkate alarak ekserji–enerji oranını tanımlamakta olup, bu modele ait ifade Denklem (1)'de verilmiştir (Petela, 2003). Spanner modeli ise radyasyonun iş potansiyelini farklı bir termodinamik bakış açısıyla ele almakta ve bu yaklaşımın matematiksel ifadesi Denklem (2)'de sunulmaktadır (Spanner, 1964). Jeter modeli, güneş radyasyonunu yüksek sıcaklıklı bir ısı kaynağı olarak değerlendirerek ideal Carnot çevrimi prensibine dayalı bir ekserji tanımı yapmakta olup, bu modele ait ifade Denklem (3)'te verilmiştir (Jeter, 1981). Bu üç klasik modele ek olarak, Mohammed–Mengüç modeli, sabit hacimli (izokorik) bir kontrol hacmi yaklaşımı benimseyerek, güneş ve çevre arasındaki radyatif enerji etkileşimini daha gerçekçi sınır koşulları altında değerlendirmekte ve ilgili ekserji ifadesi Denklem (4)'te sunulmaktadır (Mohammed ve Mengüç, 2018). Bu model, özellikle yüksek sıcaklık farklarının söz konusu olduğu uygulamalarda daha temkinli ve fiziksel açıdan gerçekçi sonuçlar üretmesi bakımından literatürde dikkat çekmektedir.

$$\psi_P = 1 - \frac{4}{3}\frac{T_a}{T_s} + \frac{1}{3}\left(\frac{T_a}{T_s}\right)^4 \quad (1)$$

$$\psi_S = 1 - \frac{4}{3}\left(\frac{T_a}{T_s}\right) \quad (2)$$

$$\psi_J = 1 - \frac{T_a}{T_s} \quad (3)$$

$$\psi_{MM} = 1 - \frac{4}{3}\frac{\left(T_s {T_a}^3 - {T_s}^4\right)}{\left({T_s}^4 - {T_a}^4\right)} \quad (4)$$

2.3. Panel Eğim Açısının Güneş Radyasyonu Üzerindeki Etkisi

Eğik bir yüzeye ulaşan toplam güneş radyasyonunun ekserji içeriği, yüzeye gelen toplam radyasyon bileşenleri ile sistemin ekserji–enerji oranının çarpımı olarak tanımlanmaktadır. Bu kapsamda, eğik yüzeye gelen toplam radyasyon (H_{Total}); doğrudan (H_{Beam}), difüz ($H_{Diffuse}$) ve yerden yansıyan ($H_{Reflected}$) bileşenlerin toplamı şeklinde ifade edilmekte olup, ilgili ilişki Denklem (5)'te sunulmuştur. Toplam radyasyon değeri belirlendikten sonra, seçilen teorik modele bağlı olarak hesaplanan ekserji–enerji oranı (Ψ) ile çarpılarak sistemin net ekserji değeri elde edilmektedir. Bu yaklaşım, güneş radyasyonunun yalnızca miktarını değil, aynı zamanda termodinamik kalitesini ve maksimum faydalı iş potansiyelini de dikkate alan daha gerçekçi bir değerlendirme sunmaktadır (Muneer ve Saluja, 1985).

$$H_{\mathbf{T}otal} = \Psi_{exergy\ ratio}\left(H_{\mathbf{B}eam} + H_{\mathbf{R}eflected} + H_{\mathbf{D}iffuse}\right) \quad (5)$$

Eğik yüzeye gelen toplam güneş radyasyonunun doğru bir şekilde hesaplanabilmesi için, literatürde güvenilirliği ve hesaplama kolaylığı nedeniyle yaygın olarak kullanılan Liu ve Jordan (1960) izotropik modeli tercih edilmiştir (Liu ve Jordan,

1960). Bu yaklaşımda, yatay düzlem için verilen aylık ortalama küresel güneş radyasyonu; panel eğim açısı, coğrafi konum ve temel güneş geometrisi parametreleri dikkate alınarak eğik yüzey üzerindeki doğrudan, yayılı ve yerden yansıyan bileşenlerine ayrıştırılmaktadır. Hesaplama süreci; deklinasyon açısı, saat açısı ve gün batımı saat açısı gibi temel güneş geometrisi parametrelerinin belirlenmesi, geometrik dönüşüm katsayılarının hesaplanması ve radyasyon bileşenlerinin ayrıştırılmasını kapsamakta olup, kullanılan temel matematiksel bağıntılar Duffie ve Beckman (2020) tarafından önerilen standart analiz yöntemleri izlenerek Denklem (6)–(16) arasında sunulmuştur (Duffie ve ark., 2020). Bu kapsamda, yayılı radyasyonun gökyüzü kubbesi boyunca eşit olarak dağıldığını varsayan izotropik model yaklaşımı benimsenmiş (Cooper, 1969; Muneer, 2007); yüzey yansıtırlığını temsil eden albedo katsayısı (ρ) ise çalışma alanının arazi özelliklerini yansıtacak şekilde ve güncel literatüre uygun olarak 0.26 alınmıştır (González-Rodríguez ve ark., 2025).

$$H_B = (H - H_d)R_b \tag{6}$$

$$R_b = \frac{\cos(Ø - \beta)\cos(\delta)\sin(\omega_s') + \omega_s'\left(\frac{\pi}{180}\right)\sin(Ø - \beta)\sin(\delta)}{\cos(Ø)\cos(\delta)\sin(\omega_S) + \omega_S\left(\frac{\pi}{180}\right)\sin(Ø)\sin(\delta)} \tag{7}$$

$$H_R = \frac{H\,\rho\,(1 - \cos\beta)}{2} \tag{8}$$

$$H_S = H_d\,R_d \tag{9}$$

$$H_d = H\left(1 - 1.13\frac{H}{H_0}\right) \tag{10}$$

$$H_o = \left(\frac{24}{\pi}\right)G_{sc}\,k\left[\cos Ø\cos\delta\sin\omega_s + \left(\frac{\pi}{180}\right)\sin Ø\sin\delta\omega_s\right] \tag{11}$$

$$k = 1 + 0.033\cos\left(360\frac{n}{360}\right) \tag{12}$$

$$\delta = 23.45^{\circ} \sin\left(360 \frac{n + 284}{365}\right) \quad (13)$$

$$\omega_s = \cos^{-1}(-\tan \emptyset . \tan \delta) \quad (14)$$

$$\omega_s' = \min\left[\frac{\omega = \cos^{-1}(-\tan \emptyset \tan \delta)}{\cos^{-1}(-\tan(\emptyset - \beta) \tan \delta}\right] \quad (15)$$

$$R_d = (1 + \frac{\cos \beta}{2}) \quad (16)$$

Denklem (6)–(16)'da kullanılan parametreler şu şekilde tanımlanmaktadır: H, yatay düzlemde ölçülen aylık ortalama küresel güneş radyasyonunu; H_S, eğik yüzeye gelen yayılı radyasyon bileşenini ifade etmektedir. R_b, eğik düzlem üzerine gelen direkt ışınımının yatay düzlem üzerine gelen ışınım miktarına oranıdır; R_d, yayılı radyasyon için eğik yüzey dönüşüm katsayısını temsil etmektedir. ∅, çalışma alanının enlemini; β, panel eğim açısını; δ, güneş deklinasyon açısını; ω_s ve ω'_s, sırasıyla yatay ve eğik yüzeyler için gün batımı saat açılarını göstermektedir. H_o, atmosfer dışı güneş radyasyonunu; G_{sc}, güneş sabitini; k, Dünya–Güneş mesafesine bağlı düzeltme katsayısını ve n, yılın gün numarasını ifade etmektedir.

3. ARAŞTIRMA BULGULARI

3.1. Güneş Radyasyonunun Ekserji Modelleri Açısından Karşılaştırılması

Aylık ortalama çevre sıcaklıkları ile ekserji/enerji oranları birlikte değerlendirildiğinde, tüm modeller için hesaplanan oranların yıl içinde sıcaklıktaki değişime duyarlı bir davranış sergilediği görülmektedir. Çevre sıcaklığının artış gösterdiği yaz aylarında ekserji/enerji oranları kademeli olarak azalırken, kış aylarında sıcaklığın düşmesiyle birlikte bu oranların arttığı belirlenmiştir. Özellikle Temmuz ve Ağustos aylarında minimum

değerlere ulaşılması, ekserji oluşumunun güneş ile çevre arasındaki sıcaklık farkına doğrudan bağlı olduğunu göstermektedir. Bu durum, çevre sıcaklığının yükselmesinin güneş radyasyonunun maksimum faydalı iş potansiyelini sınırlayan temel etkenlerden biri olduğunu ortaya koymaktadır.

Tablo 1'de verildiği üzere model bazlı karşılaştırma yapıldığında, Petela ve Spanner yaklaşımlarının yılın tüm aylarında tamamen örtüşen sonuçlar ürettiği görülmektedir. Bu uyum, her iki modelin de benzer termodinamik varsayımlara dayanmasıyla açıklanabilir. Mohammed–Mengüç modeli ise farklı bir teorik çerçeveye sahip olmasına rağmen klasik modellerle oldukça yakın sonuçlar vermiş ve ekserji/enerji oranları yaklaşık 0.9330–0.9373 aralığında hesaplanmıştır. Buna karşılık, Jeter modeliyle elde edilen oranlar diğer modellere kıyasla belirgin biçimde daha yüksek gerçekleşmiş olup, değerler yaklaşık 0.9497–0.9530 aralığında değişmektedir. Jeter modelinin daha yüksek ekserji tahminleri üretmesi, güneş radyasyonunu yüksek sıcaklıklı bir ısı kaynağı olarak ele alan ve Carnot verimine dayanan yaklaşımının doğal bir sonucudur. Genel olarak değerlendirildiğinde, modeller arasındaki farkların sınırlı olduğu, ancak kullanılan termodinamik kabullerin ekserji/enerji oranlarının mutlak seviyesini etkilediği açıkça görülmektedir.

Tablo 1. Farklı ekserji modelleri için aylık ekserji/enerji oranlarının değişimi

Aylar	Sıcaklık (K)	Ekserji/Enerji Oranı			
		Ψ_P	Ψ_S	Ψ_J	Ψ_{MM}
Ocak	282	0.9373	0.9373	0.9530	0.9373
Şubat	282.9	0.9371	0.9371	0.9529	0.9371
Mart	285.4	0.9366	0.9366	0.9524	0.9366
Nisan	289.2	0.9357	0.9357	0.9518	0.9357
Mayıs	294.1	0.9346	0.9346	0.9510	0.9347
Haziran	299	0.9336	0.9336	0.9502	0.9336
Temmuz	301.6	0.9330	0.9330	0.9497	0.9330
Ağustos	301.5	0.9330	0.9330	0.9498	0.9330
Eylül	297.2	0.9340	0.9340	0.9505	0.9340
Ekim	292.5	0.9350	0.9350	0.9513	0.9350
Kasım	287.4	0.9361	0.9361	0.9521	0.9361
Aralık	283.5	0.9370	0.9370	0.9528	0.9370

3.2. Panel Eğim Açısının Eğik Yüzeydeki Güneş Radyasyonu Ekserjisi Üzerindeki Etkisi

Şekil 3'te, Petela ekserji modeli kullanılarak hesaplanan eğik yüzeye gelen günlük ortalama güneş ışınımının, panel eğim açısı ve aylar boyunca gösterdiği değişim kontur diyagramı biçiminde sunulmaktadır. Dağılım desenleri, güneş geometrisindeki mevsimsel değişimlerin panel eğim açısı ile birlikte değerlendirildiğinde ışınım büyüklüğünü belirgin biçimde etkilediğini ortaya koymaktadır. Sayısal sonuçlar, yaz aylarında maksimum ışınım değerlerinin düşük eğim açılarında yoğunlaştığını göstermektedir. Haziran ayında 0° eğim açısı için hesaplanan günlük ortalama ışınım değeri 6068 Wh/m²·gün olup, aynı ayda eğim açısının 45°'ye çıkarılmasıyla bu değer 4911 Wh/m²·gün seviyesine gerilemektedir. Temmuz ayında da benzer bir eğilim gözlenmiş; 0° eğimde 5850 Wh/m²·gün olan ışınım değeri, 45° eğimde 4863 Wh/m²·gün olarak hesaplanmıştır. Bu durum, yaz döneminde güneş ışınlarının yataya yakın yüzeylere daha elverişli bir geliş açısıyla ulaşmasıyla ilişkilendirilebilir.

Kış aylarında ise ışınımın panel eğim açısına duyarlılığı ters yönde gelişmektedir. Ocak ayında 0° eğim için hesaplanan ışınım değeri 1697 Wh/m²·gün iken, eğim açısının 55°–56° aralığına artırılmasıyla maksimum değer olan 2468 Wh/m²·gün elde edilmiştir. Aralık ayında da benzer bir davranış söz konusu olup, 0° eğimde 1518 Wh/m²·gün olan ışınım değeri, 56° eğimde 2288 Wh/m²·gün seviyesine yükselmektedir. Bu sonuçlar, kış aylarında güneşin düşük yükseklik açısına sahip olması nedeniyle daha dik panel eğimlerinin yüzeye ulaşan ışınımı artırdığını göstermektedir. Ara mevsimlerde ise maksimum ışınım değerlerinin orta eğim açılarında oluştuğu belirlenmiştir. Örneğin Nisan ayında en yüksek günlük ortalama ışınım değeri 4839 Wh/m²·gün ile yaklaşık 13° eğim açısında hesaplanmıştır. Şekil 3'te gözlenen bu mevsimsel eğim kayması, panel eğim açısının sabit tutulmasının yıl boyunca maksimum ışınım kazanımı

sağlamadığını ve güneş enerjisi sistemlerinin tasarımında eğim açısının kritik bir parametre olduğunu ortaya koymaktadır.

Şekil 3. Petela modeline göre panel eğim açısı ve aylara bağlı olarak güneş ışınımı ekserjisinin değişimi

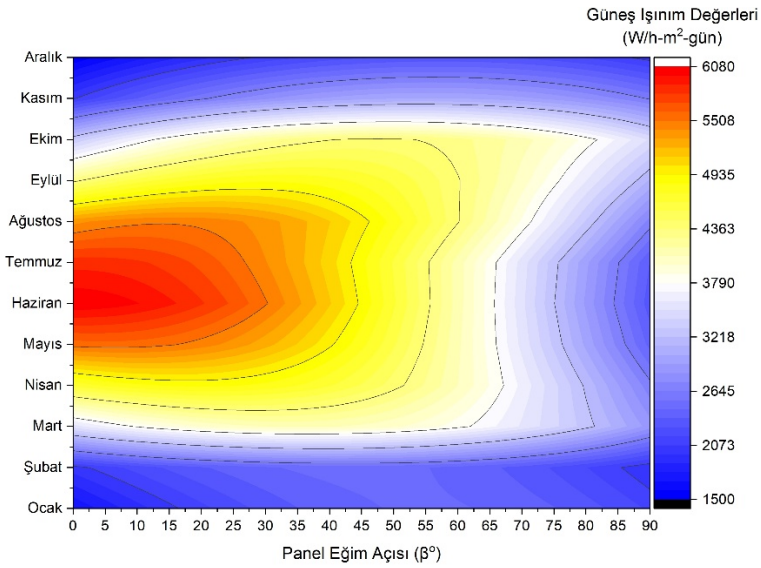

Şekil 4, Spanner ekserji modeli kullanılarak eğik bir yüzeye gelen güneş ışınımı ekserjisinin, panel eğim açısı (0°–90°) ve yıl içerisindeki aylara bağlı olarak nasıl değiştiğini göstermektedir. Spanner modelinde ekserji hesabı, ışınımın "mutlak iş potansiyeli" kavramına dayanmakta olup, panel geometrisinin etkisi özellikle eğim açısına bağlı dönüşüm katsayıları aracılığıyla daha belirgin biçimde yansımaktadır. Sonuçlar, düşük eğim açılarında (0°–20°) özellikle ilkbahar ve yaz aylarında yüksek ekserji değerlerinin elde edildiğini göstermektedir. Sayısal olarak, Haziran ayında 0° eğim açısında ekserjiye karşılık gelen ışınım değeri yaklaşık 6068 Wh/m²·gün düzeyine ulaşmakta, aynı ay için eğim açısı 45°'ye çıkarıldığında bu değer yaklaşık 4911 Wh/m²·gün seviyelerine gerilemektedir. Eğimin 90°'ye yaklaşmasıyla birlikte yaz aylarında ekserjiye

karşılık gelen ışınım değerleri belirgin biçimde azalarak 2300–2400 Wh/m²·gün bandına düşmektedir. Bu durum, yaz döneminde güneş ışınlarının yataya yakın yüzeylerde daha etkin değerlendirildiğini göstermektedir.

Buna karşılık, kış aylarında eğim açısının artması ekserji açısından daha avantajlı bir davranış sergilemektedir. Ocak ayı için 0° eğim açısında yaklaşık 1697 Wh/m²·gün olan değer, eğimin 50°–55° aralığına çıkarılmasıyla 2450 Wh/m²·gün seviyelerine yükselmektedir. Bu eğilim, düşük güneş yükseklik açılarının hâkim olduğu kış koşullarında, daha dik panel yerleşimlerinin radyasyonun kullanılabilir iş potansiyelini artırdığını ortaya koymaktadır. Spanner modeline dayalı bu sonuçlar, panel eğim açısının yalnızca enerji miktarını değil, aynı zamanda ışınımın ekserjetik kalitesini de doğrudan etkileyen kritik bir tasarım parametresi olduğunu göstermektedir.

Şekil 4. Spanner modeline göre panel eğim açısı ve aylara bağlı olarak güneş ışınımı ekserjisinin değişimi

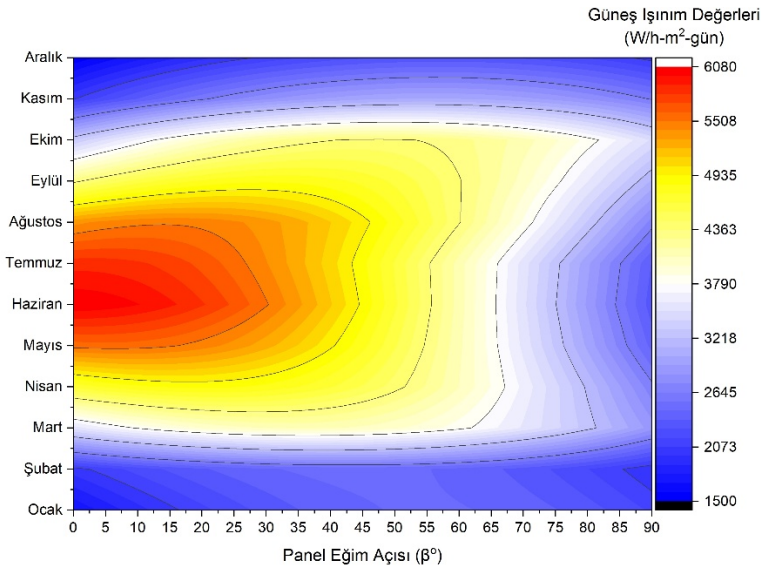

Şekil 5, Jeter ekserji modeli ile hesaplanan eğik yüzey güneş ışınımı ekserjisinin panel eğim açısı ve aylara bağlı değişimini göstermektedir. Sayısal olarak, yaz döneminde yataya yakın yüzeylerin üstünlüğü belirgindir: Haziran ayında $\beta = 0°$ için 6176 Wh/m²·gün değerine karşılık, panelin düşeye yaklaştığı durumda ($\beta = 90°$) aynı ay için değer 2344 Wh/m²·gün seviyesine gerilemektedir. Bu fark, yüksek güneş yüksekliği koşullarında ışınım geometrisinin yataya yakın yüzeylerde daha elverişli hale gelmesi ve eğimin artmasıyla etkin izdüşümün zayıflaması ile ilişkilidir.

Kış aylarında ise optimum eğimin daha yüksek değerlere kaydığı görülmektedir. Örneğin Ocak ayında $\beta = 0°$ için 1725 Wh/m²·gün iken, ekserji değeri $\beta = 55°$ civarında 2509 Wh/m²·gün düzeyine ulaşmaktadır. Bu davranış, güneşin kışın daha düşük yükseklikte seyretmesi nedeniyle eğik yüzeyin ışınımı daha etkin bir şekilde soğurması gerekliliğiyle uyumludur. Jeter modelinin Carnot verimi temelli yaklaşımı nedeniyle, elde edilen ekserji dağılımı Petela ve Spanner modellerine kıyasla sistematik olarak daha yüksek değerlere sahiptir; ancak mevsimsel ve açısal eğilimler bakımından benzer bir fiziksel davranış sergilemektedir. Bu durum, model farklılıklarına rağmen eğik yüzey ekserji analizlerinde temel belirleyicinin güneş geometrisi ve panel eğimi olduğunu göstermektedir.

Şekil 5. Jeter modeline göre panel eğim açısı ve aylara bağlı olarak güneş ışınımı ekserjisinin değişimi

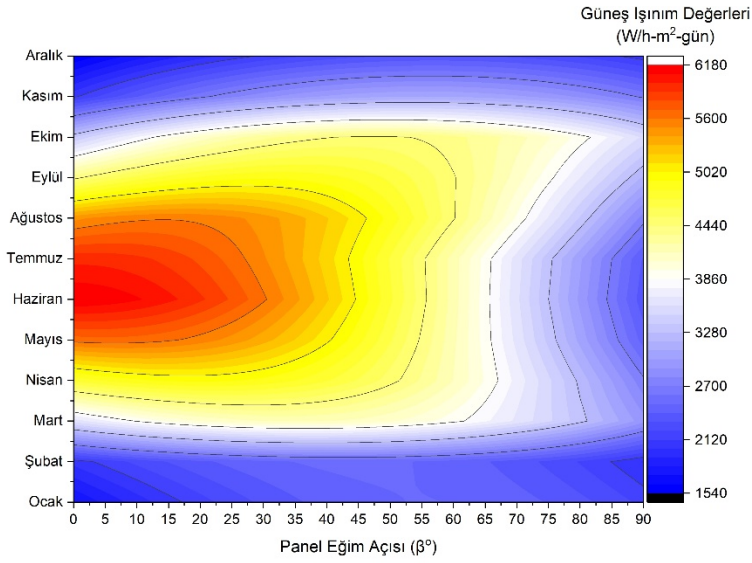

Mohammed–Mengüç modeli kullanılarak hesaplanan güneş ışınımı ekserjisi, panel eğim açısı ve mevsimsel değişkenliğe duyarlı bir dağılım sergilemektedir. Şekil 6'da sunulan sonuçlar, yaz aylarında düşük ve orta eğim açılarında belirgin bir ekserji yoğunlaşmasına işaret etmektedir. Özellikle Haziran ayında, 0–10° eğim aralığında ekserji değerleri yaklaşık 6.06–6.07 kWh m^{-2} $gün^{-1}$ seviyelerine ulaşarak yıllık maksimumlara yaklaşmaktadır. Buna karşılık, kış aylarında (Aralık–Ocak) yüksek eğim açılarında (70–90°) ekserji değerlerinin 1.5–2.0 kWh m^{-2} $gün^{-1}$ bandına gerilediği görülmektedir.

Mohammed–Mengüç modelinin formülasyonunda çevresel sıcaklık etkisinin daha sınırlı ve dolaylı biçimde temsil edilmesi, elde edilen ekserji dağılımının Petela ve Spanner modelleriyle büyük ölçüde benzer mevsimsel ve açısal eğilimler göstermesine neden olmaktadır. Bununla birlikte, eğim açısına

bağlı değişimlerin daha yumuşak bir gradyan ile gerçekleştiği ve özellikle geçiş mevsimlerinde (Nisan ve Eylül) maksimum ekserji bölgelerinin daha geniş bir eğim aralığına yayıldığı dikkat çekmektedir. Bu özellik, Mohammed–Mengüç modelinin aylık ışınım bileşenleri arasındaki dengeyi daha homojen bir biçimde yansıttığını ve sistem tasarımı açısından daha esnek bir eğim seçimine olanak tanıdığını göstermektedir. Öte yandan, Mohammed–Mengüç modeliyle elde edilen ekserji değerleri, Carnot verimi temelli Jeter modeline kıyasla sistematik olarak daha düşük seviyelerde kalmaktadır. Bu fark, Jeter modelinin teorik üst sınırı temsil eden yaklaşımına karşılık, Mohammed–Mengüç modelinin ışınım–çevre etkileşimini daha temkinli bir çerçevede ele almasıyla açıklanabilir. Buna rağmen, maksimum ve minimum ekserji bölgelerinin yıl içindeki konumu ile eğim açısına bağlı dağılım karakteri bakımından her iki modelin benzer fiziksel davranışlar sergilediği görülmektedir.

Şekil 6. Mohammed Mengüç modeline göre panel eğim açısı ve aylara bağlı olarak güneş ışınımı ekserjisinin değişimi

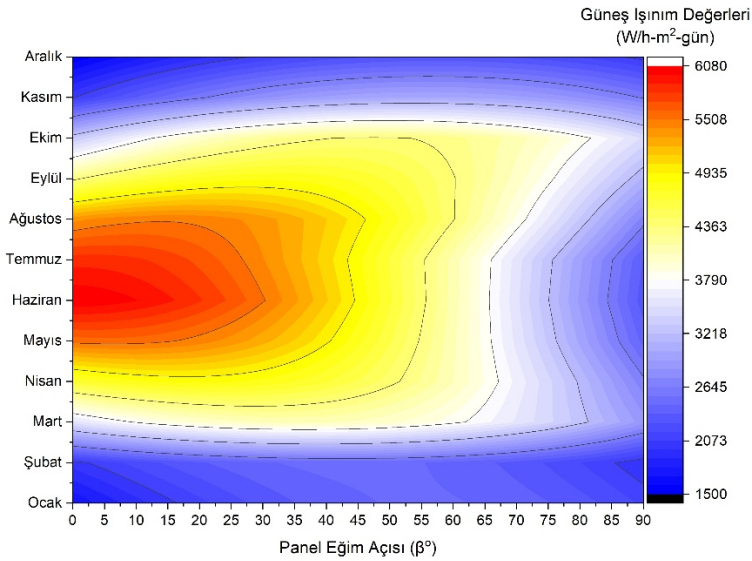

4. SONUÇ

Bu çalışmada elde edilen sonuçlar, güneş ışınımı ekserjisinin hem mevsimsel değişkenlikten hem de panel eğim açısından belirgin biçimde etkilendiğini göstermektedir. Yaz aylarında yataya yakın yüzeylerde ekserji değerleri en yüksek seviyelere ulaşırken, Haziran ayında 0–10° eğim aralığında hesaplanan ekserji potansiyeli yaklaşık 6.0–6.1 kWh m^{-2} $gün^{-1}$ düzeylerine çıkmaktadır. Buna karşılık, kış aylarında güneş ışınlarının düşük geliş açısı nedeniyle maksimum ekserji kazanımı daha dik yüzeylerde gerçekleşmekte ve Aralık–Ocak döneminde 70–90° eğimlerde ekserji değerleri yaklaşık 1.5–2.0 kWh m^{-2} $gün^{-1}$ aralığında kalmaktadır.

Model karşılaştırmaları, Petela ve Spanner yaklaşımlarının neredeyse çakışan sonuçlar ürettiğini, Mohammed–Mengüç modelinin bu iki modele çok yakın ancak eğim açısına bağlı değişimleri daha yumuşak bir dağılımla temsil ettiğini ortaya koymuştur. Buna karşın, Carnot verimi temelli Jeter modeli, tüm aylar ve eğim açıları boyunca diğer modellere kıyasla yaklaşık %1.5–2.0 daha yüksek ekserji değerleri sunarak teorik üst sınırı temsil etmiştir. Genel olarak sonuçlar, güneş enerjisi sistemlerinin değerlendirilmesinde yalnızca toplam enerji miktarına dayalı yaklaşımların yetersiz kaldığını; panel yönelimi ve çevresel koşulları dikkate alan ekserji temelli analizlerin sistem tasarımı ve optimizasyonu açısından daha gerçekçi ve güvenilir bir çerçeve sunduğunu göstermektedir.

KAYNAKÇA

Bakirci, K. (2012) "General models for optimum tilt angles of solar panels: Turkey case study", *Renewable and sustainable energy reviews*, 16(8), 6149-6159.

Bayrak, F., Abu-Hamdeh, N., Alnefaie, K. A. ve Öztop, H. F. (2017) "A review on exergy analysis of solar electricity production", *Renewable and Sustainable Energy Reviews*, 74, 755-770.

Benghanem, M. (2011) "Optimization of tilt angle for solar panel: Case study for Madinah, Saudi Arabia", *Applied energy*, 88(4), 1427-1433.

Beyazit, N. İ., Bulut, H. ve Ünal, F. (2019) "Diyarbakır ili için uzun dönemli güneş radyasyonunun ekserji analizi", *Harran Üniversitesi Mühendislik Dergisi*, 4(2), 1-6.

Caliskan, H. (2017) "Energy, exergy, environmental, enviroeconomic, exergoenvironmental (EXEN) and exergoenviroeconomic (EXENEC) analyses of solar collectors", *Renewable and Sustainable Energy Reviews*, 69, 488-492.

Cooper, P. I. (1969) "The absorption of radiation in solar stills", *Solar energy*, 12(3), 333-346.

Çevik, A. (2021) "Uzun süreli verilere dayalı güneş radyasyonunun ekserji ve enerji analizi", *Karamanoğlu Mehmetbey Üniversitesi Fen Bilimleri Enstitüsü*.

Duffie, J. A., Beckman, W. A. ve Blair, N. (2020) *Solar Engineering of Thermal Processes, Photovoltaics and Wind, 5th Edition*.

González-Rodríguez, L., Jamil, B., Kallioğlu, M. A., Cabrera-Reina, A., Marzo, A., García-Tuñon, W., Volke, M., Lobos, F. ve Laguarda, A. (2025) "Tilted solar UV

radiation estimation and its role in advanced solar water treatment systems", *Solar Energy*, 295, 113521.

Gürfidan, R., Yiğit, F. ve Kabul, A. (2025) "Exergy focused optimum solar panel tilt angle determination with improved hybrid model: The case of Turkey", *Engineering Applications of Artificial Intelligence*, 145, 110220.

Hepbasli, A. (2008) "A key review on exergetic analysis and assessment of renewable energy resources for a sustainable future", *Renewable and sustainable energy reviews*, 12(3), 593-661.

Jeter, S. M. (1981) "Maximum conversion efficiency for the utilization of direct solar radiation", *Solar energy*, 26(3), 231-236.

Kabul, A., Yiğit, F. ve Duran, A. (2024) "Estimating The Solar Exergy Potential of Surfaces With Different Tilt Angles", *Konya Journal of Engineering Sciences*, 12(3), 756-772.

Kaltakkıran, G. (2023) "Ölçüm Verilerine Dayalı Global Güneş Radyasyonunun Ekserji Analizi: Erzurum İli Örneği", *Journal of Studies in Advanced Technologies*, 1(2), 94-104.

Liu, B. Y. ve Jordan, R. C. (1960) "The interrelationship and characteristic distribution of direct, diffuse and total solar radiation", *Solar energy*, 4(3), 1-19.

Luo, D., Liu, J., Wu, H., Zhang, G., Pan, Z. ve Huang, J. (2025) "Advancing smart net-zero energy buildings with renewable energy and electrical energy storage", *Journal of Energy Storage*, 114, 115850.

Mohammed, H. N. ve Mengüç, M. P. (2018) "Solar radiation exergy and quality performance for Iraq and Turkey", *International Journal of Exergy*, 25(4), 364-385.

Muneer, T. (2007) *Solar radiation and daylight models*. Routledge.

Muneer, T. ve Saluja, G. S. (1985) "A brief review of models for computing solar radiation on inclined surfaces", *Energy conversion and management*, 25(4), 443-458.

Özalp, M. (2025) "Dünya Yenilenebilir Enerji Görünümü ve Geleceği", *Akademik Hassasiyetler*, 12(28), 649-681.

Petela, R. (2003) "Exergy of undiluted thermal radiation", *Solar energy*, 74(6), 469-488.

Rodríguez, E., Cardemil, J. M., Starke, A. R. ve Escobar, R. (2022) "Modelling the exergy of solar radiation: a review", *Energies*, 15(4), 1477.

Saidur, R., BoroumandJazi, G., Mekhlif, S. ve Jameel, M. (2012) "Exergy analysis of solar energy applications", *Renewable and Sustainable Energy Reviews*, 16(1), 350-356.

Spanner, D. C. (1964) "Introduction to thermodynamics."

Uçkan, İ. (2017) "Exergy analysis of solar radiation based on long term for Van city", *Politeknik Dergisi*, 20(3), 579-584.

Yadav, A. K. ve Chandel, S. S. (2013) "Tilt angle optimization to maximize incident solar radiation: A review", *Renewable and Sustainable Energy Reviews*, 23, 503-513.

HYBRID ADDITIVE MANUFACTURING: AN INTEGRATED APPROACH TO ADVANCED MANUFACTURING

Nafel DOGDU[1]

1. INTRODUCTION

Additive manufacturing (AM) is an innovative manufacturing approach based on the layer-by-layer transformation of computer aided three dimensional designs (CAD) into physical objects. This technology fundamentally differs from conventional manufacturing methods by eliminating the need for molds and offering a high degree of geometric freedom [1]. First introduced in the 1980s through polymer based rapid prototyping techniques such as stereolithography, AM was initially used solely for design verification and conceptual modeling. However, with the development of laser and arc based metal additive manufacturing processes, the technology rapidly evolved toward the production of functional and structural components [2]. This transformation strengthened digital design manufacturing integration and established AM as a strategic manufacturing technology for high performance sectors such as aerospace, defense, and biomedical applications [3].

Despite these advantages, standalone AM processes face fundamental technical limitations, including surface roughness, limited dimensional accuracy, residual stresses, and microstructural anisotropy [4–6]. In particular, crack formation,

[1] Lecturer, PhD, Vocational School of Technical Sciences, Akdeniz University, ORCID: 0000-0001-8172-0832.

porosity, and reproducibility issues in mechanical properties reported for high strength aluminum and titanium alloys constitute major factors limiting the industrial reliability of these processes [7,8]. These challenges have also been clearly emphasized in comprehensive review studies assessing the current state of metal additive manufacturing [9,10].

To overcome these limitations, Hybrid Additive Manufacturing (HAM) approaches have been developed. HAM aims to establish more controlled and integrated production chains by combining the geometric freedom of AM with machining, metal forming, surface treatment, and secondary energy fields that is, energy sources integrated into the AM process to enable surface, quality, and microstructural control [11–13]. While early HAM systems relied on sequential subtractive machining applied after AM, modern systems enable conventional and advanced material removal processes to be performed alternately or simultaneously on the same platform during the production process [14,15].

The historical development of HAM has not been limited to metallic structures but has expanded toward biomedical, electronic, and functional systems. In particular, multi material biofabrication approaches have enabled the integration of mechanical load bearing capacity and biological functionality within a single structure [16,17]. Similarly, in aerospace and space applications, hybrid manufacturing has been reported to successfully produce components with complex geometries and high surface quality requirements [18].

From the perspective of functional systems, hybrid manufacturing approaches offer significant opportunities for microstructural control and performance optimization in chemical and biosensor applications [19,20]. Especially through the integration of printing, sintering, and laser based processes,

advanced functional components such as flexible radio frequency (RF) electronics and hybrid circuits can be produced [21]. These developments transform HAM from a purely structural manufacturing method into an engineering platform that enables multifunctional system design [22].

Multi energy field processes such as laser–arc hybrid additive manufacturing have gained prominence in large scale metal part production by balancing high deposition rates with acceptable surface quality [23,24]. In addition, hybrid process chains that combine metal additive manufacturing with forming processes have created new scientific research areas focused on controlling microstructure, residual stresses, and formability behavior in transition regions [25,26].

The environmental and economic impacts of HAM have also been increasingly discussed in the literature. Additive and hybrid manufacturing approaches have been shown to possess significant potential for reducing material waste and improving energy efficiency [27]. Particularly in biomedical applications, hybrid manufactured meta biomaterials have been reported to offer superior mechanical performance and biocompatibility [28–31].

Recent studies demonstrate that HAM systems not only improve geometric accuracy but also enable advanced manufacturing concepts such as multi physical lattice structures, functional gradients, and digital twin assisted process control [32,33]. Mechanism based studies aimed at explaining the physical fundamentals of these processes contribute to making hybrid manufacturing more predictable and repeatable [34].

Nevertheless, significant technical and operational challenges still hinder the widespread industrial adoption of hybrid additive manufacturing. Although porosity, surface roughness, and variability in mechanical properties can be

substantially reduced through hybrid process planning [35], controlling material gradients and ensuring seamless process integration in transition regions remain active research topics [36,37]. In engineering alloys such as titanium and stainless steel, residual stresses, microstructural evolution, and corrosion behavior continue to represent critical challenges for hybrid manufacturing [38–42].

Recent studies in pharmaceutical and dental applications further demonstrate that hybrid additive manufacturing offers significant advantages in personalized production, functional performance, and clinical accuracy [43,44].

In addition, recent studies on advanced powder processing and alloy design have shown that powder preparation techniques can significantly influence phase transformation behavior and microstructural stability. Investigations on mechanically alloyed Zr-doped NiTi powders have demonstrated that alloying strategies can strongly affect R-phase formation and austenitic transformation characteristics, highlighting the importance of material design in advanced manufacturing systems [45]**.**

In this section, the fundamental limitations encountered when additive manufacturing is applied as a standalone process in industrial production have been identified, and the ways in which hybrid additive manufacturing addresses these limitations have been explained from a holistic perspective. Hybrid additive manufacturing is considered as an approach in which additive and conventional manufacturing methods are systematically integrated within a single production chain, and the historical development, current industrial maturity level, and key advantages of the technology are summarized based on the literature. This framework provides the foundation for the following section, which examines the industrial applications of

hybrid additive manufacturing, the challenges encountered, and future development trends in greater detail.

2. INDUSTRIAL APPLICATIONS OF HYBRID ADDITIVE MANUFACTURING

HAM is a multi component manufacturing approach developed to overcome the limitations of conventional manufacturing methods and to extend the design freedom and functional production capabilities offered by AM. This technology enables the production of highly complex, customized, structural, and functional components, while simultaneously providing significant advantages in areas where AM alone remains limited, such as dimensional accuracy, surface quality, and microstructural control [18], [25], [33]. The fundamental manufacturing logic of this approach and the interactions between process stages are summarized through the simplified production workflow presented in Figure 1.

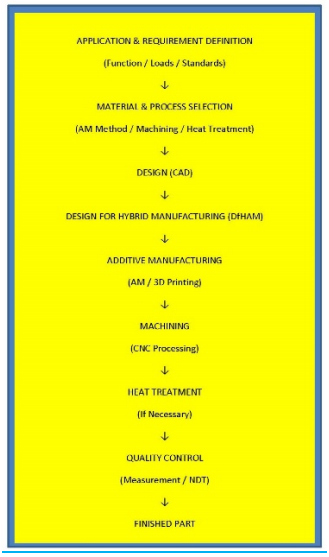

Figure 1. Workflow of hybrid additive manufacturing including pre-design, material selection, and post-processing stages.

The schematic illustrates the planned and integrated combination of the geometric freedom provided by additive manufacturing with the dimensional precision offered by machining within a single production chain.

2.1. Aerospace and Medical Applications

One of the most prominent application areas of HAM technology is the aerospace and space industry. In this sector, high cost materials such as titanium and nickel based superalloys lead to substantial material waste when processed using conventional methods. By reducing buy-to-fly ratios, HAM improves material utilization efficiency and consequently enables a reduction in production costs [26, 27], [33]. In applications such as turbine blade repair, integral impeller manufacturing, and the production of structural brackets, the design flexibility, customization capability, and ability to meet strength requirements provided by hybrid systems stand out [21], [33].

In the medical sector, hybrid additive manufacturing is effectively used in the production of patient specific orthopedic implants, biocompatible vascular stents, and high precision dental prostheses [31], [37], [43]. Particularly in biomedical applications where individualized design is of critical importance, the ability of hybrid processes to create complex geometries while improving surface quality plays a key role.

Similarly, in the tooling industry, which constitutes a fundamental component of manufacturing infrastructure, hybrid additive manufacturing systems offer significant advantages. Complex features such as internal cavities and conformal cooling channels can be produced with high efficiency and precision using HAM systems [16], [17].

2.2. Process Integration in Hybrid Manufacturing Systems

The rapid heating cooling cycles occurring during the AM stage lead to high levels of residual stresses within the part. This results in risks such as crack formation, geometric distortion, and reduced fatigue life [38]. For this reason, it has been reported that by integrating subtractive operations such as milling into HAM systems, tensile residual stresses can be reduced by up to 90%, while compressive stresses are introduced at the surface, thereby increasing the service life of the component [34], [38]. The anisotropic microstructures formed as a result of AM processes cause components to exhibit different mechanical behaviors in different directions. Secondary operations such as interlayer laser shock peening [30] or rolling [40] have been shown to render the microstructure more homogeneous and isotropic. However, such integrations also give rise to new technical challenges at the system level. In particular, the risk of damage to laser optical systems due to cooling fluids [34], tool wear [36], and microstructural incompatibilities occurring in transition zones [28] emerge as critical issues requiring careful design of HAM process chains.

In addition, the high initial investment costs of HAM machines, complex process planning requirements, the risk of contamination during powder recovery, and the lack of sufficient standardization of production processes [22], [24] constitute major barriers to the widespread industrial adoption of HAM. This indicates that HAM should be addressed not only in terms of its technical aspects but also from operational and organizational perspectives.

Nevertheless, the improvements achieved by HAM in areas where AM remains limited such as dimensional tolerances, surface quality, and porosity control are highly significant. It has

been reported that porosity can be substantially reduced through interlayer processing strategies [35], [39], surface quality can be improved, and the resulting mechanical strength can approach that of forged components [28], [38]. These improvements demonstrate that HAM plays not merely a complementary role, but a decisive role in determining overall production quality.

In this context, Table 1 presents a comparative assessment of conventional manufacturing methods, AM, and HAM based on fundamental industrial production criteria. The comparison highlights the advantages provided by HAM in terms of geometric complexity, material utilization efficiency, surface quality, microstructure control, and part repair, while also reflecting limitations related to investment cost and process complexity in a balanced manner. This evaluation enables a holistic assessment of the position of HAM among existing manufacturing approaches.

Table1. Comparison of Conventional, Additive, and Hybrid Additive Manufacturing Approaches

Criterion / Evaluation Metric	Conventional Manufacturing Methods	Additive Manufacturing (AM)	Hybrid Additive Manufacturing (HAM)
Geometric Complexity	Low limited design freedom	High complex geometries can be produced	Very high design freedom combined with precision machining
Material Utilization Efficiency (Buy-to-Fly)	Low (up to 10:1)	Moderate (3:1 – 1.5:1)	High (can be reduced to ~1.2:1)
Surface Quality and Tolerances	High (process dependent)	Low post processing often required	High controlled through interlayer or in process machining
Microstructure Control	Good homogeneous microstructure	Anisotropic microstructure limited control	Optimizable improved via secondary processes
Design Flexibility	Limited tool accessibility required	High	Integrated design and manufacturing considered simultaneously
Energy Consumption	High (especially in subtractive processes)	Moderate	Relatively low reduced number of processing steps
Part Repair and Remanufacturing	Difficult or not feasible	Possible (especially with DED based processes)	Highly effective repair and remanufacturing combined
Industrial Certification Compatibility	Compliant with existing standards	Developing varies by sector	Subject to emerging standards – increasing industrial adoption
Investment Cost	Moderate	Moderate to high	High complex equipment and software requirements
Application Areas	Automotive, aerospace, heavy industry	Medical, space, defense, dentistry	Aerospace, medical, tooling, energy, electronics

The comparison presented in Table 1 clearly demonstrates that hybrid additive manufacturing is not merely

an approach in which additive and conventional methods are used sequentially; rather, it offers a holistic manufacturing approach that integrates geometric freedom, dimensional accuracy, and microstructure control within a single production chain. In particular, the gains achieved in terms of material utilization efficiency, surface quality/tolerances, and part repair elevate HAM to a strategic position in industrial manufacturing.

2.3. Why Hybrid Additive Manufacturing Matters in Industrial Production

At present, the development of hybrid additive manufacturing (HAM) technology is not limited solely to improving production efficiency; it also demonstrates significant progress in the areas of intelligent manufacturing systems, sustainability, and standardization. The literature indicates that future research and application trends related to HAM are concentrated around specific technical, digital, and organizational themes.

In this context, artificial intelligence and machine learning–based approaches are gaining increasing importance for real time monitoring of process data and the implementation of adaptive production control [36]. Similarly, digital twin and IoT based integrations enable virtual modeling of manufacturing processes, allowing potential defects to be predicted in advance and process optimization to be carried out more effectively [40].

Another key area of future research concerns the control of transition regions in hybrid structures involving multi material usage. Ensuring mechanical and microstructural continuity in these regions is regarded as a critical objective in terms of both structural integrity and long term service performance [28], [31].

From the perspective of standardization and industrial integration, international organizations such as ASTM, ISO, and

the FDA have begun to develop testing protocols and certification frameworks specific to hybrid additive manufacturing processes [43], [44]. These developments play a fundamental role in accelerating industrial adoption and enhancing the reliability of HAM based production, particularly in the aerospace and medical sectors.

3. CONCLUSION

This book chapter demonstrates that hybrid additive manufacturing is not merely a technique aimed at improving specific manufacturing steps; rather, it offers a holistic manufacturing approach that spans the entire production chain, from design and manufacturing to quality control and part performance. It provides the reader with a clear and systematic framework to understand where the limitations of standalone additive manufacturing become evident and how hybrid approaches can overcome these limitations through specific mechanisms.

The historical development, industrial applications, and technical challenges discussed throughout the chapter indicate that hybrid additive manufacturing is not simply an emerging technology, but a rational response to contemporary manufacturing needs. In particular, the explanation of how fundamental challenges of modern manufacturing such as dimensional accuracy, microstructure control, part repair, and sustainability can be addressed through hybrid approaches enhances the practical relevance of this chapter.

Readers who benefit from this chapter will be able to more consciously assess in which application areas hybrid additive manufacturing provides a genuine advantage, under which conditions it still presents limitations, and in which directions the technology is expected to evolve in the future.

Such an assessment contributes to the formulation of more targeted research questions in academic studies and supports more informed technology selection in industrial applications.

In conclusion, this chapter serves as a guiding resource for anyone seeking to approach hybrid additive manufacturing not only from a technical perspective, but also as a strategic, systematic, and long-term manufacturing approach. The ability of readers to adapt this knowledge to their own research, design, or production processes stands out as the most significant outcome in terms of understanding the true value of hybrid additive manufacturing.

REFERENCES

[1] J. Konasch et al., “A Novel Hybrid Additive Manufacturing Process for Drug Delivery Systems with Locally Incorporated Drug Depots,” Pharmaceutics, vol. 11, no. 12, p. 661, Dec. 2019, doi: 10.3390/pharmaceutics11120661.

[2] P. Szymczyk-Ziółkowska, M. B. Łabowska, J. Detyna, I. Michalak, and P. Gruber, “A review of fabrication polymer scaffolds for biomedical applications using additive manufacturing techniques,” Biocybernetics and Biomedical Engineering, vol. 40, no. 2, pp. 624–638, Apr. 2020, doi: 10.1016/j.bbe.2020.01.015.

[3] B. Freitas, V. Richhariya, M. Silva, A. Vaz, S. F. Lopes, and Ó. Carvalho, “A Review of Hybrid Manufacturing: Integrating Subtractive and Additive Manufacturing,” Materials, vol. 18, no. 18, p. 4249, Sep. 2025, doi: 10.3390/ma18184249.

[4] S. H. Emon and D. S. Shim, “A Review of the Quality Control and Mechanical Properties in Hybrid Additive Manufacturing,” Int. J. Precis. Eng. Manuf., vol. 26, no. 9, pp. 2515–2550, Sep. 2025, doi: 10.1007/s12541-025-01329-z.

[5] R. Durga Prasad Reddy and V. Sharma, “Additive manufacturing in drug delivery applications: A review,” International Journal of Pharmaceutics, vol. 589, p. 119820, Nov. 2020, doi: 10.1016/j.ijpharm.2020.119820.

[6] S. Gao et al., “Additive manufacturing of alloys with programmable microstructure and properties,” Nat Commun, vol. 14, no. 1, p. 6752, Oct. 2023, doi: 10.1038/s41467-023-42326-y.

[7] Y. Qin et al., “Additive manufacturing of biodegradable metals: Current research status and future perspectives,” Acta Biomaterialia, vol. 98, pp. 3–22, Oct. 2019, doi: 10.1016/j.actbio.2019.04.046.

[8] P. Sarobol et al., “Additive Manufacturing of Hybrid Circuits,” Annu. Rev. Mater. Res., vol. 46, no. 1, pp. 41–62, Jul. 2016, doi: 10.1146/annurev-matsci-070115-031632.

[9] Y. Li et al., “Additive manufacturing of vascular stents,” Acta Biomaterialia, vol. 167, pp. 16–37, Sep. 2023, doi: 10.1016/j.actbio.2023.06.014.

[10] L. Zhou et al., “Additive Manufacturing: A Comprehensive Review,” Sensors, vol. 24, no. 9, p. 2668, Apr. 2024, doi: 10.3390/s24092668.

[11] A. Zhakeyev, P. Wang, L. Zhang, W. Shu, H. Wang, and J. Xuan, “Additive Manufacturing: Unlocking the Evolution of Energy Materials,” Advanced Science, vol. 4, no. 10, p. 1700187, Oct. 2017, doi: 10.1002/advs.201700187.

[12] K. O. Ahmed and M. Soshi, “Algorithmic optimization of process selection for additive-subtractive hybrid manufacturing,” Manufacturing Letters, vol. 44, pp. 314–324, Aug. 2025, doi: 10.1016/j.mfglet.2025.06.038.

[13] Z. Cheng, H. Huang, M. Yin, and H. Liu, “Applications of liposomes and lipid nanoparticles in cancer therapy: current advances and prospects,” Exp Hematol Oncol, vol. 14, no. 1, p. 11, Jan. 2025, doi: 10.1186/s40164-025-00602-1.

[14] S. C. Altıparmak, V. A. Yardley, Z. Shi, and J. Lin, “Challenges in additive manufacturing of high-strength aluminium alloys and current developments in hybrid

additive manufacturing," International Journal of Lightweight Materials and Manufacture, vol. 4, no. 2, pp. 246–261, Jun. 2021, doi: 10.1016/j.ijlmm.2020.12.004.

[15] C. Baumann et al., "Comparison of three hybrid metal additive-subtractive manufacturing processes," CIRP Annals, vol. 74, no. 1, pp. 321–325, 2025, doi: 10.1016/j.cirp.2025.04.074.

[16] C. R. Alcala-Orozco, X. Cui, G. J. Hooper, K. S. Lim, and T. B. F. Woodfield, "Converging functionality: Strategies for 3D hybrid-construct biofabrication and the role of composite biomaterials for skeletal regeneration," Acta Biomaterialia, vol. 132, pp. 188–216, Sep. 2021, doi: 10.1016/j.actbio.2021.03.008.

[17] A. Zadpoor, "Design for Additive Bio-Manufacturing: From Patient-Specific Medical Devices to Rationally Designed Meta-Biomaterials," IJMS, vol. 18, no. 8, p. 1607, Jul. 2017, doi: 10.3390/ijms18081607.

[18] M. Á. Rabalo, A. García, and E. M. Rubio, "Emerging Trends in Hybrid Additive and Subtractive Manufacturing," Applied Sciences, vol. 15, no. 11, p. 6102, May 2025, doi: 10.3390/app15116102.

[19] B. Zhang et al., "From Complex Shaping to Mirror Finish: Additive Manufacturing of Aerospace-grade Cf /SiC Space Optics," Advanced Science, p. e17980, Nov. 2025, doi: 10.1002/advs.202517980.

[20] A. Kalkal, A. K. Yadav, D. Verma, A. Sehgal, G. Packirisamy, and D. Bhatia, "Harnessing the potential of emerging additive manufacturing technologies as a game-changer for chemical and biosensing innovations," Rep. Prog. Phys., vol. 88, no. 8, p. 086701, Aug. 2025, doi: 10.1088/1361-6633/adf7ba.

[21] A. Islam et al., “Hybrid additive manufacturing of flexible copper radiofrequency electronics,” Materials Today, vol. 83, pp. 125–131, Mar. 2025, doi: 10.1016/j.mattod.2024.12.016.

[22] M. Merklein, D. Junker, A. Schaub, and F. Neubauer, “Hybrid Additive Manufacturing Technologies – An Analysis Regarding Potentials and Applications,” Physics Procedia, vol. 83, pp. 549–559, 2016, doi: 10.1016/j.phpro.2016.08.057.

[23] W. Yue, Y. Zhang, Z. Zheng, and Y. Lai, “Hybrid Laser Additive Manufacturing of Metals: A Review,” Coatings, vol. 14, no. 3, p. 315, Mar. 2024, doi: 10.3390/coatings14030315.

[24] A. Hasan and S. S. Akhtar, “Hybrid Manufacturing: A Critical Review on the Integration of Metal Additive Manufacturing and Forming,” Arab J Sci Eng, Nov. 2025, doi: 10.1007/s13369-025-10885-5.

[25] J. P. M. Pragana, R. F. V. Sampaio, I. M. F. Bragança, C. M. A. Silva, and P. A. F. Martins, “Hybrid metal additive manufacturing: A state–of–the-art review,” Advances in Industrial and Manufacturing Engineering, vol. 2, p. 100032, May 2021, doi: 10.1016/j.aime.2021.100032.

[26] J. Hafenecker et al., “Hybrid process chains combining metal additive manufacturing and forming – A review,” CIRP Journal of Manufacturing Science and Technology, vol. 46, pp. 98–115, Nov. 2023, doi: 10.1016/j.cirpj.2023.08.002.

[27] S. Jung, L. B. Kara, Z. Nie, T. W. Simpson, and K. S. Whitefoot, “Is Additive Manufacturing an Environmentally and Economically Preferred Alternative for Mass Production?,” Environ. Sci. Technol., vol. 57,

no. 16, pp. 6373–6386, Apr. 2023, doi: 10.1021/acs.est.2c04927.

[28] A. A. Zadpoor, “Mechanical performance of additively manufactured meta-biomaterials,” Acta Biomaterialia, vol. 85, pp. 41–59, Feb. 2019, doi: 10.1016/j.actbio.2018.12.038.

[29] Z. Meng et al., “Melt pool height monitoring based on dynamic laser spot in Oscillating Laser Arc Hybrid Additive Manufacturing,” Journal of Materials Processing Technology, vol. 346, p. 119117, Dec. 2025, doi: 10.1016/j.jmatprotec.2025.119117.

[30] Y. Yang et al., “Microstructure of titanium alloy in additive/subtractive hybrid manufacturing: A review,” Journal of Alloys and Compounds, vol. 1014, p. 178769, Feb. 2025, doi: 10.1016/j.jallcom.2025.178769.

[31] N. E. Putra, M. J. Mirzaali, I. Apachitei, J. Zhou, and A. A. Zadpoor, “Multi-material additive manufacturing technologies for Ti-, Mg-, and Fe-based biomaterials for bone substitution,” Acta Biomaterialia, vol. 109, pp. 1–20, Jun. 2020, doi: 10.1016/j.actbio.2020.03.037.

[32] W. W. S. Ma et al., “Multi-Physical Lattice Metamaterials Enabled by Additive Manufacturing: Design Principles, Interaction Mechanisms, and Multifunctional Applications,” Advanced Science, vol. 12, no. 8, p. 2405835, Feb. 2025, doi: 10.1002/advs.202405835.

[33] T. Tegethoff, R. Santa, J. M. Bucheli, B. Cabrera, and A. Scavarda, “Navigating Industry 4.0: Leveraging additive technologies for competitive advantage in Colombian aerospace and manufacturing industries,” PLoS ONE, vol. 20, no. 2, p. e0318339, Feb. 2025, doi: 10.1371/journal.pone.0318339.

[34] S. Webster, H. Lin, F. M. Carter Iii, K. Ehmann, and J. Cao, "Physical mechanisms in hybrid additive manufacturing: A process design framework," Journal of Materials Processing Technology, vol. 291, p. 117048, May 2021, doi: 10.1016/j.jmatprotec.2021.117048.

[35] F. Alamri, I. Barsoum, S. Bojanampati, and M. Maalouf, "Prediction of porosity, hardness and surface roughness in additive manufactured AlSi10Mg samples," PLoS ONE, vol. 20, no. 3, p. e0316600, Mar. 2025, doi: 10.1371/journal.pone.0316600.

[36] R. Sinha et al., "A hybrid additive manufacturing platform to create bulk and surface composition gradients on scaffolds for tissue regeneration," Nat Commun, vol. 12, no. 1, p. 500, Jan. 2021, doi: 10.1038/s41467-020-20865-y.

[37] J. Li, X. Cui, G. J. Hooper, K. S. Lim, and T. B. F. Woodfield, "Rational design, bio-functionalization and biological performance of hybrid additive manufactured titanium implants for orthopaedic applications: A review," Journal of the Mechanical Behavior of Biomedical Materials, vol. 105, p. 103671, May 2020, doi: 10.1016/j.jmbbm.2020.103671.

[38] P. Nandwana, R. Kannan, C. M. Fancher, T. Feldhausen, C. Herberger, and Y. Lee, "Residual strain and microstructure evolution in 316L stainless steel fabricated by hybrid additive/subtractive manufacturing," Journal of Materials Research and Technology, vol. 41, pp. 891–899, Mar. 2026, doi: 10.1016/j.jmrt.2025.11.170.

[39] W. Du, X. Li, J. Zhang, C. Chen, and S. Zhu, "Review of hybrid additive–subtractive manufacturing of stainless steel for repair applications," Additive Manufacturing

Frontiers, p. 200290, Dec. 2025, doi: 10.1016/j.amf.2025.200290.

[40] M. K. Tiwari, H. Y. Shahare, P. K, and P. Tandon, "Synergizing Additive Manufacturing and Incremental Forming: Evolution of Hybrid Additive Manufacturing Incremental Forming Process," Materials and Manufacturing Processes, vol. 40, no. 6, pp. 741–754, Apr. 2025, doi: 10.1080/10426914.2025.2469540.

[41] L. An et al., "Tailoring thermal insulation architectures from additive manufacturing," Nat Commun, vol. 13, no. 1, p. 4309, Jul. 2022, doi: 10.1038/s41467-022-32027-3.

[42] C. Liu et al., "The corrosion behaviors of Inconel 718 fabricated by additive-subtractive hybrid manufacturing in marine environment," Corrosion Science, vol. 255, p. 113133, Oct. 2025, doi: 10.1016/j.corsci.2025.113133.

[43] J. Bernatoniene, J. Stabrauskiene, J. A. Kazlauskaite, U. Bernatonyte, and D. M. Kopustinskiene, "The Future of Medicine: How 3D Printing Is Transforming Pharmaceuticals," Pharmaceutics, vol. 17, no. 3, p. 390, Mar. 2025, doi: 10.3390/pharmaceutics17030390.

[44] C. Cioloca Holban et al., "Three-Dimensional Printing and CAD/CAM Milling in Prosthodontics: A Scoping Review of Key Metrics Towards Future Perspectives," JCM, vol. 14, no. 14, p. 4837, Jul. 2025, doi: 10.3390/jcm14144837.

[45] Ü. Zeybek, "Mechanically alloyed Zr-doped NiTi powders: A study on R-Phase formation and austenitic transformation behavior," *Canadian Metallurgical Quarterly* , pp. 1–11, Oct. 2025, doi: 10.1080/00084433.2025.2575229.

NUMERICAL INVESTIGATION OF MARANGONI CONVECTION UNDER VARYING ASPECT RATIOS AND GRAVITY CONDITIONS

Ela KATI SUNAY[1]

1. INTRODUCTION

Marangoni (thermocapillary) convection is a transport mechanism that occurs as a result of tangential shear stresses acting on a fluid due to surface tension gradients formed along a free surface. The formation of Marangoni convection is directly related to temperature differences occurring along the free surface. In most liquids, surface tension decreases with increasing temperature; therefore, in systems where temperature variations exist along the free surface, the surface tension distribution loses its uniformity. The resulting surface tension gradient causes the fluid to move from regions of lower surface tension (higher temperature) toward regions of higher surface tension (lower temperature). This motion initiated along the surface leads to the formation of closed circulation cells within the fluid volume.

Marangoni convection becomes particularly significant in small-scale systems, in fluids with high Prandtl numbers, and in configurations where free-surface effects dominate. In such systems, Marangoni-driven flows strongly influence heat and mass transfer mechanisms. Consequently, Marangoni convection is of great importance not only from the standpoint of

[1] Asst. Prof. Dr., Süleyman Demirel University, Faculty of Engineering and Natural Sciences, Department of Mechanical Engineering, ORCID: 0000-0002-4135-5241.

fundamental fluid mechanics but also in many engineering and scientific applications.

Marangoni convection is encountered in a wide range of applications, including flow control in microfluidic systems, thin-film coating and drying processes, crystal growth and semiconductor manufacturing, as well as space engineering and microgravity experiments.

The characteristics of the flow structure formed in Marangoni convection depend on several parameters such as the geometric aspect ratio (Ar), temperature difference, thermophysical properties of the fluid, gravity conditions, and boundary conditions. Among these parameters, the aspect ratio (Ar) is one of the key factors determining the development of the flow structure in Marangoni convection. Variations in the aspect ratio directly influence the geometric distribution of circulation cells and the interaction between Marangoni convection and natural convection. In this context, the comparative investigation of Marangoni convection under different aspect ratios is important for revealing the role of this mechanism on the flow structure more clearly.

Under normal gravity conditions, Marangoni convection always occurs together with natural convection arising from density variations due to temperature differences. The buoyancy force generated by natural convection may modify the flow structure produced by surface tension gradients; in some configurations it may weaken Marangoni-induced circulation or influence the stability of the flow. Therefore, the flow structure observed under normal gravity conditions is not only a result of the Marangoni mechanism but also of natural convection effects. In contrast, under microgravity conditions, buoyancy forces become negligible and the flow structure is largely determined by surface tension gradients. This situation enables Marangoni

convection to be examined more clearly. In the literature, experimental and numerical studies conducted in microgravity environments have special importance in terms of isolating and understanding the fundamental physical mechanisms of Marangoni convection. In particular, studies carried out in space environments reveal that the suppression of buoyancy forces allows surface-tension-driven flows to be observed in a purer form, and therefore microgravity studies occupy an important place in academic research. For this reason, in order to reveal the interaction between Marangoni convection and natural convection and to better evaluate the fundamental behavior of the mechanism, analyses were carried out under both normal gravity and microgravity conditions in this study.

Studies investigating surface-tension-driven convection mechanisms and their effects on sensitive manufacturing applications such as semiconductor crystal growth have contributed significantly to the understanding of the fundamental physical principles of Marangoni convection. Ostrach (1982) examined surface-tension-driven flows in low-gravity environments and emphasized the importance of space research.

Wang et al. (1991) analytically investigated natural convection and Marangoni convection in a two-layer fluid system without mass transfer at the interface. In analyses based on the assumption of parallel flow, cases with horizontal and vertical heat fluxes were evaluated, and it was shown that four different convection patterns could occur in the system. The results revealed that these patterns depend on dimensionless parameters and that the interaction between buoyancy forces and surface tension effects determines the flow structure.

Sasmal and Hochstein (1994) developed a finite-volume-based numerical model to investigate Marangoni convection in a cavity with a curved and deforming free surface. In their study,

the effects of Marangoni and capillary numbers as well as the contact angle on the flow structure and heat transfer were analyzed, and the results were evaluated through streamlines, isotherms, and local Nusselt number distributions.

Zeng et al. (1999) numerically investigated the variation of the oscillation radial frequency with aspect ratio in a half-floating-zone configuration using silicone oil.

Hamed and Floryan (2000) examined Marangoni convection in a cavity with differentially heated sidewalls while considering interface deformation. Their results showed that the interface becoming tangent to the hot wall is the main mechanism limiting system stability.

Lai (2004) demonstrated that each of the dimensionless parameters appearing in the continuity, Navier–Stokes, and energy equations affects the flow behavior of high-Prandtl-number fluids undergoing oscillatory thermocapillary convection.

Peng et al. (2008) numerically investigated Marangoni convection under microgravity conditions using the finite difference method. The results showed that the flow remains steady at low Marangoni numbers and is confined near the free surface. As the Marangoni number increases, the flow extends into the liquid volume and the surface velocity increases; however, once a critical value is exceeded, the flow becomes unstable.

Selver et al. (2013) numerically investigated the interaction between surface-tension-driven flow and natural convection in silicone oil with a viscosity of 5 cSt under normal and reduced gravity conditions. The results showed that variations in gravity level significantly affect the flow characteristics and revealed the determining role of buoyancy forces in Marangoni convection.

Mielniczuk et al. (2018) investigated capillary interactions in a floating-zone configuration using an analytical model. Their results showed that gravitational effects cause a loss of symmetry in the system, leading to undesirable deformations. In order to reduce this deformation, additional tests were conducted under microgravity conditions, and more stable and symmetric structures were observed compared to those obtained under normal gravity.

Weerakoon Rathnayake et al. (2024) investigated the effect of volume ratio on the flow dynamics of fluids with different Prandtl (Pr) and Schmidt (Sc) numbers under steady and unsteady Marangoni conditions using three-dimensional numerical simulations. The results showed that, at low Prandtl numbers, the effect of volume ratio on temperature distribution is limited under steady conditions but becomes more significant under unsteady conditions. At high Prandtl numbers, however, the volume ratio significantly affects both temperature and velocity distributions. In addition, for high Schmidt and low Prandtl numbers, the concentration distribution was found to be more affected by the volume ratio, and oscillatory and irregular flow structures were observed under unstable regimes.

In the present study, the open-cavity configuration commonly used in the investigation of Marangoni convection was modeled in two dimensions, and numerical simulations were performed using the ANSYS Fluent software. In order to determine the effects of the aspect ratio (Ar) on flow velocity, stability, and structural characteristics, eight different aspect ratios were considered. Furthermore, to evaluate the interaction between Marangoni convection and natural convection, the analyses were conducted under both normal gravity and microgravity conditions.

2. NUMERICAL MODEL AND METHOD

The open-cavity configuration used in the model consists of a container in which one of the opposing long vertical walls is heated and the other is cooled, while the remaining walls and the bottom surface are insulated (Figure 1).

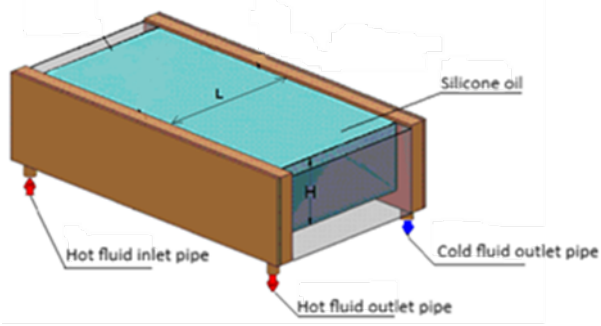

Figure 1. Open-cavity configuration (Selver et al., 2013)

As shown in Figure 1, one of the two opposing long vertical walls is defined as the heated wall, while the other is defined as the cooled wall. In this configuration, the silicone oil is heated from one side wall and cooled from the opposite wall. Due to the temperature difference, the surface tension distribution along the free surface becomes non-uniform, resulting in the formation of a surface tension gradient. This condition generates tangential stresses along the free surface and leads to the development of Marangoni convection.

In order to investigate this flow structure numerically, the ANSYS Fluent software was employed. In the study, eight different aspect ratios (Ar) were considered, and a two-dimensional geometrical model was defined for each ratio. The numerical analyses were carried out using these models. An example of the geometrical model used in the numerical simulations and its corresponding mesh structure is presented in Figure 2.

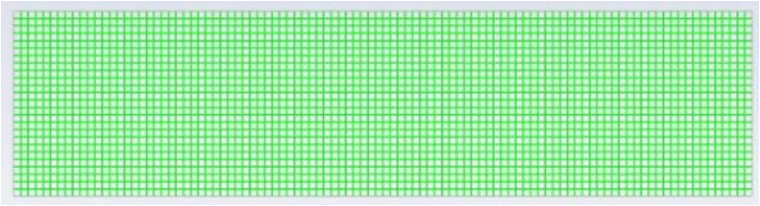

Figure 2. Geometrical model and mesh structure for Ar = 0.25

In the geometrical model shown in Figure 2, the left vertical boundary represents the heated wall, the right vertical boundary represents the cooled wall, the upper horizontal boundary represents the free surface of the silicone oil, and the lower horizontal boundary represents the bottom surface of the container. For the example model presented in Figure 2, the aspect ratio is defined as Ar = 0.25, where Ar = H/L. Here, H represents the height of the silicone oil, and L denotes the distance between the heated and cooled walls.

In the numerical simulations, the physical properties of silicone oil with a viscosity of 2 cSt were used (Masud, 1997). In order to ensure that the flow remained within the steady Marangoni convection regime, the temperature of the heated wall was maintained at T_H = 298 K, while the temperature of the cooled wall was fixed at T_C = 288 K.

In this study, eight different aspect ratios were considered: Ar = 0.25, 0.5, 0.75, 1, 1.25, 1.5, 1.75, and 2. In all models, the distance L was kept constant at 0.01 m, while the value of H was varied to obtain different aspect ratios.

Since the surface tension gradient responsible for Marangoni convection acts along the free surface of the liquid, this region is of critical importance for the numerical analysis. Therefore, particular attention was paid to the quality of the generated mesh and to the resolution near the free-surface region. The flow was assumed to be laminar, and the simulations were performed using the SIMPLER algorithm. It was assumed that the

free surface remained flat and horizontal, that no heat transfer occurred between the free surface and the surrounding environment (adiabatic condition), and that radiation effects were negligible. Under these conditions, a total of sixteen numerical simulations were carried out for eight different aspect ratios under normal gravity (9.81 m/s²) and microgravity (1.0×10^{-6} m/s²) conditions.

3. RESULTS AND DISCUSSION

Marangoni convection arises as a result of temperature differences along the free surface that modify the surface tension. In most fluids, surface tension decreases with increasing temperature, which leads to the formation of a surface tension gradient along the free surface. This gradient induces a flow along the free surface from the hotter region toward the colder region.

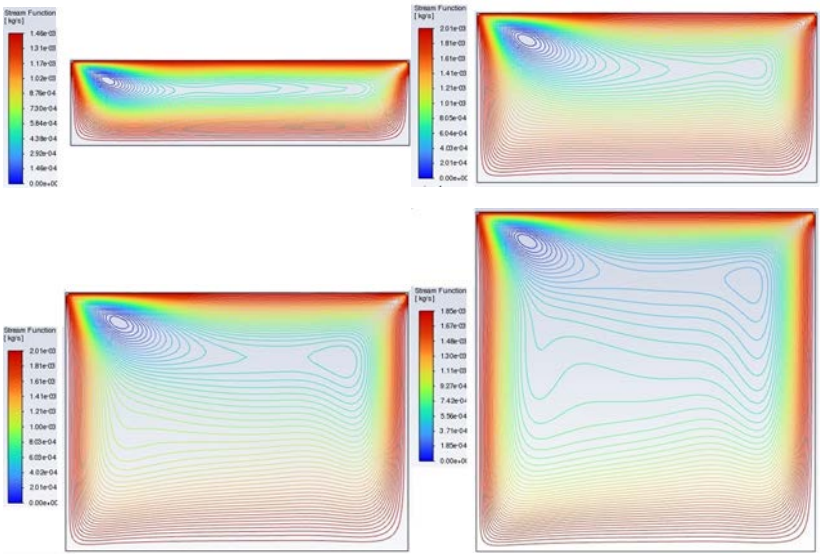

Figure 3. Streamline patterns of silicone oil undergoing Marangoni convection under normal gravity conditions for Ar=0.25, 0.5, 0.75, and 1

The streamline patterns obtained under normal gravity conditions for silicone oil configurations with aspect ratios Ar=0.25, 0.5, 0.75 and 1 are presented in Figure 3. In the geometrical model, the left vertical wall is defined as the heated wall, whereas the right vertical wall is defined as the cooled wall. Under these conditions, fluid particles move along the free surface from the hot region toward the cold region due to the surface tension effect. Examination of Figure 3 shows that, in all configurations, the convection circulation develops in such a way that it occupies a large portion of the cavity, and a second vortex cell begins to form. In the configuration with Ar=0.25 the second vortex cell appears near the center of the cavity, whereas for Ar=0.5, 0.75 and 1, the second vortex cell is observed to form closer to the cold wall.

Under normal gravity conditions, Marangoni convection generally occurs together with natural convection. Natural convection induced by density differences may influence the flow structure of Marangoni convection and, in some cases, may alter the characteristics of the surface-tension-driven flow. Therefore, studies conducted under microgravity conditions are of great importance for observing Marangoni convection more clearly and for reducing the influence of natural convection. For this reason, the numerical analyses in the present study were performed under both normal gravity and microgravity conditions.

Figure 4 presents the streamline patterns of silicone oil with a viscosity of 2 cSt undergoing Marangoni convection under microgravity conditions for configurations with aspect ratios Ar=0.25, 0.5, 0.75 and 1.

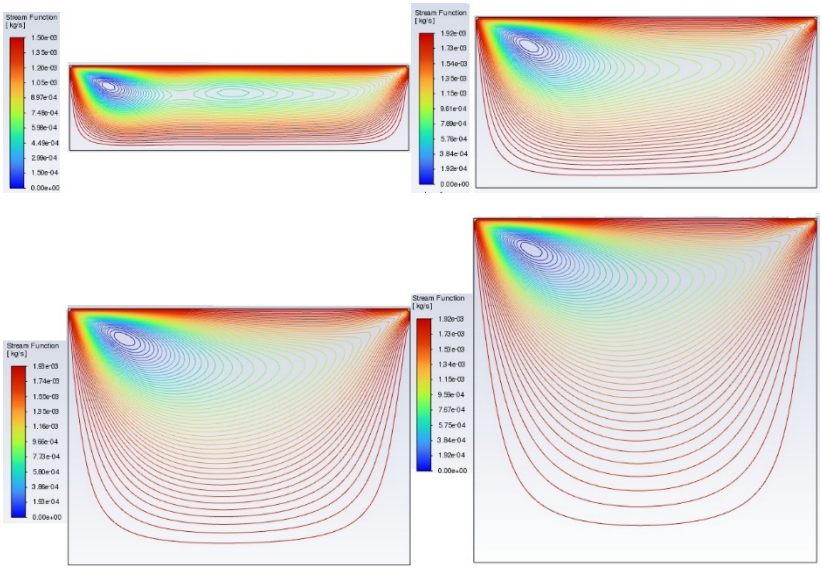

Figure 4. Streamline patterns of silicone oil undergoing Marangoni convection under microgravity conditions for Ar=0.25,0.5, 0.75, and 1

An examination of Figure 4 shows that a second vortex cell forms only in the configuration with an aspect ratio of Ar=0.25, whereas a single vortex cell is observed for Ar=0.5, 0.75 and 1. A comparison between Figures 3 and 4 reveals significant differences in terms of the shape of the convection circulation and its distribution within the cavity.

Figure 5 presents the streamline patterns of silicone oil with a viscosity of 2 cSt undergoing Marangoni convection under normal gravity conditions for configurations with aspect ratios Ar= 1.25, 1.5, 1.75 and 2.

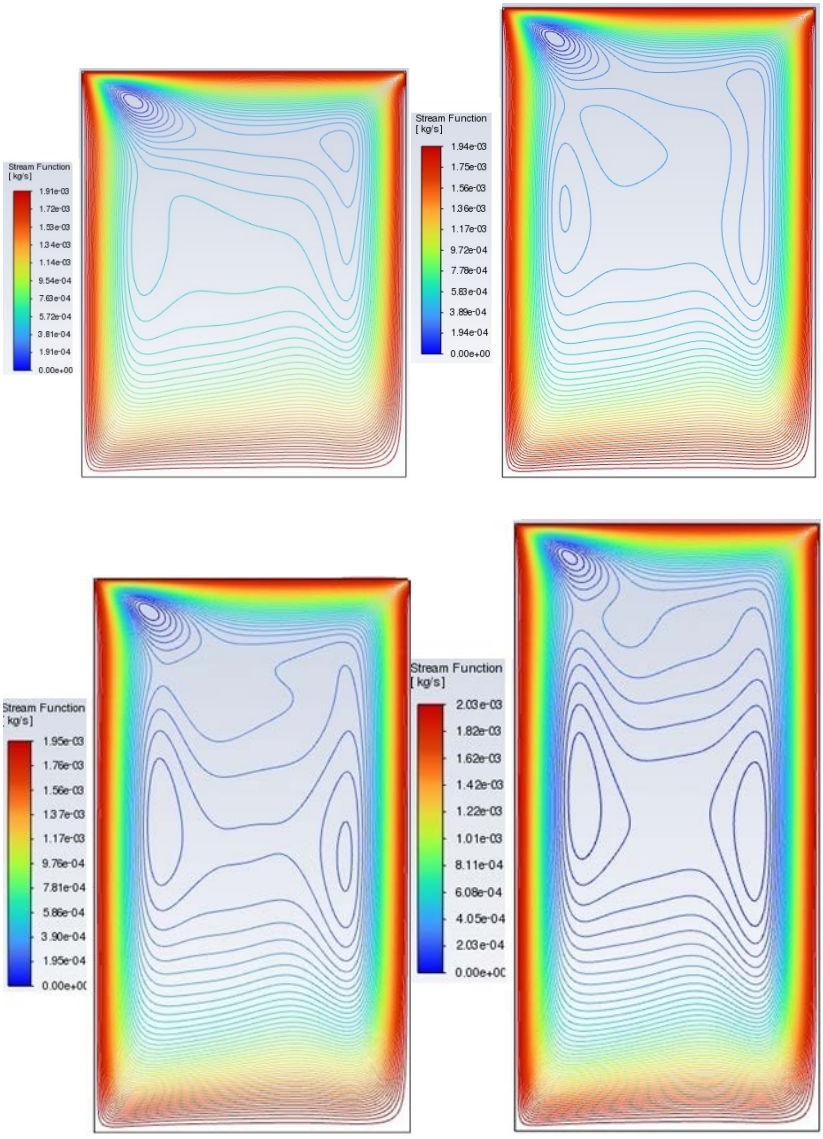

Figure 5. Streamline patterns of silicone oil undergoing Marangoni convection under normal gravity conditions for Ar=1.25, 1.5, 1.75, and 2

An examination of Figure 5 shows that, similar to Figure 3, the convection circulation develops in such a way that it occupies a large portion of the cavity in all configurations. In

addition, multiple vortex cells are observed in all configurations. It is also observed that as the aspect ratio increases, the structure of the convection circulation changes and the irregularity within the flow gradually increases.

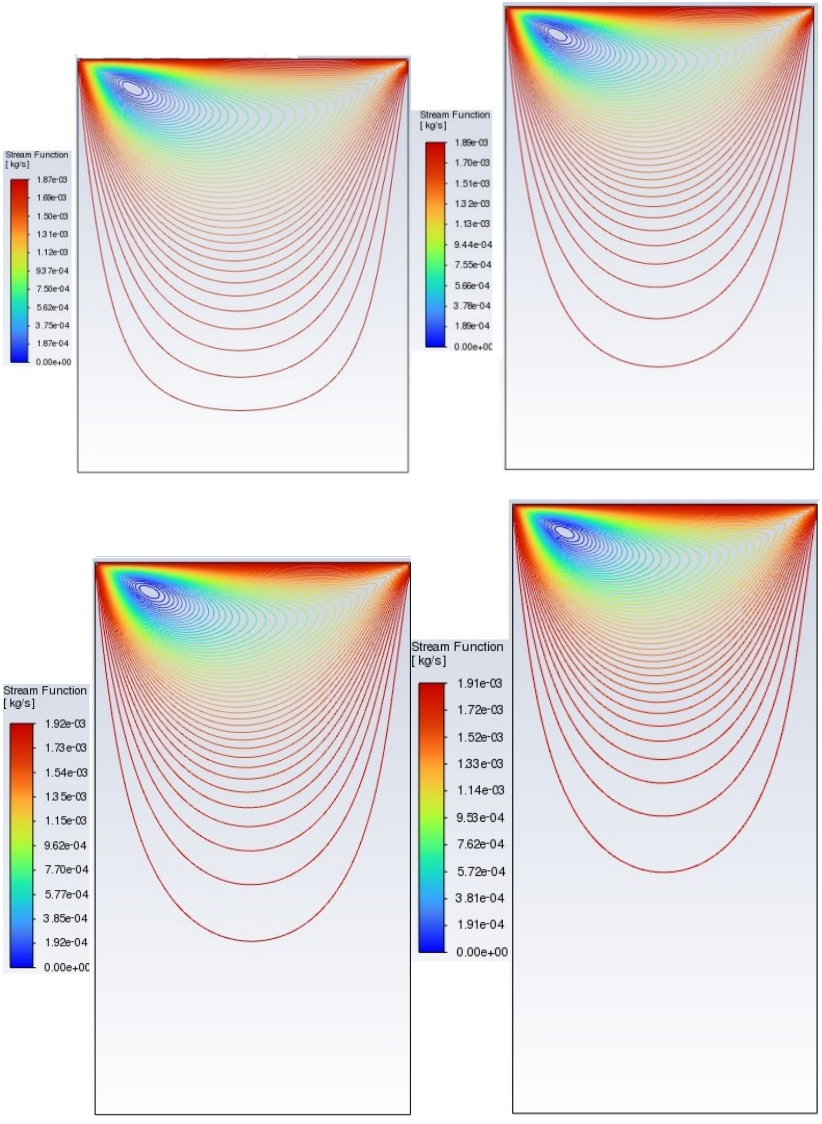

Figure 6. Streamline patterns of silicone oil undergoing Marangoni convection under microgravity conditions for Ar=1.25, 1.5, 1.75, and 2

In order to examine Marangoni convection more clearly and to reduce the influence of natural convection, numerical analyses were also performed under microgravity conditions for aspect ratios Ar = 1.25, 1.5, 1.75 and 2. Figure 6 presents the streamline patterns of silicone oil with a viscosity of 2 cSt undergoing Marangoni convection under microgravity conditions for configurations with these aspect ratios.

An examination of Figure 6 shows that a single vortex cell forms in all configurations, and the structure of the convection circulation remains largely unchanged while the overall flow pattern is preserved. As the aspect ratio increases, the convection circulation becomes concentrated near the upper region of the cavity and the flow does not penetrate into the deeper regions of the cavity. As a result, a stagnant flow region forms in the lower part of the cavity.

Under normal gravity conditions, a temperature gradient develops from the bottom toward the top of the configuration due to the effect of natural convection. For this reason, in all configurations presented in Figures 3 and 5, the convection circulation develops in such a way that it occupies the entire cavity. In contrast, in the analyses performed under microgravity conditions (Figures 4 and 6), the buoyancy effect is largely eliminated and the flow is governed only by surface-tension-driven Marangoni forces. In this case, since the temperatures in the regions where vortex cells exist are higher than those in the stagnant region below, the fluid density in the stagnant region becomes greater. Consequently, this limits the penetration depth of the vortex cells into the fluid.

The temperature distributions of silicone oil undergoing Marangoni convection inside the configuration under normal gravity conditions for aspect ratios Ar = 0.25, 0.5, 0.75, 1, 1.25, 1.5, 1.75 and 2 are presented in Figures 7 and 8.

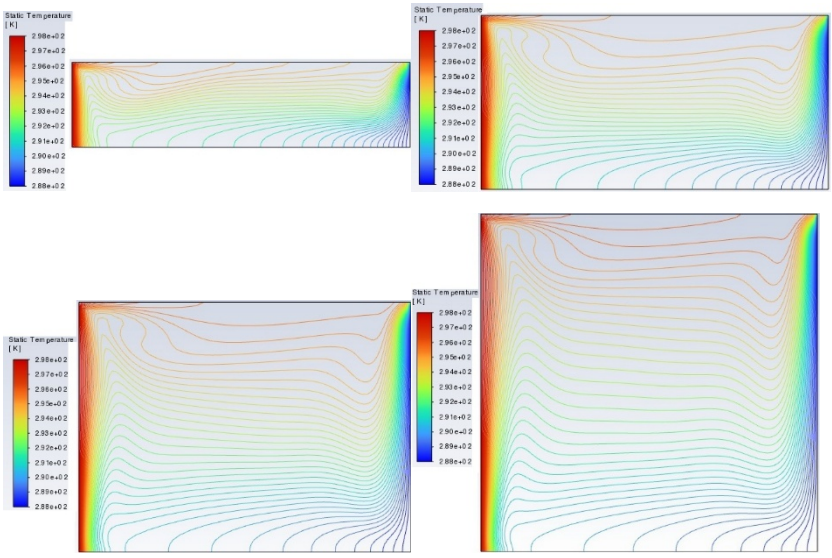

Figure 7. Isotherm patterns of silicone oil undergoing Marangoni convection under normal gravity conditions for Ar = 0.25, 0.5, 0.75 and 1

An examination of Figures 7 and 8 shows that, in all configurations, the isotherms become denser near the heated wall, indicating that the temperature gradient is more pronounced in this region. As the aspect ratio increases, the isotherms within the configuration exhibit a more regular and nearly parallel structure. In addition, under normal gravity conditions, the temperature distribution is not confined only to the region near the free surface due to the influence of natural convection, but also extends toward the lower regions of the configuration. This indicates that buoyancy forces and Marangoni convection develop simultaneously, causing the convection circulation to spread over a larger portion of the configuration volume. Therefore, under normal gravity conditions, heat transfer occurs under the combined influence of surface-tension-driven Marangoni flow and natural convection induced by density differences.

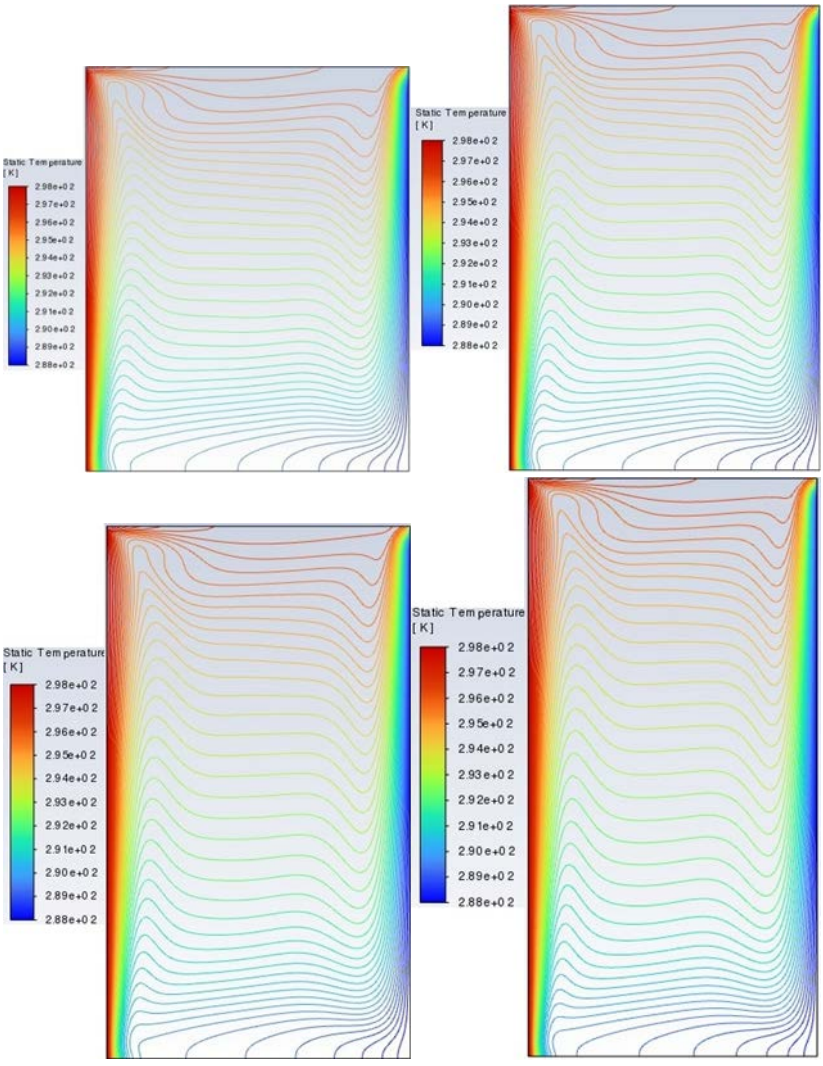

Figure 8. Isotherm patterns of silicone oil undergoing Marangoni convection under normal gravity conditions for Ar = 1.25, 1.5, 1.75 and 2

Figures 9 and 10 present the temperature distributions of silicone oil undergoing Marangoni convection within the configuration under microgravity conditions for aspect ratios Ar=0.25, 0.5, 0.75, 1, 1.25, 1.5, 1.75 and 2.

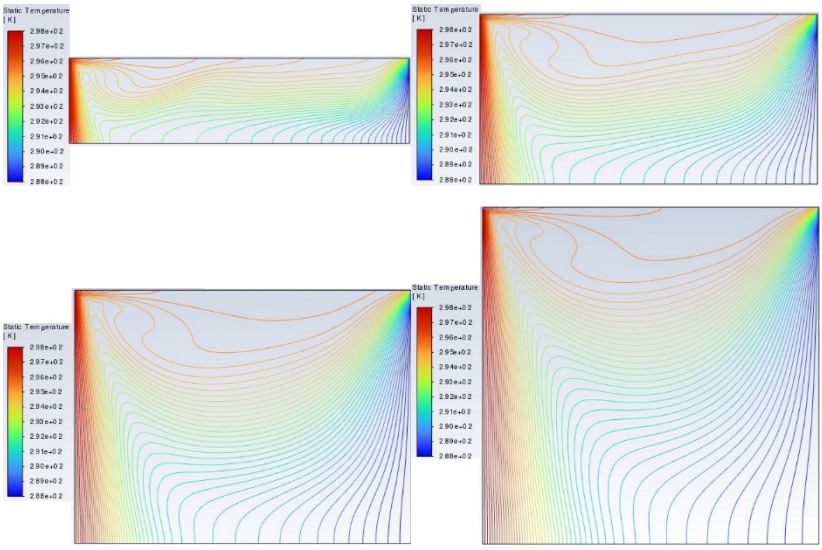

Figure 9. Isotherm patterns of silicone oil undergoing Marangoni convection under microgravity conditions for Ar = 0.25, 0.5, 0.75 and 1

An examination of Figures 9 and 10 shows that, in all configurations, a distinct temperature distribution forming a semicircular pattern near the free surface of the liquid is observed. At smaller aspect ratios, the temperature distribution appears as more horizontally oriented isotherms extending downward from the free surface. As the aspect ratio increases, the isotherms in the regions located beneath the semicircular temperature field formed near the free surface tend to extend in a more vertical direction. This behavior is associated with the fact that, under microgravity conditions, the flow is largely governed by the surface tension gradient and the Marangoni-driven surface flow becomes concentrated in the upper regions. As a result, the flow weakens in the lower regions of the configuration, and this behavior can be clearly observed in the streamline patterns presented in Figures 4 and 6.

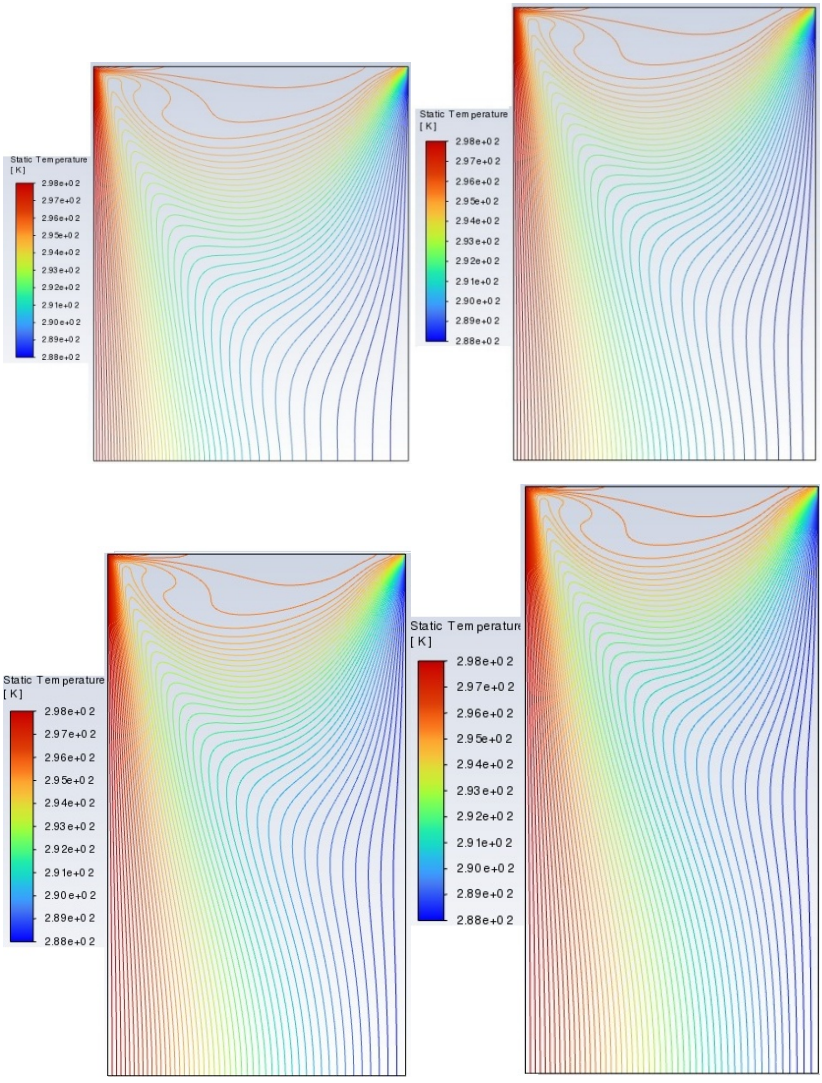

Figure 10. Isotherm patterns of silicone oil undergoing Marangoni convection under microgravity conditions for Ar = 1.25, 1.5, 1.75 and 2

A comparison of Figures 7, 8, 9 and 10 shows that, under microgravity conditions, the isotherms differ significantly from those obtained under normal gravity conditions due to the elimination of the buoyancy force associated with natural convection.

4. CONCLUSION

In this study, Marangoni convection occurring in silicone oil with a viscosity of 2 cSt inside an open cavity configuration was investigated using numerical analysis. In order to examine the effect of the aspect ratio on flow behavior and temperature distributions, numerical analyses were performed for eight different aspect ratios: Ar = 0.25, 0.5, 0.75, 1, 1.25, 1.5, 1.75 and 2. These analyses were carried out under both normal gravity and microgravity conditions, and the obtained results were evaluated based on streamline patterns and isotherm distributions.

An examination of the results obtained under normal gravity conditions indicates that Marangoni convection develops together with natural convection. Due to the buoyancy force arising from density differences, the convection circulation develops in such a way that it occupies a large portion of the configuration. As the aspect ratio increases, changes occur in the structure of the convection cells, and multiple vortex cells are observed particularly at higher aspect ratios. In addition, it was determined that the convection circulation is significantly influenced by the geometry and that the irregularity of the flow field increases as the aspect ratio becomes larger.

In the analyses performed under microgravity conditions, the elimination of buoyancy forces associated with natural convection results in flow behavior that is largely governed by the Marangoni convection mechanism driven by surface tension gradients. Under these conditions, the convection cells exhibit a more regular structure and a single vortex cell is formed in most configurations. Furthermore, as the aspect ratio increases, the convection circulation becomes concentrated in regions closer to the free surface and the penetration depth of the flow into the lower regions of the configuration decreases. As a result, more

stagnant flow regions develop in the lower part of the configuration.

An examination of the isotherm distributions shows that under normal gravity conditions the temperature distribution is not confined only to the region near the free surface; due to the effect of natural convection, it extends toward the lower regions of the configuration and forms a more regular layered structure. In contrast, under microgravity conditions a distinct temperature distribution forming a semicircular pattern near the free surface is observed. In the regions below this zone, the isotherms tend to be oriented more vertically. This behavior indicates that, with the elimination of natural convection under microgravity conditions, the flow is largely controlled by Marangoni convection governed by surface tension gradients.

The obtained results demonstrate that both the aspect ratio and gravity conditions have a determining influence on the flow structure and temperature distribution.

REFERENCES

Hamed, M., & Floryan, J. M. (2000). Marangoni convection. Part 1. A cavity with differentially heated sidewalls. *Journal of Fluid Mechanics*, 405, 79–110.

https://doi.org/10.1017/S002211209900734X

Lai, C. L. (2004). Multiple-scale analysis of oscillatory thermocapillary convection of high Prandtl number fluids in a rectangular cavity. *International Journal of Heat and Mass Transfer, 47*, 1069–1078.

Masud, J. (1997). *The influence of gravity on thermocapillary flows in high Prandtl number fluids* (Doctoral dissertation). Department of Mechanical & Aerospace Engineering, Case Western Reserve University, Cleveland, OH.

Mielniczuk, O., Millet, O., Gagneux, G., & El Youssoufi, M. S. (2018). Characterisation of pendular capillary bridges derived from experimental data using inverse problem method. *Granular Matter, 20,* 14–23.

Ostrach, S. (1982). Low-gravity fluid flows. *Annual Review of Fluid Mechanics, 14*, 313–345.

Peng, L., Fan, J.-Y., & Li, Y.-R. (2008). Numerical simulation of thermocapillary convection in detached solidification under microgravity. *Microgravity Science and Technology, 20*(3–4), 231–235.

https://doi.org/10.1007/s12217-008-9016-5

Sasmal, G. P., & Hochstein, I. (1994). Marangoni convection with a curved and deforming free surface in a cavity. *Journal of Fluids Engineering, 116*(3), 577–582. https://doi.org/10.1115/1.2910316

Selver, R., Katı Sunay, E., & Özçelik Alan, M. (2013). Akışkanın yüzey gerilim hareketlerinin farklı yerçekimi vektörleri altında incelenmesi. *Makine Teknolojileri Elektronik Dergisi, 10*(4), 57–71.

Wang, C. H., Sen, M., & Vasseur, P. (1991). Analytical investigation of Bénard–Marangoni convection heat transfer in a shallow cavity filled with two immiscible fluids. *Applied Scientific Research, 48,* 35–53.

Weerakoon Rathnayake, N. N., Okano, Y., Minakuchi, H., & Dost, S. (2024). A numerical simulation study of the effect of deformed free surface on the thermo-solutal Marangoni convection in a shallow cavity. *Journal of Chemical Engineering of Japan, 57,* 2421265. https://doi.org/10.1080/00219592.2024.2421265

Zeng, Z., Mizuseki, H., Higashino, K., & Kawazoe, Y. (1999). Direct numerical simulation of oscillatory Marangoni convection in cylindrical liquid bridges. *Journal of Crystal Growth, 204,* 395–404.

ADVANCED SOLAR TECHNOLOGIES: GLOBAL TRENDS AND TECHNO-ECONOMİC ANALYSİS

Tugba GURLER[1]

Safiullah SHIRZAD[2]

1. INTRODUCTION

All renewable energies ultimately derive from the sun, including such as wind, wave, hydro, or biomass energy sources, which can be called indirect solar energy or secondar energy sources. For example, the earth's surface has an uneven distribution of the light coming from the sun; this causes differences in pressure which are the main reason for wind energy. Unbalanced evaporation and precipitation on the earth cause the hydrological cycle, and the process of the photosynthesis of biomass resources also depends on the level of light coming from the sun, Direct solar energy, harvested by PV cells to generate electricity (explained in more detail below), is a clean and inexhaustible form of energy which can make a significant contribution to global energy problems

The first significant attempts to convert solar energy into mechanical power were made in the 19th century, mainly to produce low-pressure steam for motors. Augustin Mouchot, a French pioneer in this field, constructed and ran a number of solar-powered steam engines throughout Europe and North

[1] Assistant Prof, Hitit Universuty, Faculty of Engineering and Natural Sciences, Departmant of Mechanical Engineering, ORCID: 0000-0003-3255-5521.

[2] Graduate, Hitit University, Institute of Graduate Studies Department of Interdisciplinary Energy Systems Engineering, ORCID: 0009-0000-8724-0418

Africa between 1864 and 1878 (See in Figure 1) . A printing machine was successfully driven by one of his engines, which he prominently showed at the 1878 International Exhibition in Paris (see Figure 1) (Mouchot, 1878; 1880 as cited in Kalogirou, 2009).

Figure 1. A printing press at the 1878 Paris exposition powered by a parabolic collector (Mouchot, 1878; 1880 as cited in Kalogirou, 2009)

However, a model constructed in Tours was found to be economically unfeasible by the French government due to its high expenditures. In Algeria, a later version was installed. Mouchot created a solar collector in the form of a truncated cone in 1875, which was a significant advancement in solar collector technology. With a diameter of 5.4 meters, a collection area of 18.6 m², and moving parts weighing a considerable 1400 kg, this collector was constructed from silver-plated metal plates. Abel Pifre, a contemporary of Mouchot, was creating his own solar engines at about the same time (Meinel and Meinel, 1976; Kreider and Kreith, 1977 as cited in Kalogirou, 2009). Pifre's collectors resembled Mouchot's truncated cone designs because they were parabolic reflectors made of several tiny mirrors.

Innovation quickly made its way to the US from across the Atlantic. The first steam engine to run entirely on solar power is claimed to American engineer John Ericsson. He went on to build eight distinct systems, all of which employed air or water as the working fluid and parabolic troughs (Jordan and Ibele, 1956 as cited in Kalogirou, 2009).

In 1901, A. G. Eneas built a large-scale solar-powered water pump for a farm in California. The system featured a 10-meter-wide focusing collector, which was essentially a large, inverted umbrella-like structure. 1,788 mirrors on its inner surface were angled to capture the sun's full energy and focus the rays onto a boiler at the focal point. A traditional compound engine and centrifugal pump were subsequently powered by the resultant steam (Kreith and Kreider, 1978 as cited in Kalogirou,2009). At the St. Louis World's Fair in 1904, a Portuguese priest by the name of Father Himalaya unveiled a massive solar furnace. For its time, its design—which resembled a big, off-axis parabolic horn—was seen as fairly modern (Meinel and Meinel, 1976) as cited in Kalogirou, 2009. Frank Shuman and C. V. Boys collaborated on what may have been the most complex effort of this era in 1912. In Meadi, Egypt, they set out to construct the biggest solar-powered irrigation facility in the world.

The equipment, which was operational by 1913, focused sunlight onto absorber tubes using long parabolic cylinders. Each cylinder measured 62 meters in length, and the overall surface of the several banks was an astounding 1200 square meters. According to Kreith & Kreider (1978) as cited in Kalogirou, 2009, the plant could produce 37 to 45 kW continuously for up to five hours. Despite its technical achievements, the plant was shut down in 1915 as a result of World War I's economic turmoil and the declining cost of fossil fuels.

Over the subsequent 50 years, engineers and scientists continued to refine focusing collector technology to heat working fluids and power machinery. These efforts have largely converged on two main technological paths: central receiver systems and distributed receiver systems. Both use various optical configurations, such as point-focus and line-focus concentrators, to capture and intensify sunlight. Central receiver systems, for instance, utilize vast fields of The operating temperature of solar receivers can vary widely, from around 100°C in low-temperature trough systems to nearly 1500°C in more advanced dish and central receiver designs (SERI, 1987 as cited in Kalogirou, 2009).

Megawatt-scale power is produced by several large-scale solar plants in the modern period, either for industrial process heat or electricity. In 1979, Albuquerque, New Mexico, saw the start of the first commercial solar facility in history. This plant produced 5 MW of power using 220 heliostats. Later, a second, bigger facility with a 35 MW thermal output was built near Barstow, California. The majority of solar thermal plants nowadays are built to generate electricity or heat for industrial uses; they frequently produce superheated steam at temperatures of 673 K, or roughly 400°C. Small-scale, traditional desalination plants that run on thermal or electrical energy can be powered by this steam since it can be utilized directly or to produce electricity.

A parallel area of solar application, focused on residential hot water and space heating, first emerged in the mid-1930s but only gained significant traction in the late 1940s. At that time, the vast majority of homes relied on coal-fired boilers for heating. The initial concept was straightforward: to use solar energy to heat water that could then be circulated through existing radiator systems (Kalogirou, 2009).

During the earl 1960s commercial manufacturing of solar water heaters began and quickly expanded into a global industry.

The most common configuration for these systems is the thermosiphon type. An insulated storage tank with a capacity of 150 to 180 liters and two flat-plate solar collectors with a combined absorber area of 3 to 4 m² make up a typical device, which is supported by a frame. These systems frequently include a heat exchanger connected to a central heating system or an additional electric immersion heater to provide a steady supply of hot water during times of low sunlight. The forced circulation system is another well-liked concept. Only the solar collectors on the roof are visible in this configuration. The system is completed with a network of pipes, a circulation pump, and a differential thermostat to regulate operation. The hot water storage tank is situated indoors, usually in a utility room.

While this type is often preferred for its cleaner architectural appearance, it is generally more expensive to install than a thermosiphon system, particularly for smaller residential applications (Kalogirou, 1997 as cited in Kalogirou, 2009).

2. SOLAR PHOTOVOLTAIC (PV) TECHNOLOGIES: MATERIAL ADVANCEMENTS

The photovoltaic (PV) effect was first observed in selenium by the French physicist Edmond Becquerel in 1839. More than a century later, in 1958, the development of silicon solar cells achieved a conversion efficiency of 11%, though their astronomical cost—around $1,000 per watt—made them impractical for most applications. Their first practical use was in the space program, where the premium on a reliable power source outweighed the expense. Alternative photovoltaic materials, such gallium arsenide (GaAs), were discovered as a result of research conducted throughout the 1960s. These materials were far more costly than silicon, even though they could tolerate higher

operating temperatures. Global installed solar capacity peaked at around two gigawatts by the end of 2002 (Lysen, 2003). Semiconductors, which transmit electricity more effectively than insulators but not as well as metals, are used to make photovoltaic cells.

The most widely used semiconductor for this purpose is silicon (Si), along with compounds such as cadmium sulphide (CdS), cuprous sulphide (Cu_2S), and gallium arsenide (GaAs).

A distinct category is amorphous silicon (a-Si) cells. Unlike traditional crystalline cells, these are made from a thin, homogeneous layer of silicon atoms without a regular crystal structure. This material absorbs light far more efficiently than crystalline silicon, allowing the cells to be much thinner. For this reason, amorphous silicon is classified as a thin-film PV technology. It can be deposited onto a variety of substrates, both rigid (like glass) and flexible (like plastic or steel), making it well-suited for curved surfaces or foldable modules. The main trade-off is efficiency; amorphous cells typically achieve only about 6%, which is lower than their crystalline counterparts. However, their simpler manufacturing process makes them significantly cheaper to produce, making them ideal for cost-sensitive applications where top-tier efficiency is not a priority.

Amorphous silicon is essentially a glassy alloy composed of silicon and approximately 10% hydrogen. Its appeal for thin-film solar cells stems from several key properties:

1. Material Abundance: Silicon is one of the most common elements on Earth and is non-toxic.
2. High Light Absorption: It absorbs sunlight so effectively that the active layer needs to be only about 1 micrometer thick. This is a fraction of the 100 micrometers or more required for crystalline silicon

cells, drastically reducing the amount of material needed.

3. Substrate Versatility: It is possible to directly apply thin films of a-Si on low-cost supporting materials like glass, sheet steel, or even plastic foil.

Other potential materials are gaining pace in the PV business in addition to silicon-based solutions. Among them are copper indium di selenide (CIS) and cadmium telluride (CdTe). These technologies' primary benefit is that, in contrast to crystalline silicon, they can be produced using comparatively inexpensive industrial techniques, and they usually provide greater module efficiencies than amorphous silicon. In addition to that, crystalline silicon panels continue to be expensive.

To further decrease the levelized cost of electricity generated by photovoltaics, there is a strong need for multi-junction architectures that can surpass the fundamental efficiency ceiling of single-junction devices (Aydin et al., 2024). A particularly promising approach to achieving this is the use of all-perovskite tandem solar cells. These devices exploit the unique ability of perovskite materials to have their bandgaps precisely tuned (Marti & Araújo, 1996). This tunability makes it possible to stack two or more sub cells, each with complementary bandgaps, within a single device. The key advantage of this configuration is a significant reduction in energy losses from photon thermalization. As a result, all-perovskite tandems have achieved record certified power conversion efficiencies (PCEs) exceeding 30%, thus outperforming both single-junction silicon cells, which peak at 27.4%, and single-junction perovskite cells, which max out at 26.7% (Green et al., 2025). Furthermore, certified efficiencies for all-perovskite tandem mini-modules have reached 24.8%, a notable improvement over the 23.2% efficiency of single-junction perovskite modules (Green et al., 2025). Individual PV cells are put together into modules that are

intended to generate a particular voltage and current when exposed to light in order to provide a workable power source. After that, these modules can be joined in parallel to increase current or in series to raise voltage. Because of their great versatility, photovoltaic systems can be connected with other electrical power sources or run independently (off-grid). Photovoltaic (PV) systems fall into two basic categories: stand-alone (off-grid) and grid-connected systems. They are used for a wide range of purposes, such as powering communications equipment on Earth and in space.

Stand-alone PV systems are designed for locations that are difficult to access or simply not served by the main electricity grid. Operating independently, these systems typically store the energy they generate in batteries for later use. A standard configuration include one or more PV modules to generate power, a bank of batteries for storage, and a charge controller to manage the flow of electricity and protect the batteries. Often, an inverter is also incorporated to convert the direct current (DC) produced by the modules into the alternating current (AC) required by standard household appliances.

In contrast, grid-connected PV systems are integrated directly with the local electricity network. This connection allows for two-way energy exchange. The PV system's electricity can be used right away to power the building during the day, which is a typical situation for offices and commercial buildings.

Alternatively, particularly for residential systems where the occupants might be away during the day, the excess power can be sold back to an electricity supply company. Then, during the evening or at times when the solar system isn't producing enough power, electricity can be purchased from the network as usual. In this setup, the electrical grid itself effectively acts as an unlimited storage system, eliminating the need for on-site battery

banks. Beside all those, recent developments shows the integration of these systems togethers, as PVT (photovoltaic thermal systems), (Gurler et al., 2018).

When photovoltaic technology began to be deployed in large-scale commercial applications around two decades ago, typical system efficiencies were below 10%. Today, commercial module efficiencies have improved significantly, reaching approximately 23%. In laboratory settings, experimental cells have achieved efficiencies exceeding 30%, although these high-performance units are not yet commercially available.

3. REGIONAL TRENDS AND BIBLIOGRAPHIC ANALYSIS

The rapid development of photovoltaic (PV) technologies has resulted in a substantial increase in scientific publications addressing various aspects of solar energy systems, including materials, system optimization, artificial intelligence applications, and energy management strategies. In order to understand the structure and evolution of this research field, bibliographic and keyword-based analyses have become essential tools for identifying dominant research themes, emerging technological directions, and potential knowledge gaps.

In this study, a comprehensive bibliographic dataset consisting of 900 research articles published in 2026 was collected from the ScienceDirect database. The selection of articles was based on keywords related to photovoltaic technologies, solar energy systems, optimization techniques, machine learning, and intelligent energy management. The bibliographic data were analyzed using VOSviewer software, a widely used bibliometric visualization tool that enables the mapping of relationships between keywords, research themes, and scientific clusters through co-occurrence analysis.

The visualization produced by VOSviewer illustrates the relationships among keywords extracted from the analyzed publications. In these maps, each node represents a keyword, while the size of the node reflects the frequency of its occurrence within the dataset. Links between nodes indicate co-occurrence relationships, meaning that the connected keywords frequently appear together in the same research articles. Additionally, the spatial distribution of nodes and their clustering provide insights into the structure of the research field and the interaction between different research themes.

Figure 2 presents the keyword co-occurrence network derived from the dataset. The figure shows that several keywords form central nodes within the network, including “photovoltaic,” “solar energy,” and “photovoltaic systems.” These keywords represent the core themes of contemporary solar energy research. Surrounding these central nodes are several thematic clusters that highlight major research directions. One prominent cluster relates to artificial intelligence and data-driven methods, including keywords such as machine learning, deep learning, photovoltaic power forecasting, and fault detection. This indicates the increasing role of AI-based techniques for performance prediction, system monitoring, and intelligent control of photovoltaic systems.

Another important cluster observed in the network relates to advanced photovoltaic materials and emerging technologies, including keywords such as organic solar cells, perovskites, and flexible photovoltaic devices. These topics reflect ongoing efforts to improve solar cell efficiency, reduce production costs, and develop lightweight or flexible solar modules suitable for diverse applications. Additional keywords such as computational fluid dynamics (CFD) highlight research focused on system performance optimization and energy harvesting efficiency. Overall, the network demonstrates that modern photovoltaic

research is increasingly interdisciplinary, combining material science, energy engineering, computational modeling, and artificial intelligence.

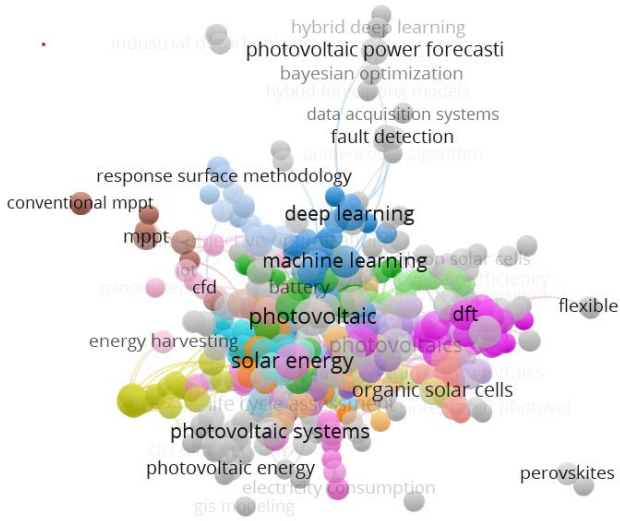

Figure 2. Keyword co-occurrence network of photovoltaic research topics generated using VOSviewer based on 900 articles from the ScienceDirect database (2026).

To further examine the intensity of research activity within different thematic areas, a density visualization map was generated, as shown in Figure 3 In this visualization, the color gradient represents the concentration of research topics based on keyword frequency and co-occurrence intensity. Areas with brighter colors indicate higher research density, while darker regions represent relatively lower research activity. The density map clearly shows that the highest concentration of research is centered around photovoltaic technologies, solar energy systems, and machine learning applications, indicating that these topics are currently the most extensively investigated in the field.

The strong presence of keywords related to deep learning, photovoltaic power forecasting, and fault detection suggests that data-driven optimization techniques are becoming increasingly

important for improving the reliability and operational efficiency of solar energy systems. Meanwhile, emerging topics such as perovskite solar cells, flexible photovoltaics, and organic solar cells appear in regions of lower density, indicating that although these areas are gaining increasing attention, they still represent developing research domains with considerable potential for future investigation.

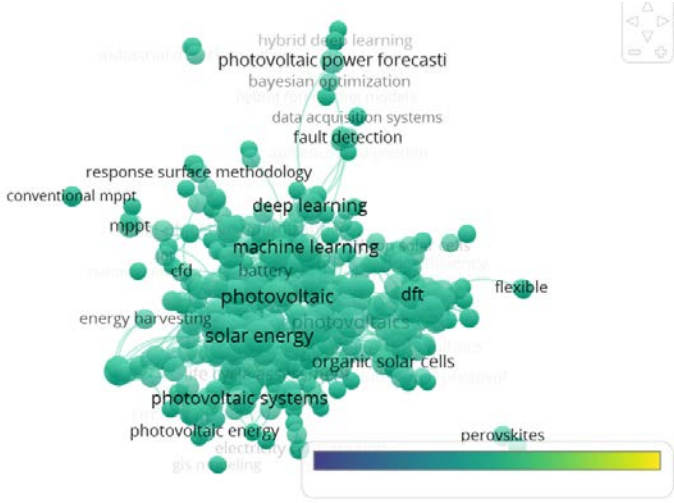

Figure 3. Density visualization of photovoltaic research topics generated using VOSviewer from keyword co-occurrence data.

Despite the significant growth in photovoltaic research, the bibliographic analysis highlights several important research needs and gaps. First, many existing studies tend to focus on either photovoltaic material development or system-level optimization separately, with limited integration between these domains. A more comprehensive approach that simultaneously considers advanced photovoltaic materials, intelligent control strategies, and system performance optimization remains necessary.

Second, although machine learning and deep learning techniques are increasingly applied for photovoltaic power

forecasting and fault detection, their practical integration into real-time photovoltaic system management and energy optimization frameworks is still relatively limited. Many studies remain theoretical or simulation-based, leaving opportunities for further research on real-world implementation and operational integration.

Furthermore, the bibliographic results reveal that emerging technologies such as perovskite solar cells and flexible photovoltaic systems are still underrepresented compared to traditional photovoltaic technologies. These technologies have the potential to significantly improve solar energy deployment in applications such as building-integrated photovoltaics (BIPV), portable energy systems, and lightweight solar installations. Therefore, further research is required to address issues related to long-term stability, scalability, and commercial feasibility of these advanced materials.

Finally, although photovoltaic research has expanded globally, there remains a need for more region-specific analyses that consider geographical, climatic, and policy-related factors influencing solar energy adoption. Regional studies are particularly important for optimizing photovoltaic system design, improving energy planning strategies, and supporting sustainable energy transitions in different parts of the world.

In this context, the present bibliographic analysis provides valuable insights into current research trends, emerging technologies, and potential research opportunities in the photovoltaic sector. By analyzing a large dataset of 900 scientific articles using VOSviewer, the study contributes to a better understanding of the evolving knowledge structure of photovoltaic research and highlights key areas that require further investigation.

4. TECHNOECONOMIC ANALYSIS

Techno-economic analysis is a comprehensive evaluation method that integrates both the technical performance and the economic feasibility of a project. It is widely used in energy system planning, particularly in renewable energy technologies such as solar photovoltaic (PV), wind, and hybrid energy systems. The purpose of techno-economic analysis is to determine whether a project is technically viable and economically profitable under given operating conditions (Short et al., 1995; IRENA, 2012).

The technical analysis focuses on the design, configuration, and operational performance of the energy system. In solar photovoltaic applications, this includes the selection and evaluation of different system configurations such as fixed PV systems, single-axis or dual-axis tracking systems, and floating photovoltaic systems, as well as the assessment of their electrical and mechanical components, energy production potential, and system efficiency. Technical performance is usually simulated using specialized software tools such as PVsyst, HOMER Pro, and the System Advisor Model (SAM), which allow researchers to estimate system output under different environmental and operational conditions.

While PVs were once considered a prohibitively expensive solar technology, the costs have dropped considerably. Based on the recent datas the cost of the solar pv technologies have dropped considerably, as shown in table.1 (IRENA, 2025).

Table 1. Total installed cost, capacity factor and LCOE trends by technology, 2010 and 2024

	Total installed costs (2023 USD/kW)			Capacity factor (%)			Levelized cost of electricity (2023 USD/kWh)		
	2010	2023	Percent change	2010	2023	Percent change	2010	2023	Percent change
Bioenergy	3 010	2 730	-9%	72	72	0%	0.084	0.072	-14%
Geothermal	3 011	4 589	52%	87	82	-6%	0.054	0.071	31%
Hydropower	1 459	2 806	92%	44	53	20%	0.043	0.057	33%
Solar PV	5 310	758	-86%	14	16	14%	0.46	0.044	-90%
CSP	10 453	6 589	-37%	30	55	83%	0.393	0.117	-70%
Onshore wind	2 272	1 160	-49%	27	36	33%	0.111	0.033	-70%
Offshore wind	5 409	2 800	-48%	38	41	8%	0.203	0.075	-63%

Source: (International Renewable Energy Agency(IRENA), 2025)

The economic analysis, on the other hand, evaluates the financial feasibility of the project by estimating investment costs, operational and maintenance costs, system lifetime, and the overall economic return of the system. Several economic indicators are commonly used in techno-economic studies to assess project profitability and financial sustainability. These indicators are ;

Net Present Value (NPV) represents the difference between the present value of the project's revenues and the present value of its costs over the system lifetime. A positive NPV indicates that the project is economically feasible.

$$NPV = \sum_{t=0}^{n} \frac{C_t}{(1+r)^t} \quad (1)$$

Where: C_t= net cash flow at year t ; r= discount rate; t= time period; n= project lifetime

Levelized Cost of Energy (LCOE) represents the average cost of producing electricity over the entire lifetime of the system. It is widely used to compare the economic competitiveness of different energy technologies.

$$LCOE = \frac{\sum_{t=0}^{n} \frac{I_t + O_t + M_t}{(1+r)^t}}{\sum_{t=0}^{n} \frac{E_t}{(1+r)^t}} \quad (2)$$

Where: I_t= investment expenditures in year t; O_t= operation costs; M_t= maintenance costs; E_t= electricity generated in year t; r= discount rate; n= system lifetime

Internal Rate of Return (IRR) is the discount rate that makes the net present value equal to zero. It represents the expected rate of return of the investment.

$$0 = \sum_{t=0}^{n} \frac{C_t}{(1+IRR)^t} \quad (3)$$

A project is generally considered attractive if the IRR is greater than the required rate of return.

Payback Period (PP) is the time required for the project to recover its initial investment from the generated cash flows. The payback period provides a simple measure of how quickly the investment becomes profitable.

$$PP = \frac{Investment}{Annual\ Net\ Cash\ FlowInitial} \quad (4)$$

In modern renewable energy studies, these techno-economic evaluations are frequently conducted using advanced simulation tools such as HOMER Pro, PVsyst, and SAM, which

integrate technical system modeling with financial analysis to support decision-making for energy planning and investment.

5. CONCLUSION

This chapter has provided a comprehensive overview of advanced photovoltaic technologies, their evolution from early historical applications of solar concentration to modern high-efficiency systems. The fundamental principles of photovoltaic energy conversion were examined alongside the diverse range of PV technologies currently available, including crystalline silicon, thin-film, and emerging material systems. The bibliographic analysis of 900 research articles using VOSviewer revealed the evolving structure of photovoltaic research. Keyword co-occurrence networks demonstrated that artificial intelligence and machine learning techniques have become increasingly integrated into PV research, particularly for power forecasting, fault detection, and system optimization. The density visualization confirmed that while traditional PV materials remain heavily investigated, emerging topics such as perovskite solar cells, flexible photovoltaics, and organic solar cells represent growing research frontiers with substantial future potential. Notably, the analysis identified a persistent gap between materials-focused research and system-level optimization studies, suggesting opportunities for more integrated approaches that simultaneously address efficiency enhancement and practical implementation challenges.

In addition to technological advancements, the practical implementation of photovoltaic systems also requires careful techno-economic evaluation to ensure their feasibility and long-term sustainability. While high efficiency remains a critical parameter in PV development, the economic viability of solar technologies depends on factors such as installation cost,

operational and maintenance expenses, system lifetime, and overall energy yield. Therefore, techno-economic indicators such as the Levelized Cost of Energy (LCOE), Net Present Value (NPV), Internal Rate of Return (IRR), and Payback Period are commonly used to assess the financial performance of photovoltaic systems. As PV technologies continue to evolve toward higher efficiencies and improved materials, integrating technical performance with economic assessment will remain essential for guiding future deployment strategies and supporting the global transition toward sustainable energy systems.

REFERENCES

Aydin, D., Gürler, T., & Sözen, A. (2024). Experimental investigation of a novel photovoltaic–thermal based solar still system. *Solar Energy*, 258, 1–12.

Branker, K., Pathak, M. J. M., & Pearce, J. M. (2011). A review of solar photovoltaic levelized cost of electricity. *Renewable and Sustainable Energy Reviews, 15*(9), 4470–4482. https://doi.org/10.1016/j.rser.2011.07.104

Green, M. A., Dunlop, E. D., Hohl-Ebinger, J., Yoshita, M., & Ho-Baillie, A. W. Y. (2025). Solar cell efficiency tables (Version 65). *Progress in Photovoltaics: Research and Applications*, 33(1), 3–12.

Gurler, T., Aydin, D., & Sözen, A. (2018). Performance analysis of a solar still integrated with photovoltaic/thermal collector. *Energy Conversion and Management*, 171, 1191–1200.

International Renewable Energy Agency (IRENA). (2025). *Renewable power generation costs in 2024.* Abu Dhabi, UAE: IRENA. (Accessed online 07/03/2026)

International Renewable Energy Agency (IRENA). (2012). *Renewable energy technologies: Cost analysis series*. IRENA.

Jordan, R. C., & Ibele, W. (1956). A theory of solar distillation. *Journal of Applied Meteorology*, 1(2), 229–236.

Kalogirou, S. A. (1997). Solar thermal collectors and applications. *Progress in Energy and Combustion Science*, 30(3), 231–295.

Kalogirou, S. (2009). Solar energy engineering: Processes and systems. Academic Press.

Kreider, J. F., & Kreith, F. (1977). Solar heating and cooling: Engineering, *practical design, and economics*. New York, NY: McGraw-Hill.

Kreith, F., & Kreider, J. F. (1978). *Principles of solar engineering*. Washington, DC: Hemisphere Publishing.

Lazard. (2023). *Levelized cost of energy analysis – Version 16.* Lazard Ltd.

Lysen, E. H. (2003). *The history of solar energy*. London, UK: Earthscan.

Marti, A., & Araújo, G. L. (1996). Limiting efficiencies for photovoltaic energy conversion in multigap systems. *Solar Energy Materials and Solar Cells*, 43(2), 203–222.

Meinel, A. B., & Meinel, M. P. (1976). *Applied solar energy: An introduction*. Reading, MA: Addison-Wesley.

Mouchot, A. (1878). *La chaleur solaire et ses applications industrielles*. Paris, France: Gauthier-Villars.

Mouchot, A. (1880). *Solar energy and its industrial applications*. Paris, France: Gauthier-Villars.

Solar Energy Research Institute. (1987). *Solar energy technologies handbook*. Golden, CO: SERI.

ADDITIVE MANUFACTURING OF SANDWICH STRUCTURES: PROCESSES AND CORE ARCHITECTURES

Neslihan TOP[1]

1. INTRODUCTION

Sandwich structures are multilayered structural systems created by placing a lightweight core material between two thin, rigid surface layers (Kamble, 2024; Ma et al., 2021a). In this configuration, the surface layers carry bending and in-plane loads, while the core layer resists shear stresses, providing the structure with high bending rigidity, buckling resistance, and energy absorption capacity (Sarvestani et al., 2018). Therefore, sandwich structures stand out as structural solutions offering high mechanical performance with low weight. In sandwich structures, surface layers can be made of metal or composite materials. Steel and aluminum alloys are commonly used for metal surfaces, while glass, carbon, and aramid fiber-reinforced polymer composites are widely used for composite surfaces due to their high strength and rigidity properties (Sahu et al., 2022). Core structures typically consist of foam or cellular geometries, with honeycomb and corrugated core structures being among the most common architectures. Due to their high specific rigidities, energy absorption capacities, and thermal insulation properties, sandwich structures are widely used in the aerospace, automotive, marine, and construction industries (Ma et al., 2021b; Top et al., 2025; Sahib et al., 2023). However, conventional manufacturing

[1] Assist. Prof. Dr., Gazi University, Faculty of Technology, Dept. of Industrial Design Engineering, ORCID: 0000-0002-0771-6963.

methods often require multi-stage production processes, and core geometries are generally limited to simple structures.

In recent years, additive manufacturing (AM) technologies have emerged as a significant alternative method in sandwich structure production. This approach, encompassing technologies such as photopolymerization, material extrusion, and powder-bed fusion, allows for the production of complex core geometries, offering significant design freedom in sandwich structure design. These advancements have enabled the creation of sophisticated structural configurations such as complex cellular core architectures, TPMS-based surfaces, and biomimetic core designs. In this context, examining the fundamental principles and manufacturing methods of sandwich structures becomes increasingly important. In this context, it is important to examine the fundamental structural principles, manufacturing methods, and core architectures of sandwich structures. This section first introduces the basic structural principles and material systems used in sandwich structures, followed by a discussion of manufacturing methods and core architectures, and finally reviews the role of additive manufacturing technologies in the design and production of sandwich structures based on the existing literature.

2. FUNDAMENTALS OF SANDWICH STRUCTURES

Sandwich structures are multilayer structural systems consisting of two thin, high-rigidity surface layers with a lightweight core layer in between (Figure 1a). This configuration offers significant advantages in engineering applications by providing high flexural rigidity and strength with low mass.

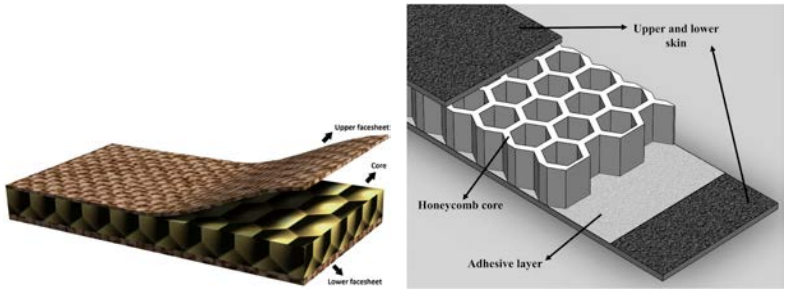

Figure 1. (a) A typical sandwich panel (Sadiq and Kovacs, 2025) (b) Schematic representation of sandwich structure (Mirzaei et al., 2025)

The mechanical behavior of sandwich structures largely depends on the functional load sharing between the surface layers and the core. The surface layers increase the bending rigidity and moment-carrying capacity of the structure, while the core layer, by creating a distance between the two surfaces, carries shear stresses and prevents local buckling, thereby increasing the stability of the structure. The thickness of the core affects energy absorption and allows it to withstand high compressive stress under constant stress. (Gibson & Ashby, 1997). Load transfer between the surface layers and the core is typically achieved through epoxy-based adhesives or resin systems (Figure 1b). This structure is often used in applications subjected to compressive or aerodynamic loads due to its high flexural rigidity and buckling resistance.

In structural sandwich applications, the thickness of the surface layers is typically around a few millimeters, while the core layer exhibits a significantly thicker structure in comparison, sometimes exceeding 50 mm in some applications (Birman and Kardomateas, 2018). However, in most practical engineering applications, the core thickness remains below this value. These aspect ratios constitute the characteristic geometric feature of sandwich structures and reveal the classic sandwich structure behavior where the surface layers carry bending loads and the

core layer carries shear stresses. The surface layers and core materials of sandwich structures may not always be homogeneous. Surface layers are often made of fiber-reinforced composites such as carbon fiber reinforced polymer, glass fiber, aluminum alloys, carbon or kevlar fiber, and aramid fiber composites, while metallic materials such as aluminum and steel are also used in some applications(Castanie et al., 2020; Junaedi et al., 2024; Sun et al., 2026). Surface layers can consist of a single metal layer, or they can be made of multilayered (laminated) or woven composite materials. Core materials, on the other hand, mostly consist of lightweight and cellular structures such as low-density foams, honeycomb structures, or metal foams (Sadiq & Kovacs, 2025). In conventional manufacturing methods, sandwich panels are typically obtained by bonding surface layers to a core; this process is usually accomplished using methods such as vacuum bagging, hot pressing, or autoclave curing. However, these methods limit the production of complex internal geometries, add extra weight to the structure due to additional adhesive layers, and can prolong production time. These limitations have increased interest in additive manufacturing (AM) technologies for the production of sandwich structures in recent years. Thanks to its layered manufacturing principle, AM allows for the direct production of complex cellular core geometries without the need for molds, enabling the production of designs such as TPMS-based surfaces, biomimetic architectures, and advanced cellular structures. This makes it possible to enhance the mechanical performance and energy absorption capacity of sandwich structures, thereby expanding their potential for use as lightweight, high-performance structures, particularly in the aerospace, automotive and energy sectors.

3. ADDITIVE MANUFACTURING TECHNIQUES FOR SANDWICH STRUCTURES

Additive manufacturing technologies offer more integrated production approaches compared to conventional methods in the production of sandwich structures. In conventional manufacturing processes, the surface layers and core are typically prepared in separate production stages and then joined together using adhesives or mechanical fasteners. This multi-stage manufacturing approach both complicates the production process and can lead to the formation of weak junction regions, particularly at the interface between the surface layer and the core. Thanks to the layered manufacturing principle, in additive manufacturing processes, the surface layers and core region of sandwich structures can be produced integrally in a single production process. This provides better structural continuity between the different components of the structure and reduces mechanical weaknesses arising from interfaces. (Figure 2a). However, hybrid manufacturing strategies are also used in some applications (Hou et al., 2013). In this approach, the core structure is produced using additive manufacturing methods, while the surface layers are prepared using traditional composite or metal manufacturing techniques and then bonded to the core via adhesive or mechanical connections (Figure 2b). Hybrid manufacturing approaches are preferred, particularly for industrial engineering applications requiring segmented composite surface layers with high strength and high rigidity.

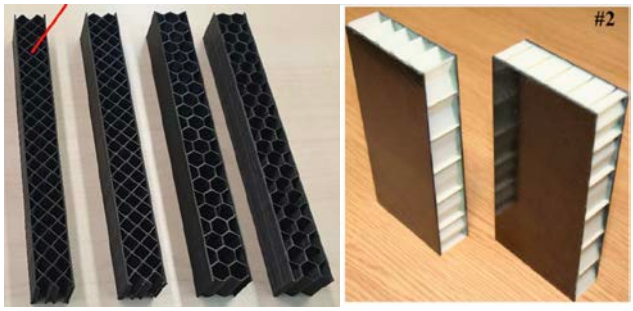

(a) **(b)**

Figure 2. 3B baskılı sandwich yapılar: (a) core and skins are integrally (Faidallah et al., 2023) (b) Hybrid sandwich structures (Hou et al., 2013)

One of the most important advantages of additive manufacturing (AM) technologies is that they enable the direct fabrication of core structures with complex internal geometries. Thanks to AM, complex core geometries, advanced core designs such as TPMS-based structures and biomimetic architectures can be produced. Such architectures offer significant structural advantages such as high specific rigidity, improved energy absorption capacity, and more efficient load-carrying behavior. In addition, AM processes contribute to the performance-oriented optimization of sandwich structures by enabling the design and production of functionally stepped core structures (Birman and Kardomateas, 2018). Because of these characteristics, additive manufacturing technologies play a significant role in the development of lightweight and high-performance sandwich structures, particularly for use in the aerospace, automotive, and energy sectors (Castanie et al., 2020; Sarvestani et al., 2018; Ma et al., 2021b). The main AM methods commonly used in sandwich structure production include material extrusion (FDM/FFF), VAT photopolymerization (SLA/DLP), and powder bed fusion (SLM/SLS) technologies. These methods offer a wide range of applications in the design and production of sandwich

structures by providing different material systems and manufacturing capabilities.

3.1. Material Extrusion (MEX/FDM / FFF)

Material extrusion (MEX), also known in the literature as Fused Deposition Modeling (FDM) or Fused Filament Fabrication (FFF), is one of the most widely used methods among polymer-based additive manufacturing technologies. This process is based on the principle of melting thermoplastic filaments and depositing them in layers onto the printing plate through a nozzle (Figure 3). Common materials used in the MEX process include Acrylonitrile Butadiene Styrene (ABS) and Polylactic Acid (PLA). PLA is frequently preferred for its good printability, suitable mechanical properties, and biodegradability (Faidallah et al., 2023). The selection of materials and the optimization of production parameters can significantly improve the mechanical performance of structures produced using MEX (Pollard et al., 2017). However, the microstructure resulting from the AM process can lead to disadvantages such as mechanical anisotropy, weak interlayer bonding, and internal porosity not found in cast polymers (Leśniowski et al., 2025). While parameters such as layer height, printing direction, infill pattern, and nozzle characteristics play a decisive role in the production of sandwich core structures, anisotropy resulting from layer direction and thermal residual stresses generated during printing are among the important factors to be considered in evaluating the energy absorption behavior (Mirzaei et al., 2025).

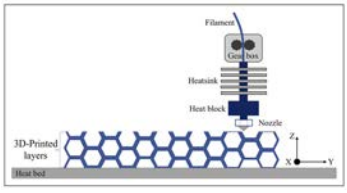

Figure 3. Schematic representation of MEX process (Mirzaei et al., 2025).

There are numerous studies in the literature on the use of MEX-based layered manufacturing methods in the production of sandwich structures, and a significant proportion of these studies focus on the effect of different core geometries on mechanical behaviour. Faidallah et al. (2023) demonstrated that rhombus geometry offers higher mechanical performance in one-piece rhombus and honeycomb core sandwich structures made of PLA material. Similarly, Sugiyama et al. (2018) reported that rhombus core design provides the highest strength and stiffness values in sandwich structures fabricated by continuous carbon fiber reinforced 3D printing. Brejcha et al. (2025) reported that structures with flax fiber–reinforced face sheets and a foamed PLA core exhibited good flexural performance, while Mirzaei et al. (2025) showed that core orientation plays a decisive role in the energy absorption capacity of sandwich structures with carbon fiber face sheets. Furthermore, in studies combining different manufacturing approaches, Dikshit et al. (2016) revealed that core geometry significantly affects external plane compressive strength and damage behavior, while Vellaisamy and Munusamy (2024) and Haldar et al. (2021) reported that cell size, core thickness, and core-surface layer interaction are determining factors in the energy absorption capacity and compressive strength of sandwich structures.

Various studies exist that utilize different material systems and core topologies in MEX-based additive manufacturing processes. Bharath et al. (2021) produced sandwich structures with one-piece HDPE surface layers and a glass microballoon-reinforced synthetic foam core using the FFF method and showed that the microballoon ratio increased the specific modulus and strength. Türkoğlu et al. (2023) reported that auxetic core designs offer higher load-carrying and energy absorption capacities compared to honeycomb geometry. Zaharia et al. (2020) and Junaedi et al. (2024) demonstrated that core topology and density

significantly affect mechanical performance in sandwich structures with biopolymer and gyroid cores. In recent years, research on the use of 3D-printed sandwich structures in advanced engineering applications has increased. In this context, Yazdi et al. (2024) investigated the behavior under explosive loading, while de Castro et al. (2021) developed PLA-based sandwich panels in which both the face sheets and the core were produced in a single manufacturing step.

Studies in the literature show that the MEX method provides high design flexibility in sandwich structure manufacturing and that the mechanical performance of sandwich structures can be significantly improved, especially by optimizing the core geometry.

3.2. VAT Photopolymerization (SLA / DLP)

Photopolymerization is an additive manufacturing method based on the principle of curing liquid photopolymer resins layer by layer with the help of a light source. This manufacturing approach, encompassing technologies such as stereolithography (SLA) and digital light processing (DLP), is widely used in the production of sandwich structures, particularly those with complex geometries, due to its high surface quality and dimensional accuracy (Figure 4). Thanks to these technologies, complex core architectures that are difficult to produce with conventional manufacturing methods can be manufactured with high precision, and new design possibilities are emerging to improve the mechanical performance of sandwich structures.

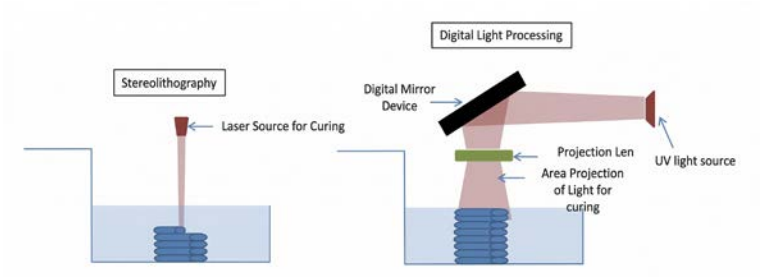

Figure 4. VAT Polimerization method: (a) SLA (b) DLP (Lee et al., 2018)

The literature shows that additive manufacturing methods based on VAT photopolymerization are increasingly used in sandwich structure production. Yıldız et al. (2024) produced Al_2O_3 honeycomb sandwich structures using an SLA based additive manufacturing method and investigated the effects of debinding atmosphere on condensation and mechanical properties. Williams et al. (2011) demonstrated that cores produced by the SLA method provide higher flexural rigidity and load-carrying capacity in carbon-epoxy sandwich structures. Similarly, Ma et al. (2021) investigated the compressive behavior of sandwich panels produced by the SLA method and reported that core wall thickness significantly increased energy absorption capacity and mechanical performance.

In recent years, studies on cellular and metamaterial core structures have increased significantly. Vasile et al. (2024) investigated the mechanical behavior of different TPMS-based thin-walled metamaterial core structures produced by the SLA method and showed that some new TPMS geometries offer higher mechanical performance compared to the gyroid structure. Yazıcı et al. (2024) investigated auxetic and honeycomb core sandwich beams produced with SLA and showed that the arrowhead-shaped auxetic geometry offers higher load carrying and energy absorption capacity. Furthermore, Challapalli and Li (2021) designed novel geometric structures that can be used in sandwich

structure cores using machine learning and showed that these structures, produced by the SLA method, exhibit higher buckling and bending strength compared to the classical eight-cell structure. However, Gao et al. (2020) fabricated 3Y-TZP ceramic honeycomb sandwich structures using a DLP-based additive manufacturing method and showed that core geometry has a significant effect on bending performance, with square honeycomb cores providing higher bending strength compared to hexagonal cores.

These studies demonstrate that VAT photopolymerization-based AM methods have significant potential in the design and production of sandwich structures, and contribute to improving structural performance, particularly by enabling the development of complex core geometries.

3.3. Powder Bed Fusion (SLM / SLS)

Powder Bed Fusion (PBF) based AM methods rely on the principle of sintering or melting metal or polymer powders in layers using an energy source (usually a laser). (Figure 5). This manufacturing approach enables the high-precision fabrication of cellular and lattice core architectures with complex internal geometries, offering significant advantages in sandwich structure design. Among PBF methods, Selective Laser Melting (SLM) and Selective Laser Sintering (SLS) are particularly widely used in the production of sandwich structures made from metal and high-performance polymer materials.

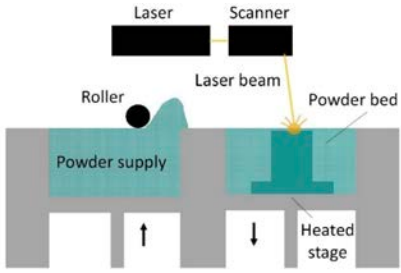

Fig 5. Representation of the PBF process (Datsiou and Ashcroft, 2024)

3.3.1. Selective Laser Melting (SLM)

SLM method is a PBF technique that allows for the complete melting of metal powders using laser energy, thus enabling the creation of dense and high-strength structures. This method is widely used, especially in the production of sandwich structures with metallic lattice cores. Yao et al. (2026) fabricated gradian-thickness TPMS core sandwich structures using the SLM method and showed that this design improved the bending stiffness, peak load capacity, and energy absorption performance through three-point bending tests and finite element analyses.

SLM technology has been shown to be effectively used in applications requiring high strength. Huang et al. (2026) investigated the near-field explosion behavior of 316L stainless steel honeycomb core sandwich structures produced by the SLM method using experimental and numerical methods and showed that filling the core with PVC foam improved the explosion resistance by increasing the energy absorption capacity of the structure. Similarly, Zhang et al. (2025) fabricated plate-reinforced X-lattice core sandwich structures and reported that these structures had high specific strength, but their compressive strength decreased significantly with increasing temperature. SLM technology is also being investigated for sandwich structures operating in high-temperature environments. Wen et al. (2026) developed a theoretical model to predict the equivalent

thermal conductivity of sandwich structures made of Ti600 alloy and validated this model with experimental and numerical analyses. The study results showed that significantly improved thermal insulation performance at high temperatures can be achieved by filling the core structure with aerogel and using a low relative density design.

3.3.2. Selective Laser Sintering (SLS)

The SLS method relies on creating layered structures by sintering polymer or ceramic powders with laser energy, and provides significant flexibility, especially in the production of lightweight cellular structures. This method allows the production of sandwich structures with different core architectures. For example, Li et al. (2021) developed meta-lattice sandwich panels by integrating the local resonance principle with cellular core sandwich structures. The results showed that these structures exhibit broadband low-frequency vibration damping capability. Similarly, Xu et al. (2025) reported that cellular sandwich panels produced by SLS method using glass fiber reinforced nylon composite have both high load carrying capacity and effective vibration damping performance. The SLS method is also used in the production of ceramic composite sandwich structures that require high temperature resistance. Zhang et al. (2020) fabricated SiCp/SiC composite sandwich panels using the SLS method and reinforced them with the PIP process. Compression tests showed that the elastic modulus and compressive strength decreased with increasing temperature, and the damage mechanisms changed at different temperatures.

Advanced core architectures that can be produced with SLS technology include cellular structures with porosity gradients. Fan et al. (2025) fabricated sandwich structures with a core architecture having a porosity gradient using the SLS method and investigated the bending behavior of these structures with

analytical models, experiments and numerical analyses. PBF methods are not limited to structural applications but are also used in functional material systems. Yang et al. (2019) developed a sandwich-structured nanocomposite consisting of $Na_3V_2(PO_4)_3$/N-doped carbon layers and showed that this structure provides high capacity and long cycle life as a cathode material for sodium ion batteries.

PBF-based additive manufacturing methods offer significant advantages, particularly in producing complex core architectures, utilizing high-performance materials, and designing functional sandwich structures. Therefore, techniques such as SLM and SLS make significant contributions to improving sandwich structure design in engineering applications requiring high strength, energy absorption, and vibration damping performance.

4. CORE ARCHITECTURES

One of the most important contributions of additive manufacturing technologies to sandwich structure design is that they enable the direct production of complex core architectures that are difficult or uneconomical to produce with traditional manufacturing methods. In sandwich building design, the core architecture is one of the fundamental elements that defines the internal geometry of the structure and determines the overall structural organization. The core structure not only forms an interlayer between two surface layers but also determines the mechanical behavior and structural character of the sandwich panel through properties such as cell shape, connection pattern, pore distribution, and topological continuity. While traditional sandwich structure designs have been largely limited to relatively simple cellular geometries such as foam, honeycomb, and corrugated, the development of additive manufacturing

technologies has made it possible to develop much more complex basic architectures in this field (Birman & Kardomateas, 2018).

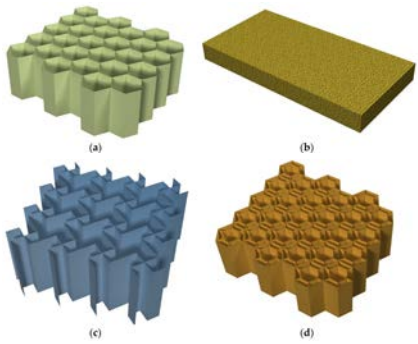

Figure 6. Typical core configurations: (a) Honeycomb, (b) foam, (c) 2D auxetic architecture, and (d) Bio inspired architecture (Sadiq & Kovács, 2025).

Thanks to the additive manufacturing principle, advanced internal geometries such as three-dimensional cellular networks, topologies composed of continuous surfaces, and biomimetic structures can be produced, thus moving beyond classical cell-based approaches in nuclear design. In this context, the main architectural approaches that stand out with the design freedom provided by additive manufacturing include lattice structures, triple periodic minimal surface (TPMS) based cores, biomimetic architectures, and functional gradient core designs (Al-Khazraji et al., 2022). Among traditional core architectures, honeycomb structures are among the most commonly used designs, and in addition to hexagonal cell arrangements, square, triangular, circular, and auxetic variations also exist (Choudhari et al., 2022). More advanced architectures, such as TPMS-based cores, offer homogeneous pore distribution and a highly customizable internal cavity architecture thanks to seamless surface networks based on continuous and periodic surface geometries such as gyroid, diamond, and Schwarz (Figure 7a) (Vasile et al., 2024).

Furthermore, since these structures can be easily modified parametrically, they allow for controlled design of architectural parameters such as cell size, surface thickness, and internal channel continuity.

Biomimetic core architectures are designs developed by drawing inspiration from structural organisations found in nature (Figure 7b). The biomimetic approach enables the transfer of biological structures and functions from nature into sandwich composite design, improving interface compatibility and structural performance between heterogeneous materials (Che et al., 2024). From an architectural perspective, the most striking feature of the biomimetic approach is that it typically presents geometric patterns that are hierarchical, directional or locally differentiated (Figure 7b). Therefore, unlike classical periodic structures, biomimetic cores can incorporate more organic, disordered, or multiscale topologies. Additive manufacturing technologies have made it possible to produce such complex geometries, leading to biomimetic core designs becoming more visible in the sandwich structure literature.

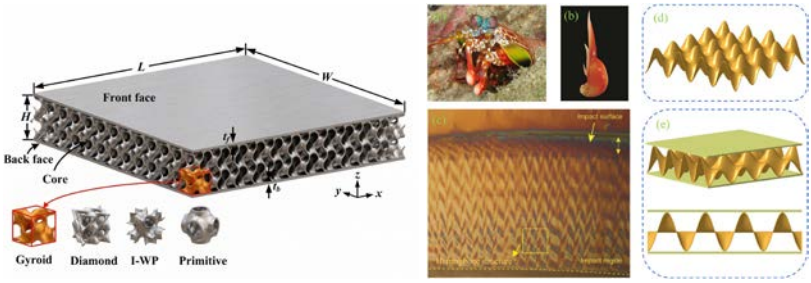

Figure 7. (a) TPMS core architectures for sandwich panels (Mo et al., 2026) (b) Bio-inspired sinusoidal sandwich structure (Yang et al., 2017)

Core architectures such as honeycomb, TPMS, and bio-inspired structures exhibit different geometric configurations, each offering distinct topological and morphological characteristics. Additive manufacturing technologies have not

only facilitated the production of these structures but also enabled the development of hybrid, graded, and application-specific core designs. Therefore, in modern sandwich structure design, the core architecture is considered not merely an internal filling form but a key design parameter that defines the geometric character of the structure.

5. CONCLUSIONS AND FUTURE PERSPECTIVES

Sandwich structures hold a significant place among engineering solutions that can provide high structural efficiency with low weight. Thanks to their lightweight core structure located between two thin surface layers, these systems are widely used, especially in the aerospace, automotive, and energy sectors. While traditional manufacturing methods have mostly been limited to simple basic geometries, the development of additive manufacturing technologies has led to a significant transformation in sandwich structure design. Additive manufacturing processes allow for the direct production of complex internal geometries without the need for molds, offering significant design freedom in sandwich structure design. This allows for the creation of more complex designs, including advanced cellular structures, TPMS-based geometries, and biomimetic core architectures, in addition to traditional honeycomb core structures. This architectural diversity makes it possible to optimize sandwich structures for different engineering applications.

Sandwich structure research is expected to increasingly focus on functionally graded core architectures, multi-material additive manufacturing strategies, and artificial intelligence–assisted design methodologies. In addition, the integration of sustainable and recyclable materials is anticipated to become a

key component of future developments in this field. With continued advances in additive manufacturing technologies, sandwich structures are likely to evolve toward lighter, more complex, and application-specific designs with enhanced structural and functional performance.

REFERENCES

Bharath, H., Bonthu, D., Gururaja, S., Prabhakar, P., & Doddamani, M. (2021). Flexural response of 3D printed sandwich composite. Composite Structures, 263, 113732. https://doi.org/10.1016/j.compstruct.2021.113732

Birman, V., & Kardomateas, G. A. (2018). Review of current trends in research and applications of sandwich structures. Composites Part B: Engineering, 142, 221–240. https://doi.org/10.1016/j.compositesb.2018.01.027

Brejcha, V., Böhm, M., Holeček, T., Jerman, M., Kobetičová, K., Burianová, I., Černý, R., & Pavlík, Z. (2025). Comparison of bending properties of sandwich structures using conventional and 3D-printed core with flax fiber reinforcement. Journal of Composites Science, 9(4). https://doi.org/10.3390/jcs9040182

Castanie, B., Bouvet, C., & Ginot, M. (2020). Review of composite sandwich structure in aeronautic applications. Composites Part C: Open Access, 1, 100004. https://doi.org/10.1016/j.jcomc.2020.100004

Challapalli, A., & Li, G. (2021). Machine learning assisted design of new lattice core for sandwich structures with superior load carrying capacity. Scientific Reports, 11(1), 18552. https://doi.org/10.1038/s41598-021-97870-2

Che, S., Qu, G., Wang, G., Hao, Y., Sun, J., & Ding, J. (2024). A review of the biomimetic structural design of sandwich composite materials. Polymers, 16(20). https://doi.org/10.3390/polym16202925

Choudhari, C. J., Thakare, P. S., & Sahu, S. K. (2022). 3D printing of composite sandwich structures for aerospace applications. In A. Praveen Kumar, K. K. Sadasivuni, B. AlMangour, & M. S. Abdul Majid (Eds.), High-

performance composite structures (Composites Science and Technology). Singapore: Springer. https://doi.org/10.1007/978-981-16-7377-1_3

Datsiou, K. C., & Ashcroft, I. (2024). Numerical investigation of laser powder bed fusion of glass. Glass Structures & Engineering, 9, 185–200. https://doi.org/10.1007/s40940-024-00257-0

de Castro, B. D., Magalhães, F. C., Panzera, T. H., & Campos Rubio, J. C. (2021). An assessment of fully integrated polymer sandwich structures designed by additive manufacturing. Journal of Materials Engineering and Performance, 30(7), 5031–5038.

Dikshit, V., Yap, Y. L., Goh, G. D., Yang, H., Lim, J. C., Qi, X., & Wei, J. (2016). Investigation of out-of-plane compressive strength of 3D printed sandwich composites. IOP Conference Series: Materials Science and Engineering, 139(1), 012017.

Faidallah, R. F., Hanon, M. M., Szakal, Z., & Oldal, I. (2023). Study of the mechanical characteristics of sandwich structures FDM 3D-printed. Acta Polytechnica Hungarica, 20(6), 7–26.

Fan, M., Zeng, T., Wu, R., Cui, Y., Xu, G., Wang, X., Cheng, S., & Zhao, J. (2024). Bending behaviors of 3D printed sandwich structures with functionally graded porous lattice cores. Thin-Walled Structures, 206, 112655. https://doi.org/10.1016/j.tws.2024.112655

Gao, S., Wang, C., Xing, B., Shen, M., Zhao, W., & Zhao, Z. (2020). Experimental investigation on bending behaviour of ZrO_2 honeycomb sandwich structures prepared by DLP stereolithography. Thin-Walled Structures, 157, 107099.

Gibson, L. J., & Ashby, M. F. (1997). Cellular solids: Structure and properties (2nd ed.). Cambridge University Press. https://doi.org/10.1017/CBO9781139878320

Haldar, A., Managuli, V., Munshi, R., Agarwal, R., & Guan, Z. (2021). Compressive behaviour of 3D printed sandwich structures based on corrugated core design. Materials Today Communications, 26, 101725. https://doi.org/10.1016/j.mtcomm.2020.101725

Hou, Y., Tai, Y. H., Lira, C., Scarpa, F., Yates, J. R., & Gu, B. (2013). The bending and failure of sandwich structures with auxetic gradient cellular cores. Composites Part A: Applied Science and Manufacturing, 49, 119–131.

Huang, J., Li, X., Zheng, X., Ma, L., Wang, Y., Chen, P., & Xie, J. (2026). Investigation of 316L stainless steel sandwich honeycomb structure subjected to near-field blast loading. Journal of Materials Research and Technology, 41, 6541–6558. https://doi.org/10.1016/j.jmrt.2026.02.213

Junaedi, H., Abd El-baky, M. A., Awd Allah, M. M., & Sebaey, T. A. (2024). Mechanical characteristics of sandwich structures with 3D-printed bio-inspired gyroid structure core and carbon fiber-reinforced polymer laminate face-sheet. Polymers, 16(12). https://doi.org/10.3390/polym16121698

Kafkaslıoğlu Yıldız, B., Yıldız, A. S., Kul, M., Tür, Y. K., Işık, E., Duran, C., & Yılmaz, H. (2024). Mechanical properties of 3D-printed Al_2O_3 honeycomb sandwich structures prepared using the SLA method with different core geometries. Ceramics International, 50(2), 2901–2908. https://doi.org/10.1016/j.ceramint.2023.11.028

Kamble, Z. (2024). Advanced structural and multi-functional sandwich composites with prismatic and foam cores: A

review. Polymer Composites, 45(18), 16355–16382. https://doi.org/10.1002/pc.27849

Lee, J. M., Sing, S. L., Zhou, M., & Yeong, W. Y. (2018). 3D bioprinting processes: A perspective on classification and terminology. International Journal of Bioprinting, 4(2), 151. https://doi.org/10.18063/ijb.v4i2.151

Leśniowski, J., Stawiarski, A., & Barski, M. (2025). Enhancing the performance of FFF-printed parts: A review of reinforcement and modification strategies for thermoplastic polymers. Materials, 18(22). https://doi.org/10.3390/ma18225185

Li, H., Hu, Y., Huang, H., Chen, J., Zhao, M., & Li, B. (2021). Broadband low-frequency vibration attenuation in 3D printed composite meta-lattice sandwich structures. Composites Part B: Engineering, 215, 108772. https://doi.org/10.1016/j.compositesb.2021.108772

Ma, Q., Rejab, M. R. M., Hanon, M. M., Idris, M. S., & Siregar, J. P. (2021a). 3D-printed spherical-roof contoured-core (SRCC) composite sandwich structures for aerospace applications. In High-performance composite structures: Additive manufacturing and processing (pp. 75–91). Singapore: Springer.

Ma, Q., Rejab, M., Siregar, J., & Guan, Z. (2021b). A review of the recent trends on core structures and impact response of sandwich panels. Journal of Composite Materials, 55(18), 2513–2555.

Mirzaei, J., Zarei, H. R., & Khodamoradi, M. K. (2025). Experimental analysis of energy absorption characteristics in composite sandwich structures with 3D-printed honeycomb core under quasi-static compression. Journal of Thermoplastic Composite Materials.

Mo, D., Zhou, T., Cai, S., Shi, M., Guo, Y., Cheng, Y., & Zhang, P. (2026). Elevated blast resistance of sandwich panel with bio-inspired triply periodic minimal surface core. Composite Structures, 379, 119963. https://doi.org/10.1016/j.compstruct.2025.119963

Pollard, D., Ward, C., Herrmann, G., & et al. (2017). The manufacture of honeycomb cores using fused deposition modeling. Advanced Manufacturing: Polymers & Composites Science, 3(1), 21–31. https://doi.org/10.1080/20550340.2017.1306337

Sadegh Yazdi, M., Hosseinzadeh, M. H., Nadimi, V., & Hajitabar, A. (2024). Experimental, numerical and optimization investigation of sandwich structures with 3D-printed sacrificial core under explosive loading. Materials Today Communications, 41, 111073. https://doi.org/10.1016/j.mtcomm.2024.111073

Sadiq, M. A., & Kovács, G. (2025). Optimization of composite sandwich structures: A review. Machines, 13(7). https://doi.org/10.3390/machines13070536

Sahib, M. M., Kovács, G., & Szávai, S. (2023). Weight optimization of all-composite sandwich structures for automotive applications. In Vehicle and Automotive Engineering 4 (pp. 720–733). Cham: Springer.

Sahu, S. K., Sreekanth, P. S. R., & Reddy, S. V. K. (2022). A brief review on advanced sandwich structures with customized design core and composite face sheet. Polymers, 14(20), 4267. https://doi.org/10.3390/polym14204267

Sarvestani, H. Y., Akbarzadeh, A. H., Niknam, H., & Hermenean, K. (2018). 3D printed architected polymeric sandwich panels: Energy absorption and structural performance. Composite Structures, 200, 886–909.

Sugiyama, K., Matsuzaki, R., Ueda, M., Todoroki, A., & Hirano, Y. (2018). 3D printing of composite sandwich structures using continuous carbon fiber and fiber tension. Composites Part A: Applied Science and Manufacturing, 113, 114–121. https://doi.org/10.1016/j.compositesa.2018.07.029

Sun, W., Liu, F., Wang, G., Shi, S., Wen, Z., & Chen, B. (2026). Improving the impact resistance of carbon fiber sandwich panels with short aramid fiber epoxy (SAFE). Structures, 84, 111058.

Top, N., Gökçe, H., & Şahin, İ. (2025). Enhancing thermal insulation with sandwich structures produced by additive manufacturing. Heat Transfer Research, 56(17).

Türkoğlu, İ. K., Kasım, H., & Yazıcı, M. (2023). Experimental investigation of 3D-printed auxetic core sandwich structures under quasi-static and dynamic compression and bending loads. International Journal of Protective Structures. https://doi.org/10.1177/20414196221079366

Vasile, A., Constantinescu, D. M., Coropețchi, I. C., Sorohan, Ș., & Apostol, D. A. (2024). Definition, fabrication, and compression testing of sandwich structures with novel TPMS-based cores. Materials, 17(21), 5150.

Vellaisamy, S., & Munusamy, R. (2024). Experimental study of 3D printed carbon fibre sandwich structures for lightweight applications. Defence Technology, 36, 71–77. https://doi.org/10.1016/j.dt.2023.11.019

Wen, T., Xiao, S., Duan, S., Wang, P., Zhang, R., Song, B., & Lei, H. (2026). Additively manufactured Ti600 lattice sandwich structures with ultra-low thermal conductivity: Theoretical model and experiment. Applied Thermal

Engineering, 284, 129161. https://doi.org/10.1016/j.applthermaleng.2025.129161

Williams, R. R., Howard, W. E., & Martin, S. M. (2011). Composite sandwich structures with rapid prototyped cores. Rapid Prototyping Journal, 17(2), 92–97.

Xu, L., Yang, Z., Zhang, Z., Li, E., Zhou, J., & Li, B. (2025). Lightweight composite meta-lattice structures with inertial amplification design for broadband low-frequency vibration mitigation. Composites Part B: Engineering, 292, 112091. https://doi.org/10.1016/j.compositesb.2024.112091

Yang, W., He, W., Zhang, X., Yang, G., Ma, J., Wang, Y., & Wang, C. (2019). $Na_3V_2(PO_4)_3$/N-doped carbon nanocomposites with sandwich structure for cheap, ultrahigh-rate, and long-life sodium-ion batteries. ChemElectroChem, 6(7), 2020–2028.

Yang, X., Ma, J., Shi, Y., Sun, Y., & Yang, J. (2017). Crashworthiness investigation of the bio-inspired bi-directionally corrugated core sandwich panel under quasi-static crushing load. Materials & Design, 135, 275–290.

Yao, S., Gu, X., Xie, M., Xu, P., Tang, M., Tan, J., & Hao, G. (2026). 3D-printed gradient TPMS sandwich structures: A study on bending performance. Applied Sciences, 16(4). https://doi.org/10.3390/app16042129

Yazıcı, M. E., Kanber, B., & Dağlı, S. (2024). Investigation of bending behavior of two and three-dimensional honeycomb and auxetic sandwich beams. Journal of Sandwich Structures & Materials, 26(6), 945–968.

Zaharia, S. M., Enescu, L. A., & Pop, M. A. (2020). Mechanical performances of lightweight sandwich structures produced by material extrusion-based additive

manufacturing. Polymers, 12(8). https://doi.org/10.3390/polym12081740

Zhang, K., Zeng, T., Xu, G., Cheng, S., & Yu, S. (2020). Mechanical properties of SiCp/SiC composite lattice core sandwich panels fabricated by 3D printing combined with precursor impregnation and pyrolysis. Composite Structures, 240, 112060. https://doi.org/10.1016/j.compstruct.2020.112060

Zhang, Z., Wang, J., Wang, Y., Zhang, Q., Jiao, J., Liu, J., Sui, Y., & Wei, X. (2025). Superior compressive performance of a novel plate-added X-lattice core sandwich structure at elevated temperatures. Composites Part A: Applied Science and Manufacturing, 196, 108992. https://doi.org/10.1016/j.compositesa.2025.108992

UÇAK KANAT RİBLERİNDE UYGULANAN BOŞALTMA GEOMETRİLERİNDE GERİNİM ENERJİ DAVRANIŞLARININ KIYASLANMASI[1]

Oğuzhan ERTAŞ[2]

Fırat KAFKAS[3]

1. GİRİŞ

Havacılık endüstrisinde hava aracı yapısal tasarım süreçleri, hava aracının uçuş zarfları içerisinde emniyetli bir şekilde görev icrasından ödün vermeksizin operasyonel verimliliği maksimize edecek hafif, yüksek performanslı ve istenen fonksiyonları yerine getirecek tasarımların gerçekleştirilmesi ve geliştirilmesi üzerine kurgulanmaktadır. Yapısal kütlenin minimize edilmesi, doğrudan bir ağırlık avantajı sağlamasının yanı sıra, yakıt verimliliğinin artırılması, ihtiyaç olan güç ihtiyacının düşürülmesi ve dolayısıyla itki sistemlerinin optimize edilmesini sağlamaktadır. Bunun yanında aerodinamik tasarım parametrelerinin idealize edilmesi üzerinde de doğrudan pozitif etkiler yaratmaktadır (Niu, 2002).

Bir hava aracını oluşturan gövde, kanat ve kuyruk gibi ana bileşenler arasında kanatlar, aerodinamik taşıma kuvvetinin üretildiği merkez olması sebebiyle kritik bir öneme sahiptir.

---

[1] Bu kitap bölümü, "Uçak Yapısal Elemanlarında Boşaltma Geometrilerinin Sonlu Elemanlar Analizi ile Karşılaştırılması ve Optimizasyonu" isimli tez çalışmasından üretilmiştir.

[2] Gazi Üniversitesi, Fen Bilimleri Enstitüsü, İmalat Mühendisliği Ana Bilim Dalı, ORCID: 0009-0007-4662-3157.

[3] Gazi Üniversitesi, Teknoloji Fakültesi, İmalat Mühendisliği, ORCID: 0000-0003-3257-7413.

Hava aracının havada tutunmasını sağlayan ve uçuş performansını doğrudan belirleyen bu yapılar, tasarım süreçlerinde en fazla hassasiyet gösterilen bölümlerin başında gelmektedir (Leishman, 2025).

Bu nedenle, kanat yapısının mekanik bütünlüğünü korurken aynı zamanda fonksiyonel bir ağırlık azaltma stratejisi izlemek, havacılık mühendisliğinin temel önceliğidir.

Yapısal optimizasyon çalışmaları, yalnızca rastgele bir hafifletme işlemi değil; emniyet katsayılarını ve yük aktarım yollarını bozmadan gerçekleştirilen, stratejik önemi yüksek bir disiplindir. Bu süreçte tasarımın başarısı, dış yükler altında yapıda depolanan gerinim enerjisinin nasıl dağıldığı ve malzemenin bu enerjiyi ne kadar verimli taşıdığıyla doğrudan ilişkilidir. Belirlenen hacim kısıtları içerisinde kalarak ağırlık ve yapısal rijitlik arasında en ideal dengeyi kurabilmektir. Gerinim enerjisi verileri, uçak bileşenlerinin hem kütle verimliliğini hem de mekanik bütünlüğünü doğrulamak için kritik bir çerçeve sunmaktadır. Bu bağlamda, hava aracı bileşenlerinin tasarımında ağırlık verimliliğini artıracak her türlü müdahale ve gerinim enerjisi odaklı analizler, uçağın genel operasyonel başarısı için önemli bir gerekliliktir (Brink, 2024).

Hava aracı yapısal elemanı, üzerine etki eden bir P yükü altında deformasyona uğradığında bu yük fiziksel bir iş yapmaktadır. Gerçekleştirilen bu iş yapısal sistem içerisinde kaybolmamakta ve yapı bünyesinde elastik gerinim enerjisi olarak depolanmaktadır. Analiz edilen bu enerji miktarı, yapının dış yüklere karşı gösterdiği direncin ve dolayısıyla yapısal rijitliğin sayısal bir ifadesi olarak kabul edilmektedir (Megson, 2007).

Gerinim Enerjisinin matematiksel gösteri Eşitlik 1'de gösterilmiştir. Gerinim enerjisi değeri, kuvvet – yerdeğiştirme grafiğinin altında kalan alana eşittir (Yao, 2021).

$$U = \int_0^{y_d} P \, dy_d \tag{1}$$

(U: Gerinim Enerjisi(J), y_d: Deformasyon Miktarı(m), P: Yük(N))

Literatür incelemeleri sonucunda görülmektedir ki ağırlık azaltma ve yapısal dayanım arasındaki bu denge, tasarım süreçlerinde dikkatle önemsenmesi gerekmektedir. Bu noktada özgül gerinim enerjisi kavramı, hafifletme çalışmaları sırasında en uygun geometrinin belirlenmesinde ve farklı boşaltma şekillerinin verimliliğini kıyaslamaya olanak tanır.

Eşitlik 2'de gösterilen özgül gerinim enerjisi, gerinim enerjisinin yapısal eleman kütlesine oranlanmasıyla elde edilir (Shuguang Yao, 2021).

$$\upsilon_s = \frac{U}{m} \tag{2}$$

(υ_s: Özgül Gerinim Enerjisi(J/kg), U: Gerinim Enerjisi(J), m: Kütle(kg))

Bir geometrinin yüksek özgül gerinim enerjisine sahip olması, malzemenin dış yükleri karşılamada çok daha etkin kullanıldığını ve birim kütle başına en iyi performansı sunduğunu ifade eder. Dolayısıyla bu çalışma, kanat riblerinde yapılacak ağırlık azaltma işlemlerinde hangi geometrik formun daha avantajlı olduğunu bu verimlilik değeri üzerinden analiz etmektedir.

2. YAPISAL YÜKLERİN HESAPLANMASI

Kanat tarafından üretilen aerodinamik yükler, yüzeyler üzerindeki basınç değişimlerinin bir bileşkesi olarak ortaya çıkar. Geniş kanat alanı sayesinde bu basınç farkları, uçağın havada tutunmasını sağlayan toplam taşıma kuvvetini meydana getirir. Oluşan bileşke aerodinamik kuvvet, serbest akış doğrultusuna dik yöndeki taşıma ve akışla aynı doğrultudaki sürükleme bileşenlerine ayrılarak analiz edilir (Sadrehaghighi, 2023).

Hava aracı kanat bileşeni, görev süreçleri boyunca karşılaştıkları yükler açısından üç temel sınıfta değerlendirilir. Bu yük grupları; uçuş esnasında yapıyı etkileyen aerodinamik yükler, atalet yükleri ve uçağın pist üzerindeki hareketleri sırasında oluşan yer yükleridir (Gudmundsson, 2022).

Kanat yapılarının tasarım aşamasına geçilebilmesi için öncelikle etki eden yüklerin kesin bir şekilde tanımlanması gerekir. Bir hava aracına ait temel tasarım senaryoları; operasyonel hız limitleri ve ivme değerleri esas alınarak belirlenir. Bu yapısal gereksinimler, uçuş hızı ile yük faktörü arasındaki ilişkiyi ortaya koyan ve literatürde V-n diyagramı olarak tanımlanan grafiksel gösterimden elde edilir (Sökmen, 2006).

Maksimum kalkış ağırlığı 150 kg'ı aşan ağır sınıf İnsansız Hava Araçları (İHA) için operasyonel uçuş limitleri, sivil havacılık sertifikasyonlarını (CS-23) temel alan STANAG 4671 standardı çerçevesinde tanımlanır. Söz konusu yönerge uyarınca, standart bir hava aracının uçuş zarfı kısıtlamaları tipik olarak +3.8g üst sınırı ile -1.5g alt sınırı arasında belirlenmektedir (NATO, 2007).

Yapısal analiz aşamasının en kritik basamaklarından biri, kanat üzerindeki aerodinamik yüklerin, yani kanat yüklemesinin doğru bir şekilde belirlenmesidir. Bu yüklemenin tahmin edilmesine yönelik literatürde farklı metodolojiler yer almaktadır.

Bunlar arasında Schrenk Yaklaşımı, karmaşık CFD akış analizlerine ihtiyaç duymadan kanat açıklığı boyunca taşıma kuvveti dağılımını hesaplamaya imkan tanıdığı için literatürde kendini kanıtlamış ve havacılık otoriteleri tarafından kabul görmüş bir yöntemdir (Soemaryanto, 2018).

Schrenk Yaklaşımı yöntemi, kanat üzerindeki yük dağılımını, ideal eliptik taşıma karakteristiği ile kanadın fiziksel formuna dayanan taşıma dağılımının aritmetik ortalaması üzerinden modellemektedir. Bu yaklaşım, teorik beklenti ile gerçek geometri arasındaki ilişkiyi basit ama etkili bir matematiksel kabulle birleştirir (Kamal, 2019).

Yapısal analiz süreçlerinde, hava aracının kalkış ağırlığı ve geometrik formu, üzerine etki edecek yüklerin karakteristiğini doğrudan belirleyen unsurlardır. Bu çalışmada incelenen hava aracı, NATO İHA sınıflandırma kriterleri baz alınarak, kalkış ağırlığı 600 kg'dan yüksek hava araçları için geçerli olan Sınıf III kategorisindeki standartlara uygun olarak kalkış ağırlığı belirlenmiştir. Analiz edilen modele ait kalkış ağırlığı değeri ve referans kabul edilen kanat geometrisine dair teknik veriler Tablo 2.1'de verilmiştir (Kütük, 2025).

Tablo 2.1. Hava Aracı Tasarım Değerleri

Maksimum Kalkış Ağırlığı	1250 kg
Yarı Kanat Açıklığı (b_{yk})	5.5 m
Kök Veter Uzunluğu (C_r)	1.2 m
Uç Veter Uzunluğu (C_t)	0.6 m
Sivrilik Oranı (λ)	0.5
Ok Açısı (Λ)	0°
Burulma Açısı (α_t)	0°

Kabul edilen referans değerlere göre Schrenk Yaklaşımı ile kanat üzerine etki eden yükler hesaplanmış ve yapısal analiz sürecinde bu yükler kanada etki ettirilmiştir.

Schrenk Yaklaşımında girdi olarak kullanılmak üzere hava aracının uçuş zarfı boyunca maruz kalacağı maksimum yük değeri Eşitlik 3'deki eşitliğe göre hesaplanmıştır.

$$L_T = W_{TA} \,.\, n \,.\, GK \tag{3}$$

$$L_T = (1250\ x\ 9.81)\ x\ 3.8\ x\ 1.5$$

$$L_T = 69896.25\ N$$

(L_T: Toplam Etki Edebilecek Yük(N), W_{TA}: Toplam Kalkış Yükü(N), n: Limit Yük Faktörü, GK: Güvenlik Katsayısı)

Analizlerde yarı kanat modelinin kullanılması sebebiyle Eşitlik 3 ile elde edilen tümleşik kanat yükü, Eşitlik 4 kullanılarak yarı kanat modeline etki edecek yük değerine dönüştürülmüştür.

$$L = \frac{L_T}{2} \tag{4}$$

$$L = 39948.125\ N$$

(L: Toplam Etki Edebilecek Yarı Yük(N))

Kanat yükleri, Schrenk Yaklaşımı kullanılarak Eşitlik 5, Eşitlik 6 ve Eşitlik 7'de gösterilen formülüzasyonlar ile hesaplanır.

$$L_S = \frac{L_e + L_p}{2} \tag{5}$$

(L_S: Schrenk Yaklaşımı Yükü(N/m), L_e: Eliptik Kanat Yük Dağılımı(N/m), L_p: Trapez Kanat Yük Dağılımı(N/m))

$$L_e = \frac{4L}{\pi b_{yk}} \,.\, \sqrt{1 - \left(\frac{2y}{b_{yk}}\right)^2} \tag{6}$$

(y: Kanat Açıklığı Boyunca Belirlenen Mesafe(m))

$$L_p = \frac{2L}{(1+\lambda)b_{yk}} \,.\left[1 + \frac{2y}{b_{yk}} \,.(\lambda - 1)\right] \tag{7}$$

Yukarıda belirtilen hesaplamalar ile kanat açıklığı boyunca her 0.1 m aralıklarda Schrenk Yaklaşımı yükleri hesaplanmıştır. Hesaplanan Schrenk Yaklaşımı yükleri, Eşitlik 8'de ifade edildiği gibi belirlenen aralıklardaki kanat veter uzunluğuna bölünerek, uygulanan yükler basınç değerlerine çevrilmiştir. Hesaplanan bu basınç değerleri sonlu elemanlar analizinde değişken yayılı yük olarak sınır şartlarına girdi yapılmıştır.

$$P = \frac{L_s}{C_y} \tag{8}$$

(P: Kanat Açıklığı Boyunca Etki Eden Basınç(N/m^2),

C_y: Belirlenen Aralıklardaki Veter Uzunluğu(m)

Basınç yüklerinin hesaplanmış ve Şekil 2.1.'de grafiksel gösterimi yapılmıştır.

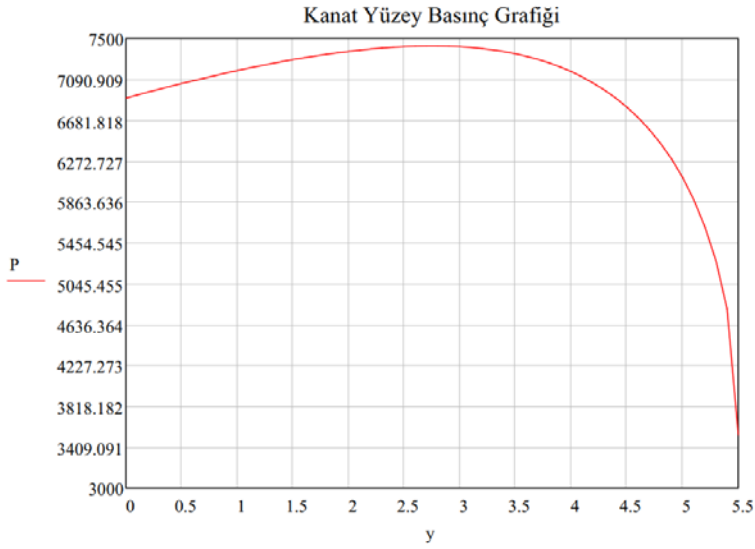

Şekil 2.1. Kanat Açıklığı Boyunca Etki Eden Basınç Yükü

3. YAPISAL TASARIM

Daha önceden belirlenen geometrik parametrelere göre kanat yapısal tasarımı yapılmıştır. Kanat tasarımında, literatürde "*Wingbox*" olarak tabir edilen tasarım geometrisi seçilmiştir. Bu tasarım yaklaşımına göre kanat veterinin %20 konumuna "*C*" kesit geometrili ön spar, kanat veterinin %65 konumuna da yine aynı kesit geometrili arka spar yerleştirilmiştir. Birbiri içine bakan ön ve arka sparın içine kanat kökünden kanat ucuna doğru artan aralıklarla "C" kesit geometrili 12 adet rib yerleştirilmiştir. Kanat komplesinin tasarımı sonrası, kanat kökünde ve kanat ucunda yer alan riblerin dışında kalan diğer riblerin duvarlarında 4 farklı geometride boşaltma işlemi uygulanmıştır. Airfoil Offset, Dörtgensel, Dairesel ve Üçgensel olmak üzere Şekil 3.1.'de gösterilen 4 farklı geometride tasarım meydana gelmiştir.

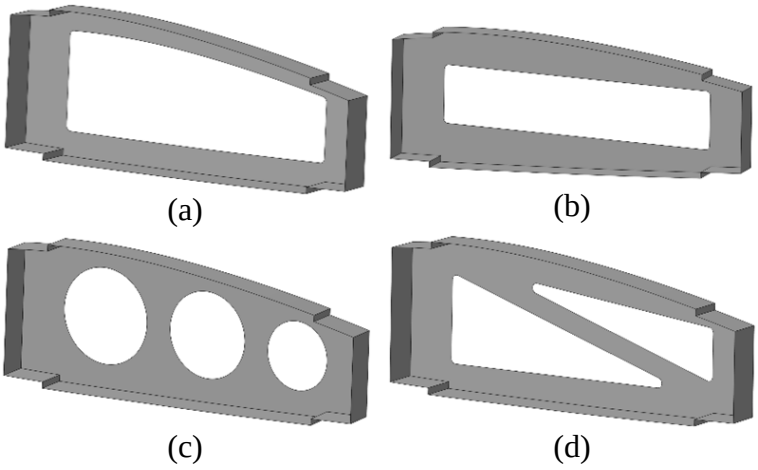

Şekil 3.1. Kanat Rib Tasarımları (a): Airfoil Offset Boşaltma Geometrili Rib, (b): Dörtgensel Boşaltma Geometrili Rib, (c): Dairesel Boşaltma Geometrili Rib, (d): Üçgensel Boşaltma Geometrili Rib

Uygulanan boşaltma işleri sonrası kanat tasarımları Şekil 3.2.'deki hali almıştır.

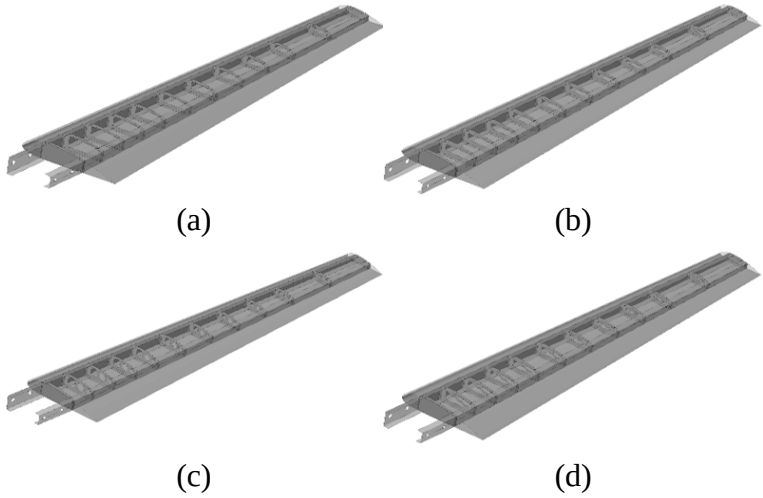

Şekil 3.2. Kanat Yapısal Tasarımı (a): Airfoil Offset Boşaltma Geometrili Tasarım, (b): Dörtgensel Boşaltma Geometrili Tasarım, (c): Dairesel Boşaltma Geometrili Tasarım, (d): Üçgensel Boşaltma Geometrili Tasarım

Kanat tasarımda yer alan Kanat Alt Kabuk, Kanat Üst Kabuk, Spar ve Riblerin kalınlıkları kabul yapılarak belirlenmiş olup, Ön ve Arka Sparlar 8 mm, Kabuklar ve Ribler 2mm olarak belirlenmiştir. Yapılan sonlu elemanlar analizleri kabul edilen bu kalınlık değerlerine göre yapılmıştır.

Yapılan tasarım çalışması sonunda boşaltmasız ve diğer 4 boşaltmalı geometri olmak üzere 5 farklı konfigürasyonda analiz geometrisi ortaya çıkmıştır. Ortaya çıkan bu geometrilerin eleman bazında ağırlık kıyaslamaları Tablo 3.1.'de gösterilmiştir.

Tablo 3.1.'deki değerlere bakıldığında referans kabul edilen boşaltma uygulanmadan tasarlanan kanat geometrisine göre rib ağırlıklarında, airfoil offset boşaltma geometrisi ile %20.56, dörtgensel boşaltma geometrisi ile %14.75, dairesel

boşaltma geometrisi ile %12.72, üçgensel boşaltma geometrisi ile %12.76 ağırlık azaltımı sağlanmıştır.

Tablo 3.1. Yapısal Elemanların Tasarımsal Ağırlık Değerleri

	Boşaltmasız Geometri	Airfoil Offset Geometri	Dörtgensel Geometri	Dairesel Geometri	Üçgensel Geometri
Yapısal Eleman	Ağırlık (kg)				
Üst Kabuk	14.803	14.803	14.803	14.803	14.803
Alt Kabuk	14.269	14.269	14.269	14.269	14.269
Ön Spar	16.903	16.903	16.903	16.903	16.903
Arka Spar	14.194	14.194	14.194	14.194	14.194
Toplam Rib Ağırlığı	3.166	2.515	2.699	2.763	2.762
Toplam Ağırlık	63.335	62.684	62.868	62.932	62.931

4. SONLU ELEMANLAR ANALİZİ

Kanat tasarımları sonrasında sonlu elemanlar analizine geçilmiş olup ANSYS Workbench platformunda analizler yapılmıştır. Sonlu elemanlar analizinin başlangıcından, sonuçların alınmasına kadar ki süreçte takip edilen aşamalar Şekil 4.1.'deki akış şemasında gösterilmiştir.

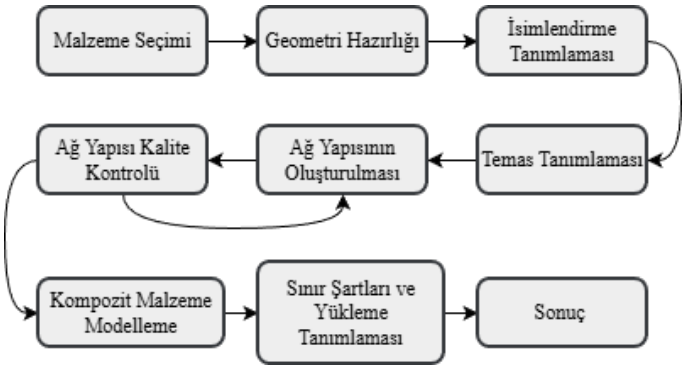

Şekil 4.1. Sonlu Elemanlar Analizi İşlem Aşamaları

Sonlu elemanlar analizine ilk olarak malzeme seçimi ile başlanmış olup ANSYS Workbech kütüphanesinde yer alan örgü yapılı Karbon Epoksi (230 GPa) Pre-preg malzeme seçilmiştir.

Malzeme seçimi sonrasında 5 farklı konfigürasyonda hazırlanan kanat tasarımları ANSYS Workbench'e yüklenmiştir.

Sonrasında analiz aşamasında ihtiyaç duyulacak yüzeylere ve elemanlara isimlendirmeler yapılarak İsimlendirme Tanımlaması aşaması tamamlanmıştır. Yüzey ve eleman isimlendirmelerinden sonra Temas Tanımlaması aşamasına geçilmiş olup, analiz çalıştırıldığında yük aktarımının gerçekleşebilmesi için kanat tasarımında birbiri ile temas kuran elemanlar arasına temaslar tanımlanmıştır.

Bir diğer aşama olarak, sayısal çözümlemenin temelini oluşturan ağ (mesh) yapısının kurgulanması sürecine geçilmiştir. Bu aşama, analiz geometrileri küçük elemanlara bölünerek matematiksel bir modele dönüştürülmesi ve çözümleyici tarafından analizin çalıştırılabilmesi sağlanmıştır. Ağ oluşturma sürecinde, yapının genelinde uygulanan boyutlandırma stratejisine ek olarak, riblerin üzerindeki kritik detayların ve geometrik süreksizliklerin modellenebilmesi için yerel ağ yoğunlaştırma işlemleri gerçekleştirilmiştir. Son aşamada ise, üretilen ağ yapısının eleman kalite metrikleri denetlenmiş, ağ kalitesinin optimizasyonu ve çözüm doğruluğunun artırılması amacıyla gerekli bölgelerde eleman boyutları revize edilerek ideal ağ formuna ulaşılmıştır.

Ağ yapısının oluşturulması sonrasında ANSYS Workbench içerisinde yer alan ACP-Pre modülü kullanılarak kanat yapısallarının kompozit elyaf dizilimleri ve modellemesi yapılmıştır. Daha önce kabulü yapılan yapısal eleman kalınlıklarına ve seçimi yapılan elyafın kalınlık değerine göre her bir yapısal elemana uygun sayıda elyaf dizilimleri yapılarak hedeflenen kalınlık sağlanmıştır. Elyaf dizilimlerinde seçilen pre-

preg elyafın örgü yapılı olması sebebiyle 0°/90° açılarda serimi gerçekleştirilmiştir.

İlgil tüm hazırlıklar tamamlandıktan sonra sınır şartlarının hazırlığına başlanmıştır. Şekil 4.2.'de görüldüğü gibi ön ve arka sparların hava aracı gövdesine girdiği ve gövdeye sabitlendiği yüzeylerden sabit mesnet verilmiştir.

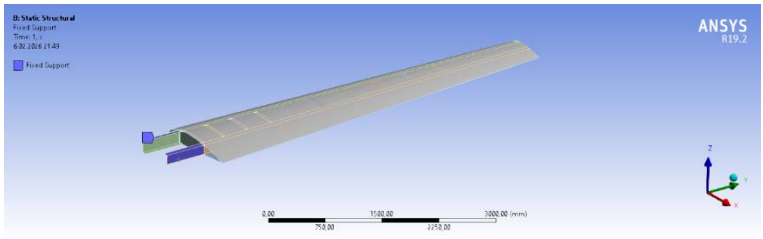

Şekil 4.2. Kanat Yapısalı Sabitleme Sınır Şartı Gösterimi

Schrenk Yaklaşımı ile hesaplanan ve Şekil 2.1.'de grafiksel gösterimi yapılan kanat basınç yükü, kanat alt kabuk yüzeyine etki ettirilmiştir. Kanat açıklığı boyunca belirlenen aralıklarda hesaplanan basınç değerleri ANSYS Workbench ortamına tablo verisi halinde eklenerek uygulanmıştır. Etki ettirilen değişken basınç yükü Şekil 4.3.'de gösterilmiştir.

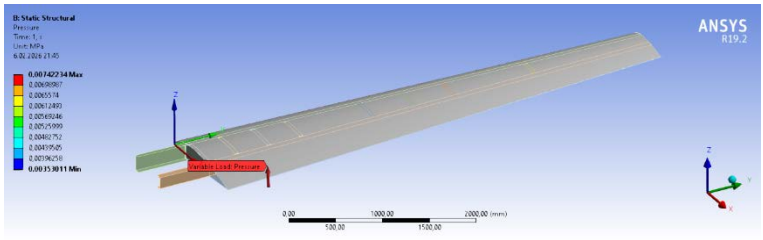

Şekil 4.3. Kanat Basınç Yükü

Sınır şartlarının tanımlanması sonrasında analiz çözdürülmüş ve boşaltma uygulanan Rib-2 ile Rib-11 arasındaki 10 rib için Toplam Gerinim Enerjisi değerleri ve her bir ribin Gerinim Enerji değerleri sonuçları alınmıştır. Analiz sonuçlarına göre, Toplam Gerinim Enerji değerleri Şekil 4.4.'de kıyaslanmıştır.

(U_T: Toplam Gerinim Enerji Değeri, T_1: Boşaltmasız Geometrili Tasarım, T_2: Airfoil Offset Geometrili Tasarım, T_3: Dörtgensel Geometrili Tasarım, T_4: Dairesel Geometrili Tasarım, T_5: Üçgensel Geometrili Tasarım)

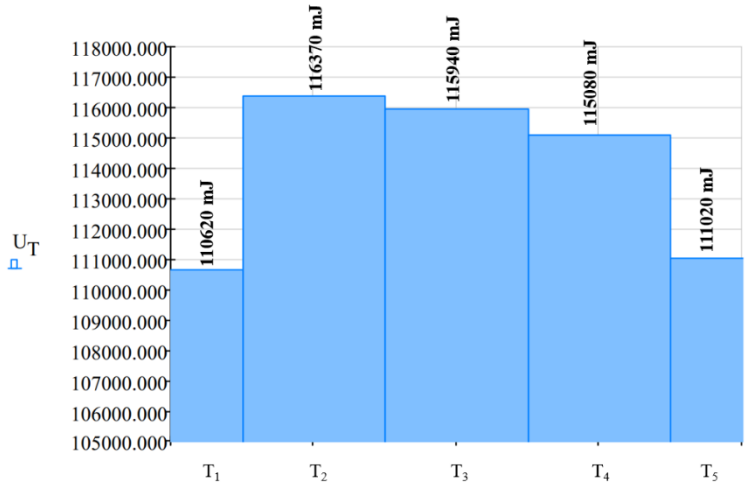

Şekil 4.4. Analiz Konfigürasyonları Toplam Gerinim Enerji Değerleri

Her bir ribde meydana gelen toplam gerinim enerji miktarları ayrı ayrı analiz sonucu alınarak alınmış olup grafiksel olarak Şekil 4.5.'de gösterilmiştir.

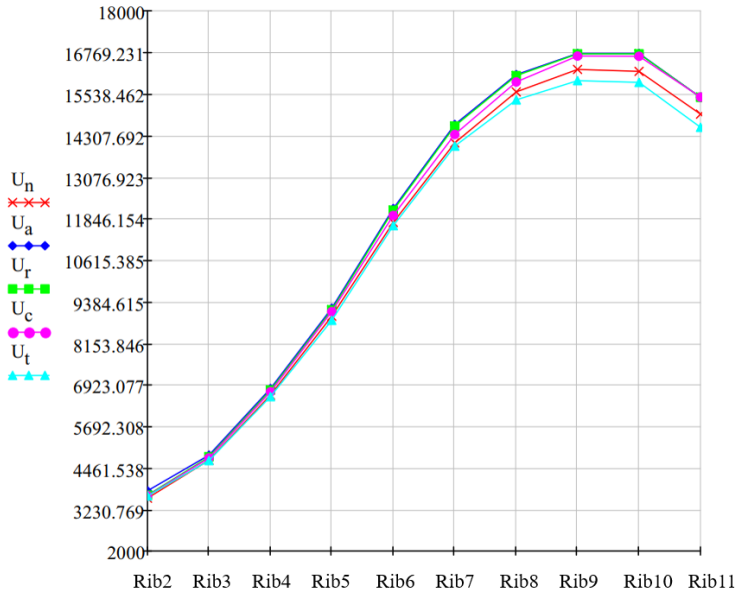

Şekil 4.5. Rib Bazlı Gerinim Enerji Değerleri

(U_n: Boşaltmasız Geometrili Tasarım Gerinim Enerjisi, U_a: Airfoil Offset Geometrili Tasarım Gerinim Enerjisi, U_r: Dörtgensel Geometrili Tasarım Gerinim Enerjisi, U_c: Dairesel Geometrili Tasarım Gerinim Enerjisi, U_t: Üçgensel Geometrili Tasarım Gerinim Enerjisi)

Şekil 4.4.'de gösterilen Rib-2 ile Rib-11 arasında yer alan riblerde meydana gelen toplam gerinim enerji değerleri mJ biriminden J birimine çevrilmiş, Rib-2 ile Rib-11 arasındaki riblerin toplam kütlesine bölünerek Eşitlik 2'de gösterildiği gibi özgül gerinim enerji değerleri hesaplanmıştır. Hesaplanan özgül gerinim enerji değerleri Şekil 4.6'da gösterilmiştir.

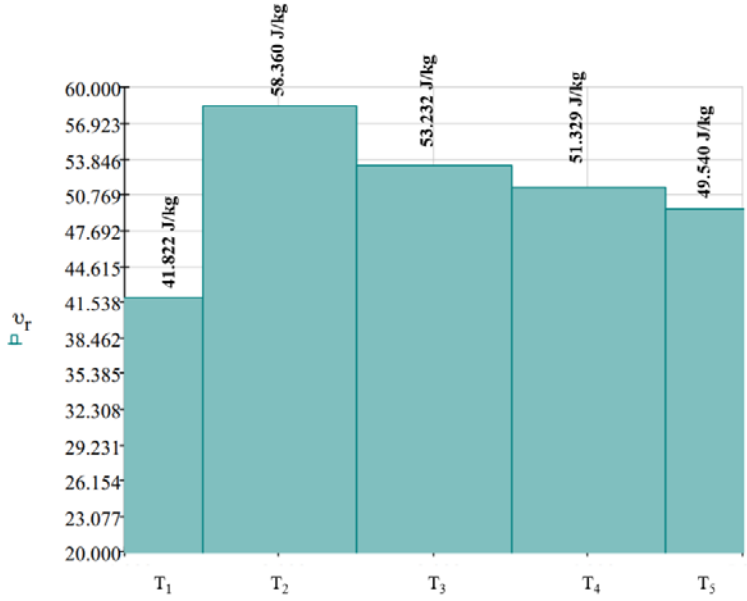

Şekil 4.6. Analiz Konfigürasyonların Özgül Gerinim Enerji Değerleri

(υ_r: Özgül Gerinim Enerji Değeri)

5. SONUÇ

Bu bölümde, kanat ribleri üzerinde uygulanan farklı boşaltma geometrilerinin yapısal ağırlık verimliliği ve gerinim enerji kapasiteleri üzerindeki etkileri karşılaştırmalı olarak analiz edilmiştir. Elde edilen veriler, ağırlık tasarrufu, toplam gerinim enerjisi ve özgül gerinim enerjisi kriterleri çerçevesinde değerlendirilmiştir.

Airfoil Offset Boşaltmalı Tasarım konfigürasyonu, 62.684 kg'lık toplam kanat ağırlığı ile en hafif tasarımı sunmaktadır.

Toplam gerinim enerjisi değerleri kıyaslandığında, en yüksek enerji depolaması 116370 mJ ile Airfoil Offset Boşaltmalı Tasarım geometrisinde gerçekleşmiştir. Bu durum, riblerin yük

altında en fazla deformasyonu bu konfigürasyonda sergilediğini, dolayısıyla diğerlerine göre daha esnek bir davranış sergilemiştir. Buna karşın Üçgensel Boşaltmalı Tasarım geometrisi, 111020 mJ ile boşaltmasız tasarıma en yakın rijitliği sergilemiştir.

Sadece ağırlık veya sadece gerinim enerji değerleri, tasarımın verimliliğini tam olarak yansıtmamaktadır. Bu noktada, birim kütle başına depolanan enerjiyi ifade eden Özgül Gerinim Enerjisi en belirleyici performans parametresidir. Boşaltmasız tasarımda 41.822 J/kg olan özgül gerinim enerji değeri, tüm boşaltmalı geometrilerde artış göstermiştir. Airfoil Offset Boşaltmalı Tasarım konfigürasyonu, 58.360 J/kg ile en yüksek özgül gerinim enerjisi değerine ulaşmıştır. Bu değer, malzemenin yapısal iş yapma kapasitesinin en yüksek olduğunun göstergesidir.

Yapılan değerlendirme sonucunda, Airfoil Offset Boşaltmalı Tasarım geometrisi en avantajlı tasarım olarak belirlenmiştir.

Seçimin temel gerekçeleri şu şekildedir:

- Maksimum Hafifleme: Toplam kanat ağırlığında en yüksek tasarrufu sağlayarak uçuş verimliliğine doğrudan katkı sunmaktadır.
- En Yüksek Özgül Verimlilik: 58.360 J/kg'lık özgül gerinim enerjisi değeri ile malzemenin en verimli şekilde kullanıldığı konfigürasyondur.

Sonuç olarak; rijitlikten bir miktar ödün verilmesine rağmen, özgül enerji verimliliği ve ağırlık kazanımı kriterleri göz önüne alındığında, Airfoil Offset Boşaltmalı Tasarım havacılık tasarım prensiplerine en uygun yapısal çözümü sunmaktadır.

KAYNAKÇA

Brink W.V.D.,Koenis T., Osinga T, Montero-Sistiaga M.(2025).“Topology Optimization for Aircraft Applications Using Hybrid and Multi-Material Methods for Different Component Scales”. Eng. Proc. 2025, 90,67. https://doi.org/10.3390/engproc2025090067.

Gudmundsson S.(2022).“General Aviation Aircraft Design Applied Methods and Procedures”.(2nd Edition) UK: Elsevier.

Kamal N.N.M.,Basri A.A., Basri E.I., Basri I.S., Abas M.F.(2019).“ Comparison Study Between Schrenk’s Approximation Method And Computational Fluid Dynamics Of Aerodynamic Loading On UAV NACA 4415 Wing”. Journal of Advanced Research in Fluid Mechanics and Thermal Sciences 64, Issue 2 (2019) 283-292.

Kütük Y.(2025). “NATO UAS(Unmanned Aircraft Systems): The Force Multiplier for Law Enforcement Agencies and The Potential Contributor to Stability Policing”. ISBN 979-12-5539-066-4.

Leishman G.(2025).“Introduction to Aerospace Flight Vehicles”. 7.12.2025 Tarihinde https://eaglepubs.erau.edu/introductiontoaerospaceflightvehicles/ adresinden erişildi.

Megson T.H.G.(2007).“Aircraft Structures for Engineering Students”.(4th Edition). UK: Elsevier.

NATO.(2007).“STANAG 4671 UAV Systems Airworthiness Requirements (USAR) For NATO Military UAV Systems”.(Edition 1).

Niu M. C.Y. (2002).“Airframe Stuctural Design”.(2nd Edition).Hongkong:Conmilit Press Ltd.

Sadrehaghighi I.(2023).“Aerodynamics of Airfoils and Wings(Including Cade Studies)”. CFD Open Series/Patch 2.75.

Soemaryanto A.R.,Rosid N.H.(2018) “Verification Of Schrenk Method For Wing Loading Analysis Of Small Unmanned Aircraft Using Navier-Stokes Based CFD Simulation”. Jurnal Teknologi Dirgantara Vol. 15 No.2.

Sökmen Ö.(2006).“Structural Optimization of a Composite Wing”.(Master Thesis).Middle East Technical University.Ankara.

Yao, S.,Chen, Z., Xu, P., Li,Z., Zhao Z.“Experimental and Numerical Study on the Energy Absorption of Polyurethane Foam-Filled Metal/Composite Hybrid Structures”. Metals 2021, 11,118. https://doi.org/10.3390/met11010118.

MAKİNE MÜHENDİSLİĞİ ALANINDA BİLİMSEL ARAŞTIRMALAR

yaz
yayınları

YAZ Yayınları
M.İhtisas OSB Mah. 4A Cad. No:3/3
İscehisar / AFYONKARAHİSAR
Tel : (0 531) 880 92 99
yazyayinlari@gmail.com • www.yazyayinlari.com